

# Buckling of Thin-Walled Circular Cylinders

September 1965

August 1968 – first revision

September 2019 – second revision

---

Month Year

## NASA STI Program . . . in Profile

Since its founding, NASA has been dedicated to the advancement of aeronautics and space science. The NASA scientific and technical information (STI) program plays a key part in helping NASA maintain this important role.

The NASA STI program operates under the auspices of the Agency Chief Information Officer. It collects, organizes, provides for archiving, and disseminates NASA's STI. The NASA STI program provides access to the NTRS Registered and its public interface, the NASA Technical Reports Server, thus providing one of the largest collections of aeronautical and space science STI in the world. Results are published in both non-NASA channels and by NASA in the NASA STI Report Series, which includes the following report types:

- **TECHNICAL PUBLICATION.** Reports of completed research or a major significant phase of research that present the results of NASA Programs and include extensive data or theoretical analysis. Includes compilations of significant scientific and technical data and information deemed to be of continuing reference value. NASA counter-part of peer-reviewed formal professional papers but has less stringent limitations on manuscript length and extent of graphic presentations.
- **TECHNICAL MEMORANDUM.** Scientific and technical findings that are preliminary or of specialized interest, e.g., quick release reports, working papers, and bibliographies that contain minimal annotation. Does not contain extensive analysis.
- **CONTRACTOR REPORT.** Scientific and technical findings by NASA-sponsored contractors and grantees.

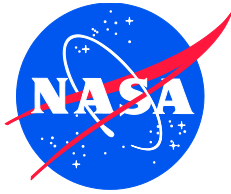
- **CONFERENCE PUBLICATION.** Collected papers from scientific and technical conferences, symposia, seminars, or other meetings sponsored or co-sponsored by NASA.
- **SPECIAL PUBLICATION.** Scientific, technical, or historical information from NASA programs, projects, and missions, often concerned with subjects having substantial public interest.
- **TECHNICAL TRANSLATION.** English-language translations of foreign scientific and technical material pertinent to NASA's mission.

Specialized services also include organizing and publishing research results, distributing specialized research announcements and feeds, providing information desk and personal search support, and enabling data exchange services.

For more information about the NASA STI program, see the following:

- Access the NASA STI program home page at <http://www.sti.nasa.gov>
- E-mail your question to [help@sti.nasa.gov](mailto:help@sti.nasa.gov)
- Phone the NASA STI Information Desk at 757-864-9658
- Write to:  
NASA STI Information Desk  
Mail Stop 148  
NASA Langley Research Center  
Hampton, VA 23681-2199

NASA/SP-8007-2018 (REV)



# Buckling of Thin-Walled Circular Cylinders

September 1965

August 1968 – first revision

September 2018 – second revision

National Aeronautics and  
Space Administration

Langley Research Center  
Hampton, Virginia 23681-2199

---

Month Year

The use of trademarks or names of manufacturers in the report is for accurate reporting and does not constitute an official endorsement, either expressed or implied, of such products or manufacturers by the National Aeronautics and Space Administration.

Available from:

NASA STI Program / Mail Stop 148  
NASA Langley Research Center  
Hampton, VA 23681-2199  
Fax: 757-864-6500

## Foreword

From 1964 to 1979, NASA developed uniform criteria for the design of space vehicles in the four following technology areas:

- Chemical Propulsion
- Environment
- Guidance and Control
- Structures

Individual topics within these technology areas were published in a series of NASA *Space Vehicle Design Criteria* monographs, the NASA SP-8000 document series. A total of forty-four NASA design criteria monographs on Structures were developed and include four monographs on the design of buckling-critical structures:

NASA SP-8007: Buckling of Thin-Walled Circular Cylinders, Revised August 1968

NASA SP-8019: Buckling of Thin-Walled Truncated Cones, September 1968

NASA SP-8032: Buckling of Thin-Walled Doubly Curved Shells, August 1969

NASA SP-8068: Buckling Strength of Structural Plates, June 1971

These monographs are known throughout the aerospace industry and provide recommendations for the design of buckling-critical thin unstiffened plates and shells subjected to various combinations of mechanical and pressure loads. In addition to these NASA monographs, two prominent NASA reports were published and are commonly used in the design of stiffened cylinders:

NASA TN D-5561: Buckling of Stiffened Cylinders in Axial Compression and Bending – A Review of Test Data, 1969

NASA CR-124075: Isogrid Design Handbook, 1973.

Recent industry and NASA experience with the development of launch vehicles structures have indicated a need for updated monographs for the design of buckling-critical structures that account for state-of-the-art structural configurations, material systems, and computational tools. This monograph provides an update to NASA SP-8007 and was prepared under the cognizance of the NASA Engineering and Safety Center (NESC). It summarizes all significant knowledge and experience accumulated from the NESC Shell Buckling Knockdown Factor (SBKF) Assessment (NESC Assessment #: 07-010-E) to date for use in the design of buckling-critical thin-walled circular cylinders. The lead of the SBKF Assessment and author of this monograph was Mark W. Hilburger of NASA Langley Research Center. A number of other individuals assisted in developing the material and reviewing the drafts. In particular, significant contributions to the State of the Art assessment were provided by Dr. Robert P. Thornburgh of the Army Research Laboratory.

The format and terminology used in this monograph is similar to previous versions of NASA SP-8007 for ease of understanding and implementation. In addition, as with the design recommendations contained in the previous versions of NASA SP-8007, this monograph is to be

regarded as a guideline to design and not as a NASA requirement, unless specified in formal program specifications. Furthermore, it is expected that the guidelines presented in this monograph will be updated as appropriate. Designers are advised to stay abreast of updates in the state-of-the-art and corresponding design criteria. Comments and recommendations on the technical content contained herein are invited and should be forwarded to the attention of the Center Chief Engineer, NASA Langley Research Center, Hampton, Virginia, 23681.

September 2019

## Table of Contents

<b>1.0</b>	<b>Introduction .....</b>	<b>1</b>
<b>2.0</b>	<b>State of the Art.....</b>	<b>2</b>
2.1	Brief History of Shell Buckling Research and NASA Design Criteria.....	2
2.1.1	Buckling of Thin-Walled Cylinders .....	4
2.1.2	Analysis Methods.....	9
2.1.3	Design Approaches .....	10
<b>3.0</b>	<b>Criteria .....</b>	<b>14</b>
3.1	General .....	14
3.2	Guide for Compliance .....	14
<b>4.0</b>	<b>References .....</b>	<b>15</b>

## List of Figures

## List of Tables

## Nomenclature

### Symbols

$N_c$	critical buckling load (Ref. 12)
$N_w$	wide column buckling load (Ref. 12)
$R$	cylinder radius
$t$	cylinder thickness
$\gamma$	classical buckling knockdown factor
$\rho_x, \rho_y$	radii of gyration in axial and circumferential directions
$(R/t)$	effective radius to thickness ratio (Ref. 12)
$\phi$	reduction (knockdown factor) (Ref. 12)

### Acronyms

ATP	automated tow placement
ET	External Tank
FEM	Finite-element method
IML	inner mold line (inner surface of structure)
KDF	knockdown factor
LaRC	Langley Research Center
LH2	liquid hydrogen
LOX	liquid oxygen
MSFC	Marshall Space Flight Center
NESC	NASA Engineering and Safety Center
OML	outer mold line (outer surface of structure)
SBKF	Shell Buckling Knockdown Factor
SLS	Space Launch System
SRB	Solid rocket booster
TA	Test article

Microsoft Office User 9/18/2018 10:11 AM

**Comment [1]:** Do these lists have to have a boarder around them? I would prefer no boarder.

## 1.0 Introduction

A structure is said to be unstable under static loading when a relatively small increase in load or a small external disturbance will cause the structure to change from one equilibrium configuration to another in a process referred to as *buckling*. For some structures, the buckling response is somewhat benign and large changes in shape develop gradually with an increase in load. In this case, the postbuckling response is *stable* and additional load can be applied to the structure until the material fails or the structure collapses. These structural response characteristics are typically found in the buckling of a flat plate or shallow curved panel. For other structures, the buckling response results in a sudden and significant change in the structural configuration. In this case, the initial postbuckling response of the structure is *unstable* and is typically accompanied by the development of large-magnitude deformations and a significant reduction load carrying capability. These structural response characteristics are typically found in the buckling of thin-walled cylindrical shells.

The primary design problem for light-weight aerospace structures is the prevention of buckling that leads to undesirable configurations such as large-magnitude displacements, large changes in global stiffness, or collapse. The critical or buckling load of a structure generally depends on its geometry, the manner in which it is stiffened, material stiffness properties, boundary conditions, and loading. Analytical methods for predicting the buckling load of shell structures were first developed in the 1920s to 1960s. However, laboratory experiments on thin-walled cylinders, during this same time period, typically yielded buckling loads that were substantially lower than the corresponding analytical predictions. This led to the development and use of conservative, empirical correlation factors, that have become known as *knockdown factors* (KDFs), in the design of buckling-critical shells. These KDFs were determined by establishing lower bounds to test data and published in a series of NASA space vehicle design criteria and reports. [Refs. 1-6]

The traditional approach for designing a thin-walled buckling-resistant shell is to predict the buckling load of the shell using a classical linear buckling analysis and then apply a knockdown factor to account for the difference between the predicted buckling load and the actual buckling load determined from tests. The linear buckling analysis typically assumes nominal structural dimensions and material properties, and simply-supported boundary conditions. This approach to shell buckling design has proved satisfactory for most design purposes and remains prominent in industry practice, as evidenced by the extensive use of the NASA design criteria. However, it has been shown over time that this design approach can result in overly conservative buckling load predictions and designs. In addition, the traditional sources of knockdown factors do not include data for modern aerospace shell structures constructed using advanced materials and manufacturing processes.

It is now well recognized that small deviations in the nominal shell-wall radius, traditionally referred to as initial *geometric imperfections*, are the primary reason for the discrepancy between the analytical predictions and the experimental results.[Refs. 7-9] In addition, unintended variations or imperfections in other structural design parameters including, but not limited to, shell-wall thickness, stiffener geometry, material stiffness, loading, and boundary conditions can also have a significant effect on the buckling response and buckling load. The advent of high-performance digital computers and advanced nonlinear structural analysis tools enable in-depth highly detailed studies of the buckling response of thin-walled buckling-critical shells and the

Microsoft Office User 9/18/2018 10:12 AM

Comment [2]: Is this reference format OK? I made it up. It is fine with me.

effects of these imperfections are, for the most part, well understood. [Refs. 10, 11] In addition, the analysis methods can accurately account for the effects of the initial imperfections, boundary conditions, and nonuniform loads and the results from these analyses generally correlate well with the experimental results. Based on these analysis tools and physical insight, semi-empirical and analysis-based knockdown factors, have become viable alternatives for some of the traditional test-based knockdown factors and classical analysis methods. [Refs. 12-14]

This monograph presents state-of-the-art practices for predicting the buckling of circular cylindrical shells subjected to various types of static loading and provides recommended procedures that yield conservative estimates of the static buckling load. To this end, a summary of the state of the art is presented in Section 2 *State of the Art* and provides the technical basis for the design criteria and recommendations. Next, the design criteria and guidelines for compliance are defined in Section 3, *Criteria*. Finally, recommended practices for the design of buckling-resistant cylindrical shells are presented in Section 4, *Recommended Practices*.

## **2.0 State of the Art**

Since the publication of NASA SP-8007 in 1965 (revised in 1968), a significant amount of research has been conducted on the buckling of thin-walled cylindrical shell structures. This research has led to advancements in several critical areas including the theory of shells and shell stability, understanding imperfection sensitivity, and high-fidelity structural analysis methods.

The goal of this section is to provide a brief assessment of the state of the art, identify important research developments and current trends, and establish the technological basis for the criteria and recommended practices presented in this monograph. In addition, some of the more common challenges and pitfalls in the design of buckling-resistant cylinders are identified and discussed.

### **2.1 Brief History of Shell Buckling Research and NASA Design Criteria**

Research on shell buckling and the development of design recommendations and methods have been well documented in the literature and only a select portion of the critical works are presented herein as they pertain to this monograph. A more detailed survey of research on shell buckling can be found in Refs. 15-25.

In the late 1920s, aircraft designs began to incorporate thin-walled load-bearing shell structures. This led to the increased study of buckling due to compression loads, and the buckling of circular cylindrical shells was a problem of particular interest. During this time, it was observed that large discrepancies existed between the theoretical buckling loads and the loads at which shell actually buckled during experimental testing. Extensive experimental investigations were conducted in an effort to resolve this problem. Not only did cylinders buckle at loads sometimes as low as 10 percent of the theoretical values, but significant scatter in the data existed, even between nominally identical cylinders tested by the same researcher. Lacking an adequate theoretical solution, empirical correlation factors, now more commonly referred to as *knockdown factors*, were established to give engineers a means to predict buckling in their designs. As a result, from the mid 1930s to late 1950s, most buckling experiments were intended to provide design data rather than insight into the fundamentals of the buckling phenomenon.

Over time, researchers began to resolve the discrepancy between the theoretical buckling load predictions and the corresponding test results. The pioneering work of von Karman and Tsien

(1941) [Ref. 7] showed that the initial postbuckling response was unstable and provided the first indications of how initial imperfections in the shell geometry could cause the large reductions in the buckling load observed in experiments. In 1950, Donnell and Wan [Ref. 8] extended this work to include the effects of initial geometric imperfections in the analysis. Their results showed that the imperfections in the cylinder act as a perturbation and cause the response to deviate from that of the idealized perfect cylinder. As a result, the cylinder exhibits a *limit point buckling* response at a load level that is significantly lower than the corresponding theoretical buckling load of the perfect cylinder, as illustrated in Figure 1. However, the analysis of these shell structures was not trivial, particularly prior to the emergence of high-performance digital computers and numerical methods that occurred in the 1970's. Simplifications in the analysis limited the results to a qualitative demonstration. Consequently, designers continued to use the classical buckling equations and applying empirical design factors that they considered appropriate. Around the same time, Koiter's asymptotic theory [Ref. 9] was applied to cylinders loaded in axial compression and provided rigorous mathematical proof of the extreme imperfection sensitivity. However, this work went relatively unknown until 1967 when it was translated from Dutch into English. Koiter's work went on to form the basis of many semi-empirical design methods such as that proposed by Almroth et. al [Ref. 12], and basic research on the effects of imperfections on the buckling of shells.

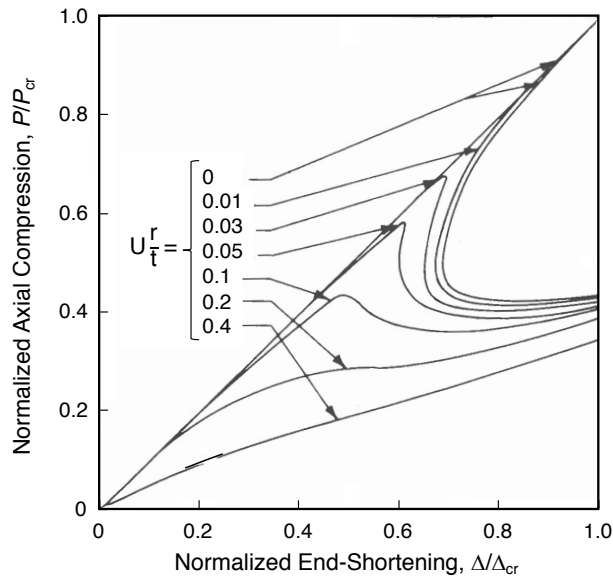


Figure 1. Effects of imperfections on the load-end-shortening response of a compression-loaded monocoque cylinder (recreated from Donnell and Wan [Ref. 8])

In the 1960s, NASA recognized a need to establish uniform design criteria for space vehicles and began to issue a series of monographs to be used as design guidelines. Monographs for the design of buckling-resistant shells included NASA SP-8007 (Buckling of Thin-Walled Circular Cylinders), NASA SP-8019 (Buckling of Thin-Walled Truncated Cones), and NASA SP-8032 (Buckling of Thin-Walled Doubly Curved Shells) [Refs. 1-3]. These monographs presented equations for determining the classical linear buckling load as well as guidance for determining the appropriate knockdown factor to use. In addition to these NASA monographs, two prominent NASA reports were published and are commonly used in the design of stiffened cylinders, including NASA TN D-5561 (Buckling of Stiffened Cylinders in Axial Compression and Bending – A Review of Test Data) and NASA CR-124075 (Isogrid Design Handbook). [Refs. 5, 6] These monographs and reports remain widely used throughout the aerospace industry.

Since the publication of the NASA design monographs, a considerable amount of research on the buckling of shells has been conducted and focused on three primary areas. The first area of research has been focused on identifying and developing an understanding of the key factors or influences that govern the buckling response and cause the discrepancy between the theoretical buckling predictions and experimentally observed behavior and to extend that understanding to the buckling of aerospace-specific structural configurations. The second area of research has been on the development of improved computational tools for the analysis of shells. This work has included the development of special purpose analytical and semi-analytical codes and finite-element methods to provide more accurate physical representations of complex as-built (i.e., imperfect) structures, as well as developing nonlinear solution methods that can accurately predict the highly nonlinear unstable collapse response of shells. In particular, high-fidelity finite-element models and nonlinear solution methods have been shown to be very effective at predicting the buckling response of both metal and composite shells, provided that careful attention is paid to capturing all of the effects that are known to influence the buckling behavior [Refs. 10, 11, 26, 27]. In addition, these high-fidelity models enable the study individual effects and determine sensitivities. The third area of research has been on the development of new design approaches for thin-walled buckling-critical shells. While significant progress has been made in all three areas of research, many challenges remain with regard to the incorporation of improved knowledge and new design approaches into the design process. A brief summary of the progress made in these areas of research is provided next.

### **2.1.1 Buckling of Thin-Walled Cylinders**

Considerable progress has been made towards understanding the buckling of thin-walled cylinders and to identify key factors that cause the discrepancy between theoretical buckling predictions and experimentally observed behavior, described previously. The scope of work considered a variety of structural configurations such as metallic and composite, stiffened, unstiffened, and sandwich cylinders; loading conditions such as axial compression, torsion, bending, internal pressure, external pressure, combined mechanical loads, and lateral loads; structural details such as cutouts, and joints; the effects of boundary conditions and nonuniform loads; prebuckling deformations; and the effects of geometric imperfections. Key areas of progress are highlighted in this section and provide the technical background for the design criteria and recommended practices presented in this monograph.

### ***Geometric Imperfection***

Geometric imperfection has been firmly established to be the primary factor in the reduction of buckling loads from the theoretical critical loads predicted by classical linear analysis methods. The importance of imperfection in the buckling phenomenon has been recognized since the early days of experimental research. However, it was not until much later that researchers started to understand the exact mechanism by which imperfection influences the stability of compressed shells. The work by Von Karman and Tsien in 1941 [Ref. 7] was the first to offer practical insight into this problem. They showed that there are multiple equilibrium positions of various *post-buckling* deformation shapes involving lower loads than those predicted by classical theory. Small imperfections can cause the shell to transition from the unbuckled equilibrium state to one of these post-buckling states during loading, thus buckling the shell at a load level lower than the classical buckling load. This led to later work by Donnell and Wan [Ref. 8] which included initial geometric imperfections in the analysis and demonstrated that it was the most likely cause of the difference between experimental buckling loads and classical analysis. Koiter's asymptotic theory [Ref. 9] was applied to cylinders loaded in axial compression and provided rigorous mathematical proof of the extreme sensitivity to initial geometric imperfections on the buckling of these thin-walled shells.

This work continued to evolve and great emphasis was placed on understanding imperfection sensitivity for a wide variety of different practical cylinder constructions and loading conditions. These studies were aided by the use of analytical, semi-analytical, and finite-element analysis tools that could perform imperfection sensitivity studies by including the effects of eigen-mode imperfections. A traditional analysis-based sensitivity study would typically use one or more eigen-mode shapes to generate an imperfection pattern and then a range of imperfection amplitudes would be assumed to generate an estimate of the imperfection sensitivity. This approach has the advantage in that it is simple to implement. However, the eigen-mode imperfection shape is not a pattern typically observed in as-built structures and the choice of mode shapes and amplitudes to include in the simulated imperfection is somewhat arbitrary. In addition, the use of an eigen-mode imperfection can cause a significant reduction in the predicted pre-buckling stiffness of the shell which is not seen in actual tests. [Ref. 26]

Efforts have been made to acquire complete surveys of actual shell geometries and characterize initial geometric imperfections. These efforts first began in the late 1960's by Arbocz and Babcock. Investigations were then carried out using these measured imperfections [Refs. 27, 28], to determine the critical role imperfection plays in the buckling of cylinders loaded in axial compression. This work was expanded to acquire complete imperfection surveys of full-scale cylindrical shells manufactured by the aerospace industry. [Ref. 29] The goal was to collect data from these imperfection surveys into an imperfection data bank that would allow future designers to more accurately predict buckling loads based on the manufacturing method used to build the shell structure [Ref. 30]. After measuring the imperfection, the data would be fit with a Fourier series representation, thus expressing the imperfection in terms of circumferential waves and axial half-waves. Their work revealed a number of common characteristics of the imperfection associated with a particular manufacturing process, later referred to as an *imperfection signature*. For example, the imperfection signature of large cylinder manufactured from a fixed number of curved panel sections were shown to have three primary Fourier series components: an out-of-roundness component (two or three circumferential full-waves), a

component with the number of circumferential waves equal to the number of panel sections, and components with the circumferential wave number equal to integer multiples of the number of panel sections. The magnitude of each of these components varied depending on specifically how the cylinder was constructed, but the overall character of the imperfection signature was consistent across similarly built cylinders. Further examples are described in detail in Ref. 25.

Other interesting but lesser known experimental work was conducted on the effects of an initial lateral load on the buckling of isotropic cylinders by Ricardo and Okubo et al. [Refs. 31, 32]. These works primarily focused on obtaining information on the buckling behavior and imperfection sensitivity of a thin-walled cylinders under various loading conditions with the objective to better understand the buckling mechanism and process. The lateral load results in a known imperfection in the form of a local inward dimple in the cylinder wall. By varying the magnitude of the lateral load, imperfection sensitivity characteristics could be investigated.

### ***Prebuckling Deformations and Stresses***

In general, the classical methods for calculating the critical stress in cylindrical shells assume that only uniform membrane stresses are present, and that there is no local bending in the shell prior to buckling. In practice however, local bending stresses and deformations are an almost unavoidable condition in both experimental tests and flight hardware. In experimental test configurations, localized bending usually arises from the support conditions between the shell and the load fixture. As a cylindrical shell is compressed axially, the Poisson expansion of the shell wall is restrained at the boundary by the support fixture, creating localized bending deformation. The magnitude and extent of this bending deformation is dependent on the radius and thickness of the cylinder, the shell wall stiffness properties, and the boundary conditions. Similar behavior can occur near stiff attachment rings or ring frames, commonly found in aerospace shell structures although the character of the response can be slightly different depending on the relative stiffness properties of the shell and the stiff ring structures. The importance of the effects of prebuckling deformations and stresses on the buckling of circular cylindrical shells was extensively investigated in the early sixties [refs. 33-35]. In addition, localized prebuckling deformations can occur in the vicinity of stiffness discontinuities in the shell, such as, joints, stiffener terminations, and cutouts or abrupt changes in the shell thickness and shell-wall mid-surface eccentricities.

In many cases, the prebuckling deformations and stresses in the shell can act like an imperfection and affect the buckling response in a similar manner to initial geometric imperfections. The out-of-plane deformations grow nonlinearly with increasing load which can result in internal load redistribution and can cause the shell to buckle long before the load reaches the classical buckling load value. Thus, the classical linear bifurcation analysis might not only over predict the buckling load, but also incorrectly predict the buckling mode. In some cases, this nonlinear effect has been observed to produce deformations large enough to even prevent instability. The consequence of this highly nonlinear behavior is that classical methods and sometimes even linear bifurcation buckling analyses may be inappropriate for determining the response of the shell. Examples of this are shown in Refs. 36-40.

### ***Boundary Conditions and Nonuniform Loading***

In addition to the prebuckling deformations and stresses induced by the constraints from the support conditions, changes in the boundary conditions, particularly in-plane, can significantly influence the buckling behavior of shells loaded in compression. The out-of-plane boundary condition, and length effects, are usually ignored in classical buckling analysis, but more rigorous analysis methods require the boundary condition to be specified as either simply supported (free rotations) or clamped (zero rotations). For each of these two transverse boundary conditions four possible in-plane boundary conditions are usually considered. It was shown by Hoff [Ref. 16] and Ohira [Ref. 41] that for very long cylinders the combination of the simply supported boundary and the zero shear stress in-plane boundary condition (free circumferential displacement) resulted in buckling loads equal to approximately half the classical values. Later work by Simitset et al [Ref. 42] showed that the reduction in buckling load of circular cylinders caused by geometric imperfection was greatly influenced by the boundary conditions at the ends, with some combinations even resulting in relatively imperfection insensitive cylinders.

Recent research efforts by Hilburger et al. [Refs. 10, 43, 44] have also investigated the effects of elastic boundary conditions representative of those found in laboratory-scale and large-scale cylinders. These studies were conducted to determine the effects of as-tested boundary conditions in an effort to improve test and analysis correlation. These elastic boundary conditions primarily affect the rotations and radial displacements near the ends of the shell. In most of the limited cases studied, the elastic boundary conditions had a minimal effect on the buckling load but often significantly changed the overall character of the prebuckling deformation response and in some instances change the location at which buckling initiated in the cylinder.

Nonuniform loading (a.k.a., loading imperfections) has also been shown to affect the buckling response and buckling load of cylinders. Nonuniform loading can come about in an as-built structure due to localized manufacturing irregularities or machining tolerances of the interface or loading surfaces which can cause deviations from the idealized uniform loading. Geier et al. and Zimmermann [Ref. 45, 46] studied nonuniform loading by installing a thin shim layer to apply a local load imperfection in experimental tests on composite shells. The nonuniform loading caused a local dimple to form in the bending boundary layer of the cylinder. This local dimple acted like an initial imperfection and caused the buckling of the cylinder to occur at lower load than the corresponding cylinder without the shim. Additional studies by Huhne et al. and Kriegesmann et al. looked at the combined effects of geometric and loading imperfections on the buckling of compression loaded shells.[Refs. 47, 48] Detailed studies on the effects of as-measured loading surface imperfections on the response of small-scale and large-scale compression-loaded cylinder test articles have been conducted by Hilburger et al. [Refs. 10, 44] The results indicated that the as-measured loading surface geometry is periodically distributed around the circumference of the cylinder and, by itself, can have a noticeable effect on the buckling load and buckling mode. However, in most cases studied, the effect of the loading imperfection remained relatively small, i.e., less than 5%, and the initial shell-wall geometric imperfection remained the primary factor in determining the actual buckling load of the cylinder.

### ***Composite Cylinders***

The high stiffness-to-weight ratios of modern fiber-reinforced composites makes them obvious candidates for use in light-weight aerospace shell structures. Like metallic cylinders, composite

cylinders can be of stiffened, unstiffened, or sandwich construction. However, the design and analysis of composite structures can be more challenging as a result of the large number of design parameters associated with the use of composite materials. Composite shells can be fabricated in several ways including built-up laminates from unidirectional or woven material, filament wound, or advanced tow placement (ATP). These different fabrication methods enable considerable flexibility in the design, and in particular can result in highly tailored structures that may not only be anisotropic, but also have shell stiffness properties that vary with location. This leads to difficulties in applying classical methods for determining critical loads and questions the applicability of the traditional design methods and design factors.

Another byproduct of the manufacturing processes used for composite shells is the irregularity of the surface and the stiffness resulting from “building up” the composite material on a tool. Filament-wound or ATP composites can exhibit distinct irregularities on the non-tool surface, e.g., undulations in the surface contour, depending on the size of fiber tow used, caused by the fibers overlapping or gapping. Laminated composite shells tend to have smoother, more uniform surfaces, except where adjacent plies meet. Most aerospace shell structures are too large to be constructed from a single sheet of composite lamina material. Thus, the manufacturer must either butt multiple laminae together or overlap them. The thermal expansion of the tool that occurs during curing often causes butt joints to open up, leaving a gap between adjacent plies which both reduces local stiffness and adds a local mid-surface eccentricity. Overlapped plies create locally thick regions which can act like stiffeners, and also add local eccentricity. The ply gaps can be of particular concern, because they have been shown to have a significant effect on the nonlinear and buckling response of thin-walled unstiffened composite cylinders in axial compression [Refs. 10, 11, 49].

### *Cutouts*

It is common for cylindrical shell structures to have one or more cutouts to allow access to the interior of the shell. Cutouts can have a significant influence on the buckling response of the shell depending on the size and shape of the cutout and the type of cutout reinforcement implemented. [Refs. 50-55] Experimental results from Refs. 50, 52 indicate that sufficiently small unreinforced cutouts will have a minimal effect on the buckling response and that other imperfections in the shell govern the global buckling response in the shell. However, for larger unreinforced cutouts, large-magnitude bending deformations occur near the edges of the cutout which leads to a local reduction in effective stiffness and cause stresses to be redistributed away from the cutout. This load redistribution and local stiffness reduction can result in a stable local buckling response around the cutout or initiate a global collapse, depending on the design. For most practical applications, however, some type of reinforcement is typically applied around the cutout to control local stresses and deformations. If done correctly, the reinforcement should restore the shell to its full load carrying capacity. However, work by Toda and Hilburger suggest that local reinforcement concepts can cause buckling to occur adjacent to the reinforcement if an abrupt stiffness change exists between the areage and the reinforcement [Refs. 51, 54, 55]. In addition, the prebuckling displacements and stresses in shells with unreinforced or reinforced cutouts grow nonlinearly with increasing load which can result in internal load redistribution and can cause the shell to buckle long before the load reaches the classical buckling load value, as described in a previous section. Thus, linear bifurcation analyses may not always produce a conservative buckling load estimate.

## ***Joints***

Large cylinders are typically manufactured by welding or mechanically fastening multiple curved panel sections into complete cylinders. In some cases, the axial joints between the panel sections can cause the development of large-magnitude prebuckling deformations and lead to reductions in the buckling load. For example, stiffened cylinders with welded joints can be particularly sensitive to this design feature. The relatively thick, unstiffened axial weld land regions typically have a higher effective membrane stiffness than the adjacent thin-walled stiffened acreage and tend to attract axial load. In addition, the local stiffness discontinuity and neutral axis eccentricity between the weld land and the acreage can cause the weld land to exhibit significant inward radial prebuckling deformations. Because the weld land region has relatively low bending stiffness, as compared to the stiffened acreage, the combination of prebuckling deformations and increased axial load can lead to a reduced buckling capability.[Ref. 56] Similar behavioral characteristics have been seen in sandwich cylinders in which the acreage sandwich structure is tapered down to a monolithic laminate and a mechanically fastened lap joint is installed.

### **2.1.2 Analysis Methods**

The development of shell theories and computational tools for the analysis of shells have provided researchers and engineers with the ability to gain tremendous insight into the buckling response of many different types of shell structures. These developments include special-purpose analytical and semi-analytical methods, and finite-element analysis capabilities, as well as solution methods that can accurately predict the complex nonlinear response of shells. Recent developments have focused more on high-fidelity finite-element models and nonlinear solution methods and have been shown to be very effective at predicting the buckling response of both metal and composite shells, provided that careful attention is paid to capturing all of the effects that are known to influence the buckling behavior [Refs. 10, 11, 57]. However, the classical analytical and semi-analytical methods still play a critical role in the analysis and design of thin-walled shells. Summaries of the important works in this area are provided in several references [Refs. 21, 27, 58]. A brief summary of methods used in design are presented here.

The most commonly used linear bifurcation buckling analysis for the design of cylindrical shells is based on the Donnell-type shell theory. [Ref. 59] The analysis assumes the shell to be geometrically perfect, under a membrane state of stress (i.e., the effects of prebuckling bending deformations due to edge restraints are neglected), and simply-supported boundary conditions. The governing system of partial differential equations are solved using a double Fourier series approximation to reduce the solution to a standard linear eigenvalue problem. This approach yields, for instance, the well-known *classical* solution for isotropic shells, for example, Batdorf, [Ref. 60], and Becker and Gerard [Ref. 61]. Other forms of the Donnell-type shell theory can be used to analyze perfect and imperfect isotropic and orthotropic stiffened shells, [Ref. 27] making this method ideally suited for efficient study of the buckling and imperfection sensitivity of a wide range of practical cylindrical shell configurations.

A semi-analytical approach can be used to develop a more accurate solution to the Donnell-type equations by including the effects of boundary conditions and a nonlinear prebuckling state. In this case, the solution assumes a Fourier series decomposition in the circumferential direction, then the resulting set of ordinary differential equations for the axial direction can be solved

numerically by means of the *shooting method* or the *finite difference method*. By using this approach, the specified boundary conditions and the effect of edge restraint are rigorously satisfied. This semi-analytical approach can be used to study the effects of classical boundary conditions and elastic boundary conditions and provide more accurate imperfection sensitivity results. The semi-analytical methods can also provide valuable results for the development and verification of finite-element models.

Finite-element methods are now very common in the design and analysis of shell structures and include two-dimensional (shell elements) and three-dimensional (solid elements) discretization. When used correctly, highly accurate solutions can be obtained in which all nonlinear effects and initial geometric imperfections are properly accounted for and structural detail features such as cutouts, joints, and stiffeners are represented. However, complex finite-element models must be carefully assembled to accurately reflect physical loads, geometry and local stiffness of the real as-built structure and the modeling assumptions need to be fully understood as the results can be very sensitive to a wide range of modeling approaches. Similarly, a variety of solution routines (e.g., linear and nonlinear, quasi-static and transient dynamic) are available to predict the prebuckling, buckling, and postbuckling response of the shell. Different solution methods and their implementation should be well understood, else an erroneous result may be obtained. It is not uncommon that the time required to create and validate an accurate finite-element model far exceeds the computational time needed to analyze the model.

One of the drawbacks to using the high-fidelity finite-element analysis methods in the early design is the relatively long model development and solution times required as compared to the simpler design-level methods. Thus, methods for reducing solution time remain an area of interest in an effort to bring increasing design fidelity into earlier stages of the design process. For example, reduced basis methods for the nonlinear analysis of shells have been proposed in an effort to reduce the number of degrees of freedom in a nonlinear system. These reduced basis techniques can be implemented in both analytically and numerically (referred to as reduction methods). The Koiter-Newton (K-N) approach has been developed by Liang et al. [Ref. 62] for the numerical solution of the buckling of thin-walled shells. The method combines concepts from Koiter's initial post-buckling analysis and Newton arc-length correction methods to obtain a solution algorithm that can predict the prebuckling, buckling, and postbuckling equilibrium path in a finite-element analysis setting. Similarly, special-purpose analytical and semi-analytical tools have been developed that enable rapid design-level analysis for the nonlinear and buckling of shells with detail features, such as cutouts, bonded repairs, and discrete stiffeners, and can be useful for preliminary design studies. [Refs. 63, 64] The results of these models can also be useful in developing and verifying finite-element models and analysis results.

### **2.1.3 Design Approaches**

Since the publication of the NASA SP-8007 monograph, other alternate design approaches have been proposed, including semi-empirical and analysis-based approaches, and have been implemented on a limited basis. Often, these alternate approaches have been used in parallel with the traditional empirical design approach and have enabled designers to safely remove some design conservatism. A brief summary of the traditional design approach from the NASA SP-8007 monograph and some of the more common alternate design approaches are described in this section.

### ***Traditional design approach***

The traditional approach for the preliminary design of a thin-walled buckling-resistant shell, as recommended in the NASA SP-8007 (1965, 1968), is to predict the buckling load of the shell using a classical linear eigenvalue analysis or approximate closed-form solution and then apply an empirical correlation factor, commonly known as a knockdown factor, to account for the difference between the predicted buckling load and the actual buckling load determined from tests. The classical eigenvalue analysis assumes nominal structural dimensions and material properties, a membrane prebuckling stress state, and simply-supported boundary conditions of a moderately long circular cylinder (i.e., length effects are neglected).

NASA SP-8007 includes buckling load calculations and design knockdown factors for a variety of cylinder constructions including isotropic and orthotropic, isotropic sandwich, and stiffened shells. The loading conditions considered include axial compression, bending, torsion, and external and internal pressure. For example, the guidance in NASA SP-8007 for determining the buckling knock-down factor  $\gamma$  for compression-loaded isotropic cylinders is to use the following equation

$$\gamma = 1 - 0.901(1 - e^{-\phi}) \quad (1)$$

$$\phi = \frac{1}{16} \sqrt{\frac{r}{t}} \quad (2)$$

Equation 1 provides a lower bound to experimental data from about 200 buckling tests on isotropic circular cylinders defined by Weingarten et al. [Ref. 65]. Similar equations are provided in SP-8007 for other loading conditions

NASA SP-8007 also provides guidance for the buckling of orthotropic cylinders. The term “orthotropic cylinders” is taken to include not only cylinders made of one or more orthotropic layers, but also stiffened cylinders with stiffener spacing sufficiently small enough that the bending and extensional properties can be approximated by a single orthotropic sheet (sometimes referred to as a *smearred stiffener approximation*). The procedure for calculating the critical buckling load for an orthotropic cylinder is more complex due to the large number of parameters associated with orthotropic shells. NASA SP-8007 also emphasizes the importance of taking into account the stiffener eccentricity, since neglecting the eccentricity typically leads to unconservative buckling loads for internally stiffened cylinders in compression. Specifically, stiffener eccentricity can result in coupling between bending and extension actions. For compression-loaded unstiffened and stiffened orthotropic shells, SP-8007 recommends the use of Eqs. (1) and (2), replacing the thickness with the geometric mean of the radii of gyration for the axial and circumferential directions,  $\rho_x$  and  $\rho_y$ .

$$\phi = \frac{1}{29.8} \left[ \frac{r}{\sqrt{\rho_x \rho_y}} \right]^{\frac{1}{2}} \quad (3)$$

For axially compressed cylinders with closely spaced moderately large stiffeners, NASA SP-8007 suggests a buckling knock-down factor of 0.75. This recommendation is based on the experimental data from Refs. 66-73. However, this factor is rarely used in practice in favor of a

more conservative factor of 0.65 as defined in the NASA TN D-5561 which reviewed data from a variety of experimental tests on stiffened cylinders and corresponds to the lowest observed buckling load across all of the tests [Refs. 66, 67, 73-76].

Another commonly used design document is the Isogrid Design Handbook [Ref. 6]. This handbook provides guidance on calculating effective material properties for isogrid-stiffened constructions and recommendations on calculating buckling loads for isogrid shells. For very lightly stiffened cylinders, it is suggested to calculate the buckling knock-down factor using Eq. (1). For moderately or heavily stiffened cylinders the knockdown factor of 0.65 from TN D-5561 is recommended.

As the design cycle evolves, finite-element (FEM)-based linear eigenvalue analysis are typically used and may include the effects of additional design details such as cutouts, joints, hard-points for attachments, discrete stiffeners, and more accurate representations of primary and secondary loads. The same knockdown factor from the preliminary design phase is often retained and applied to the FEM-based buckling load of the detailed structure.

Overall, the knockdown-factor-based design approach is a reliable and convenient approach, however, it has been shown over time that it can result in overly conservative buckling load predictions and designs. The conservatism is likely due to several factors. First, the experimental data was gathered between 1928 and 1964, and thus reflects the quality of the manufacturing processes used during this time. In addition, the importance of initial geometric imperfections on the buckling of the shells was not recognized until circa 1950, and thus may have resulted in a large variation in the quality of the test articles and the corresponding test data, as strict controls on specimen quality and test set-up were not emphasized. It is interesting to note that much of the test data generated later in that time period (1950's-1960's), corresponded to higher buckling loads, presumably due to the increased attention placed on imperfections and manufacturing quality. It is not uncommon for the buckling loads from more recent high-precision test to be 70% to 90% of the classical value, significantly higher than what would be prescribed by a traditional empirical KDF.[Ref. 77] In addition, it has been shown that stiffened cylinders typically exhibit reduced imperfection sensitivity as compared to an equivalent monocoque cylinder [Ref. 78]. One might also expect that the inclusion of local detail features such as joints, cutouts, or discrete loads associated with attachments can reduce the imperfection sensitivity as these local details can produce local perturbations in the response that act as imperfections.

Finally, these guidelines and the knock-down factors in them have not been updated since the early 1970's, thus there is considerable question as to how appropriate they are for the design of modern aerospace structures. Of particular concern is the complete absence of any experimental data using composite, orthogrid or isogrid shells in the basis for the knock-down factors.

### ***Semi-empirical design approach***

The traditional design approach remains the most commonly used approach for preliminary design, and may remain so for the foreseeable future, due to its ease of use and demonstrated reliability. However, several semi-empirical design approaches have also been proposed [Refs. 79, 80] in an effort to reduce design conservatism and provide a more general approach for the design of practical aerospace cylindrical structures. Industry has successfully implemented the approach proposed by Almroth et al.<sup>79</sup> in the design of many space vehicle applications, most notably, in the design of the Space Shuttle External Tank (ET). Their proposed design approach

was developed in an effort to extend existing empirical design data to more practical cylinder designs, such as stiffened, laminated composite, or cylinders stabilized by an elastic core (e.g., solid propellant rocket motor). This method is described in detail in Section 4.6.

The ET design successfully employed this semi-empirical design approach in parallel with NASA SP-8007 design recommendations to take advantage of enhancements due to internal pressure for both axial and shear loads, and the interaction of combined axial compression, bending and shear in the margin of safety calculations.

#### ***Analysis-based design approach***

More recently, improvements in digital computers and finite element analysis codes are enabling the development of highly accurate predictions of the buckling response of aerospace shells structures. [Refs. 13, 14] The models used to generate these predictions require detailed representations of the as-measured initial geometric imperfections, thickness and material property variations, and nonuniform loading (i.e., loading imperfections) and elastic boundary conditions, as well as any structural detail features such as cutouts, joints, and discrete stiffeners; and provide exceptional correlation between the predicted results and the actual buckling loads and buckling failure modes. Such analyses have been used to conduct detailed imperfection and design sensitivity studies and provide design buckling loads for several modern launch vehicles including the Space Shuttle solid rocket booster (SRB) cases and external tank (ET), and the Space Launch System (SLS) core stage. [Refs. 81-85]

For example, the SRB case design process utilized an analysis-based design approach. The analysis used a geometrically nonlinear finite element analysis method and included the effects of the measured shell geometric imperfection and material properties, and accurate SRB to ET interface and field joint representations. The nonlinear analysis results for the SRB hardware was correlated with the results from a full-scale buckling test. This design approach led to a reduction in structural mass as compared to the overly-conservative traditional knockdown factor approach while demonstrating a positive margin of safety. The results of this work also allowed an increase in the pre-launch wind speed allowable and a reduction in the probability of a flight delay or abort.

Similarly, the Space Shuttle ET LH2 tank, LOX tank, and interbank thrust panels were analyzed using a geometrically nonlinear analysis that included the effects of initial imperfections. Early in the ET design effort, a nonlinear FEM analysis of a detailed LH2 tank model with eigenmode imperfections was performed with various shell stability computer programs [Refs. 81, 82]. Later, a buckling analysis was performed on the LOX tank using STAGS finite element analysis code [Ref. 83] and considered both eigenmode and measured geometric imperfection shapes. The intertank thrust panels were analyzed using a nonlinear NASTRAN analysis and used linear eigenvector shapes as the initial geometric imperfection for the finite element model and included a sensitivity analysis with respect to imperfection amplitude [Ref. 84]. In all cases, subsequent structural qualification tests indicated safe design margins.

In general, these works by industry and NASA clearly indicate a desire and willingness to use alternative methods. However, the use of these methods require knowledge of or assumptions on imperfections and structural details, experience and understanding of buckling and imperfection sensitivity and may require testing if there is significant uncertainty or lack of knowledge and experience.

### ***Other methods and trends***

A broader approach to improving structural design methods was proposed by Nemeth and Starnes [Ref. 86]. This work assessed the limitations of the NASA design monographs and suggested a path forward for improving the design of buckling-critical shells. Their proposed approach separated the critical design parameters (those that are known to affect the buckling load) into those that are known and can be modeled in a deterministic manner (e.g. boundary conditions) and those that are better represented in a probabilistic manner (e.g. imperfection and material variance). They suggest a hybrid approach where the probabilistic uncertainties are incorporated into the calculation of improved knock-down factors and applied to accurate analytical models. Another issue highlighted in their work was use of a select number of high-fidelity experiments designed to validate the analysis tools rather than a vast number of experiments to characterize the design space. The analysis tools would then be used to perform numerical studies to determine shell buckling behavioral trends and design recommendations.

A key aspect of these aforementioned alternate approaches is to have some preexisting knowledge of the characteristic geometric imperfection of the structure. Researchers at Delft University and Technion in Israel have long championed the measurement and use of geometric imperfection data for the design of buckling-critical shells. To this end, their goal has been the establishment of an imperfection data-bank, which would facilitate the understanding of what imperfection signatures are common to a particular type of shell and manufacturing process. Thus, in the future, a designer would be able to use nonlinear analysis methods since the imperfection could be estimated early in the design phase. The imperfection data obtained indicated that a given manufacturing process resulted in a repeatable characteristic imperfection shape with a some about of variability. This characteristic imperfection shape was eventually referred to as an imperfection signature and became the basis for new design criteria based on these signatures. [Ref. 13]. In addition, it was recognized that the variability in the imperfection could be quantified and used in the development of a probabilistic design approach such as that proposed by Arbocz, but that requires a sufficient amount of data to establish a statistically meaningful result. Similar signatures have been investigated to a lesser extent for thickness variations and loading imperfections, some of which will be presented in this monograph.

## **3.0 Criteria**

### **3.1 General**

Structural components consisting of thin, curved isotropic or composite walls with or without stiffening shall be designed such that (1) buckling resulting in collapse of the component will not occur due to the application of design loads, and (2) buckling deformations that result from limit loads will not be so large as to impair the function of the structure or nearby components or produce undesirable changes in stiffness or loading.

### **3.2 Guide for Compliance**

Design loads for buckling are considered to be any combination of ground or flight loads that cause compressive in-plane stresses, including compression loads that result from temperature changes, external pressure, and applied mechanical loads, and any load or combination of loads that alleviate buckling. If an ultimate design factor is to be used in the design process, this factor

shall be applied only to the loads that cause compression stresses. For example, external pressure loads and destabilizing mechanical loads should be increased by the ultimate design factor but internal pressure loads should not.

## 4 Recommended Practices

### 4.1 Scope

Within the limitations imposed by the state of the art, acceptable procedures for the estimation of buckling loads for circular cylindrical shell subjected to various loading conditions are described in this section. The important problems are indicated and the source of the procedures and their limitations are discussed. Where the recommended procedure is complex and is suitably defined in a readily available reference, it is merely outlined. Where practicable, a summary of the procedure is given.

### 4.2 Isotropic Unstiffened Cylinders

Unstiffened isotropic circular cylinders subjected to various loading conditions are considered in this section. In the theoretical analysis of cylinders, it is usually necessary to take account of prebuckling deformations and stresses [Ref. 34] and end conditions [Refs. 87-89] as they can have a significant influence on the buckling response. However, the difference between rigorous solutions for various end support conditions can be obscured by the effects of initial geometric imperfections. Furthermore, the actual support conditions that exist in aerospace hardware are typically not well defined in the preliminary stages of design and the characteristics of the actual geometric imperfection may not be known. It is therefore customary to use simplified theoretical calculations that are adjusted by using a correlation or knockdown factor to account for the differences between theory and test.

#### 4.2.1 Axial Compression

Buckling and collapse coincide for isotropic circular cylinders subjected to axial compression. An equation for the buckling load of a simply supported cylinder under axial compression has been derived based on Donnell's shell theory (Ref. 90) and is given by

$$N_x = k_x \frac{\pi^2 D}{L^2} \quad (1)$$

where the buckling coefficient  $k_x$  is

$$k_x = m^2(1 + \beta^2)^2 + \frac{12}{\pi^4} \frac{(\gamma Z)^2}{m^2(1 + \beta^2)^2} \quad (2)$$

$$D = \frac{Et^3}{12(1 - \nu^2)} \quad (3)$$

$$Z = \frac{L^2}{Rt} \sqrt{1 - \nu^2} \quad (4)$$

$$\beta = \frac{nL}{m\pi R} \quad (5)$$

The cylinder length, radius, and wall thickness are denoted by  $L$ ,  $R$ , and  $t$ ; the Young's modulus and Poisson's ratio are denoted by  $E$ , and  $\nu$ ; and the number of axial half-waves and circumferential full waves of the buckling mode shape are denoted by  $m$ ,  $n$ . The knockdown factor  $\gamma$  has been added to the second term in equation 2 (associated with the cylinder curvature) to account for the differences between theoretical buckling loads and loads obtained from tests.<sup>1</sup> Minimization of Eq. 2 with respect to  $m$  and  $\beta$  results in the critical buckling coefficient. For moderately long cylinders,  $\gamma Z > 2.85$ , the buckling coefficient can be approximated by the following

$$k_x = \frac{4\sqrt{3}}{\pi^2} \gamma Z \quad (6)$$

Substitution of Eq. 6 into Eq.1 results in the familiar equation for the critical axial stress:

By assuming a value of  $\gamma$  equal to 1.0, one obtains the theoretical buckling equation given in Ref. 90.

$$\sigma_x = \frac{\gamma E}{\sqrt{3(1-\nu^2)}} \frac{t}{R} \quad (7)$$

$$= 0.605 \gamma E \frac{t}{R} \quad (\text{for } \nu = 0.3) \quad (8)$$

However, on the basis of various experimental data, it is recommended that a knockdown factor  $\gamma$  less than 1.0 be used to account for difference between the predicted buckling load and the actual buckling load determined from tests. An empirical factor is recommended from Ref. 65 given by

$$\gamma = 1 - 0.901(1 - e^{-\phi}) \quad (9)$$

where

$$\phi = \frac{1}{16} \sqrt{\frac{R}{t}} \quad (\text{for } \frac{R}{t} < 1500) \quad (10)$$

Equation 9 is shown graphically in Fig. 4.1 and provides a good lower bound for most test data (indicated by the red open circle symbols) that was compiled from the 1930's to the 1960's.

---

<sup>1</sup> This form of the buckling coefficient first appeared in the SP-8007 1965 and is likely derived from results provided in Ref. 91.

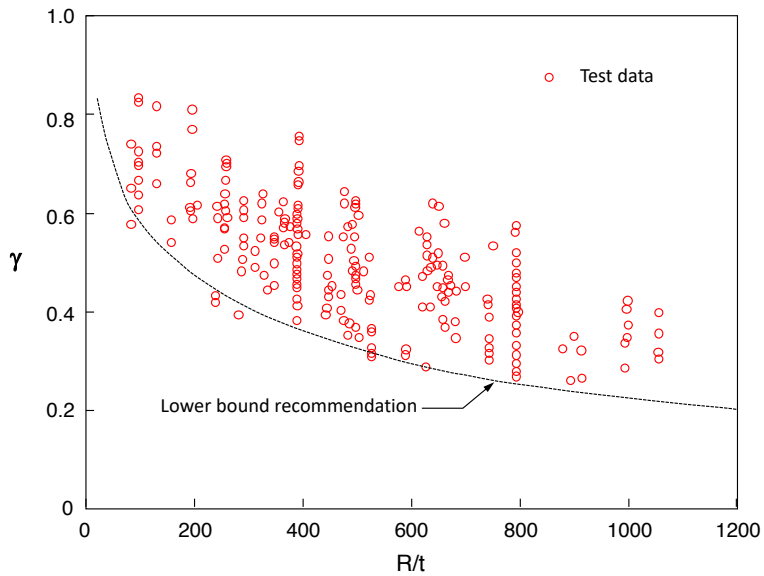


Figure 4.1 Lower bound design recommendation for thin-walled isotropic cylinders subjected to axial compression.

Notes:

- 1) Donnell's buckling load predictions given by Eq. 1 cannot predict column buckling or the interaction between shell buckling (i.e., general instability) and column buckling [Ref. 92]. In particular, the buckling load given by Eq. 1 becomes unconservative for large L/R ratios. If designing thin-walled cylindrical struts or long tanks without intermediate ring frames, the column buckling failure mode and shell buckling-column buckling interaction should be checked. Sanders' nonlinear shell theory is better suited for the prediction of the theoretical buckling loads for long cylinders.
- 2) The knockdown factor given by Eq. 5 should be used with caution for cylinders with length-to-radius ratios greater than 5 since correlation has not been verified by experiment in this range.
- 3) It is generally accepted that the knockdown factor equation given by Eq. 9 is very conservative in the design of aerospace quality cylinders. Specifically, more recent testing has produced buckling loads that are significantly higher than the lower bound design curve given by Eq. 9. These higher loads are most likely a result of greater quality control associated with the fabrication and testing of these structures and thus minimizing the effects of initial geometric imperfections and loading nonuniformities. Alternate methods for defining less conservative knockdown factors are presented in Sections 4.6 and 4.7.

When geometry and material properties are such that the computed buckling stresses are in the plastic range, the value of the Young's modulus  $E$  in Eqs. 3, 7, and 8 should be replaced by the value  $\eta E$  where

$$\eta = \frac{\sqrt{E_{sec}E_{tan}}}{E} \quad (11)$$

where  $E_{sec}$  and  $E_{tan}$  are the secant and tangent modulus of the material. Equation 11 is an approximation of the plasticity factors given in Refs. 91 and 93 and applies to moderately long cylinders. For extremely short cylinders, the appropriate plasticity factor as given in Ref 94, is given by:

$$\eta = \frac{E_{tan}}{E} \quad (12)$$

For cylinders with a length between those for which Eqs. 11 and 12 apply, it is assumed that linear interpolation between Eqs. 11 and 12 would provide satisfactory results.

#### 4.2.2 Bending

Buckling and collapse coincide for isotropic cylinders subjected to bending. It has been shown [Ref. 95] that the predicted maximum buckling axial stress due to pure bending for a finite length simply supported cylinder was approximately equal to that for uniform axial compression. Thus, the procedures given for compression-loaded isotropic cylinders may be used to obtain the critical maximum stress for isotropic cylinders in bending except that a correlation factor specific for the bending load condition should be used. The critical bending moment can be approximated by the following

$$M = \pi R^2 N_x = k_x \frac{\pi^3 D R^2}{L^2} \quad (13)$$

The knockdown factor for cylinders in bending is taken on the basis of Ref. 96 as

$$\gamma = 1 - 0.731(1 - e^{-\phi}) \quad (14)$$

where

$$\phi = \frac{1}{16} \sqrt{\frac{R}{t}} \quad (\text{for } \frac{R}{t} < 1500) \quad (15)$$

This equation should be used with caution for  $R/t > 1500$  because experimental data are not available in this range. Although the theoretical critical stress is assumed to be the same for axial compression and bending, the correlation factor for bending is greater than that for compression due to the reduced imperfection sensitivity exhibited by cylinders in bending. For sufficiently long shells, it has been shown that an interaction between the bifurcation buckling mode and the Braizer effect (cross-section ovalization) can occur, leading to lower buckling loads. [Ref 97] Thus, Braizer buckling should be checked.

### 4.2.3 External Pressure

The term *lateral pressure* corresponds to an external pressure which acts only on the curved walls of the cylinders and not on the ends (e.g., bulkheads). The circumferential stress in the cylinder wall is given by

$$N_y = \sigma_y t = pR \quad (16)$$

The term *hydrostatic pressure* corresponds to an external pressure which acts on both the curved walls and the ends of the cylinder. In this case, the circumferential and axial stresses in the shell wall are given by

$$N_y = \sigma_y t = pR \quad (17a)$$

$$N_x = \sigma_x t = \frac{pR}{2} \quad (17b)$$

Except for sufficiently short cylinders, the critical pressures for the two different types of loads are not significantly different ( $\gamma Z > 100$ ). An approximate equation for the buckling of cylinders subjected to lateral pressure is given in Ref. 90 as

$$N_y = k_y \frac{\pi^2 D}{L^2} \quad (18)$$

where

$$k_y = \frac{pRL^2}{\pi^2 D} = \frac{1}{\beta^2} \left[ (1 + \beta^2)^2 + \frac{12}{\pi^4} \frac{\gamma^2 Z^2}{(1 + \beta^2)^2} \right] \quad (19)$$

The equation for buckling of cylinders subjected to hydrostatic pressure is obtained by replacing the  $k_y$  in Eq. 18 by  $k_p$  and the factor  $\beta^2$  before the bracketed expression in Eq 19 is replaced by  $(\beta^2 + 1/2)$ . That is

$$N_y = k_p \frac{\pi^2 D}{L^2} \quad (20)$$

where

$$k_p = \frac{pRL^2}{\pi^2 D} = \frac{1}{(\beta^2 + 1/2)} \left[ (1 + \beta^2)^2 + \frac{12}{\pi^4} \frac{\gamma^2 Z^2}{(1 + \beta^2)^2} \right] \quad (21)$$

The term  $\gamma^2$  has been added to Eqs. 19 and 21 as a correction for the difference between theory and test.

The minimum values of  $k_y$  for lateral pressure and  $k_p$  for hydrostatic pressure are obtained by allowing the buckle aspect ratio  $\beta$  to vary continuously. For  $\gamma Z > 100$ ,  $k_y$  and  $k_p$  is given by the Equation (from Ref. 90):

$$k_y = k_p = 1.04 \sqrt{\gamma Z} \quad (22)$$

The critical pressure is given by

$$p_{cr} = \frac{0.855}{(1 - \nu^2)^{\frac{3}{4}}} \frac{E\sqrt{\gamma}}{\left(\frac{R}{t}\right)^{\frac{5}{2}} \left(\frac{L}{R}\right)} \quad (23)$$

For  $\nu = 0.3$ , Eq 23, simplifies to

$$p_{cr} = 0.926 \frac{E\sqrt{\gamma}}{\left(\frac{R}{t}\right)^{\frac{5}{2}} \left(\frac{L}{R}\right)} \quad (24)$$

The family of curves at high values of  $\gamma Z$  ( $\gamma Z > 4000$ ) in Fig. 4.2, which are dependent on the radius-thickness ratio of the cylinder, and which correspond to buckling of the cylinder into an oval shape ( $n = 2$ ), are derived from Ref. 98 pg. 478 as

$$k_y = k_p = \frac{3}{\pi^2} \frac{\gamma Z}{\frac{R}{t} \sqrt{1 - \nu^2}} \quad (25)$$

$$p_{cr} = \frac{\gamma E}{4(1 - \nu^2)} \left(\frac{t}{R}\right)^3 \quad (26)$$

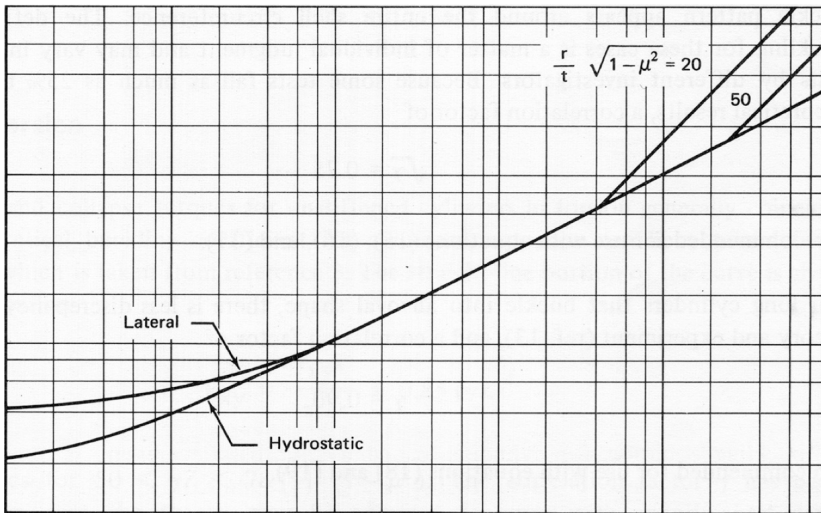
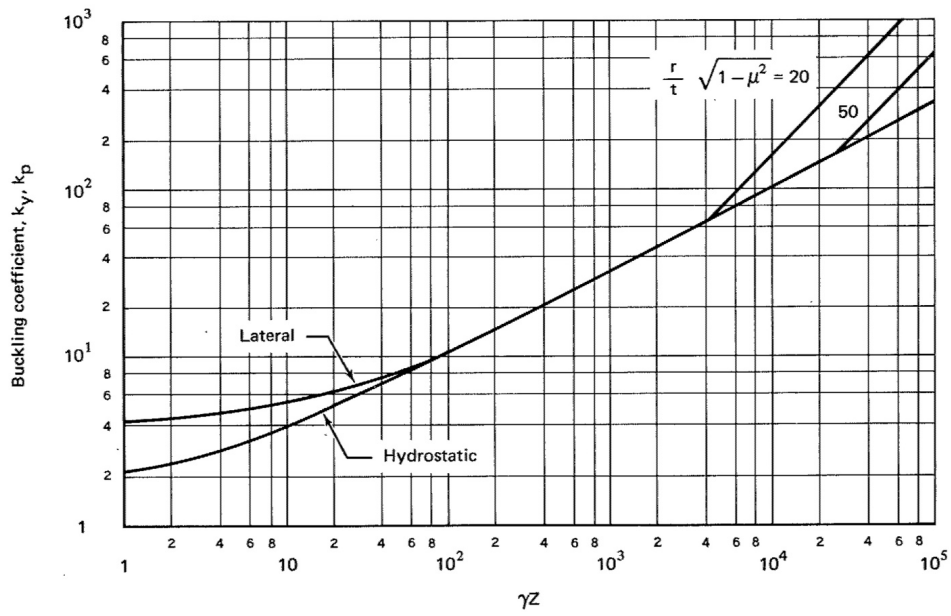


Figure 4.2 Buckling coefficients for simply supported isotropic circular cylinders subjected to external pressure.

By assuming a value of  $\gamma$  equal to 1.0, one obtains the theoretical buckling equation given in Ref. 91. However, on the basis of various experimental data, it is recommended that a knockdown factor  $\gamma$  less than 1.0 be used to account for difference between the predicted buckling load and the actual buckling load determined from tests.

It has been shown analytically (e.g., Refs. 87, 99, 100) that restraint of the cylinder ends against longitudinal movement can increase the theoretical buckling pressure by as much as 50%. Rotational constraints on the edges only affected the buckling load of relatively short cylinders. These results indicate that the effects of the boundary conditions should be assessed carefully.

Experimental data for cylinders which buckle with more than two circumferential waves  $[\gamma Z < 11.8 \left(\frac{R}{t}\right)^2 (1 - \nu^2)]$  show considerable scatter about the theoretical values given by Eq. 14 (see Ref. 101). There are several sources to the observed scatter. The end restraint of the test specimens were not always considered in detail in the analysis of the test data. Lower buckling loads may also be reported in the test data when isolated buckles appear in cylinders with large  $R/t$  or small  $L/R$  before pressure is reached at which a global buckle pattern appears around the entire circumference. The definition of the buckling for these cases is a matter of individual judgement and may vary in different tests by different investigators. For cylinders subjected to hydrostatic pressure, the induced axial compression load and imperfection sensitivity characteristics may also have a significant influence on the buckling response. Later work by Yamaki [Ref.20] indicated significantly better correlation between test and analysis due to improved testing methods and specimen fabrication. However, because some of the test loads from previous testing are as much as 25% below the theoretical results, a conservative correlation factor of

$$\sqrt{\gamma} = 0.75 \quad (27)$$

is recommended for use with Eqs. 22-24.

For long cylinders that buckle into an oval shape, there is less of a discrepancy between theory and experiment (Ref. 102), and a correlation factor of

$$\gamma = 0.90 \quad (28)$$

is recommended for use with Eqs. 25 and 26.

For relatively short cylinders under lateral pressure ( $\gamma Z < 5$ ) the plasticity factor for long, simply supported plates in axial compression may be used. It is obtained from Ref. 94 as

$$\eta = \frac{E_{sec}}{E} \left( \frac{1}{2} + \frac{1}{2} \sqrt{\frac{1}{4} + \frac{3 E_{tan}}{4 E_{sec}}} \right) \quad (29)$$

For  $100 < \gamma Z < 11.8 \left(\frac{R}{t}\right)^2 (1 - \nu^2)$ , the approximate plasticity factor is obtained from Eq 12 of Ref. 102 as

$$\eta = \frac{E_{sec}}{E} \sqrt{\left(\frac{E_{tan}}{E_{sec}}\right)^{\frac{1}{2}} \left(\frac{1}{4} + \frac{3 E_{tan}}{4 E_{sec}}\right)} \quad (30)$$

And for  $\gamma Z > 11.8 \left(\frac{R}{t}\right)^2 (1 - \nu^2)$  the approximate plasticity factor is obtained from equation (59) of Ref. 91 as

$$\eta = \frac{E_{sec}}{E} \left( \frac{1}{4} + \frac{3 E_{tan}}{4 E_{sec}} \right) \quad (31)$$

No plasticity factor is available for the range  $5 < \gamma Z < 100$ ; satisfactory results may, however, be achieved by linear interpolation with the parameter  $Z$  between the values of  $\eta$  given by Eqs. 29 and 30.

Plasticity factors for the biaxial stress state of hydrostatic pressure are unavailable. For lack of better information, the plasticity factors given by Eqs. 29 and 31 may be used.

#### 4.2.4 Torsion

Buckling and collapse of unstiffened cylinders subjected to torsion generally coincide. The theoretical buckling coefficient for cylinders in torsion  $k_{xy}$  can be obtained from Fig. 4.3, which is taken from Ref. 90. For very short cylinders the value of the critical shear-stress coefficient approaches the value of a flat plate in shear equal to 5.34 when the edges are simply supported. The straight-line portion of the curve is given by

$$k_{xy} = \frac{N_{xy} L^2}{\pi^2 D} = 0.85 (\gamma Z)^{\frac{3}{4}} \quad (32)$$

and applies for  $50 < \gamma Z < 78 \left(\frac{R}{t}\right)^2 (1 - \nu^2)$ .

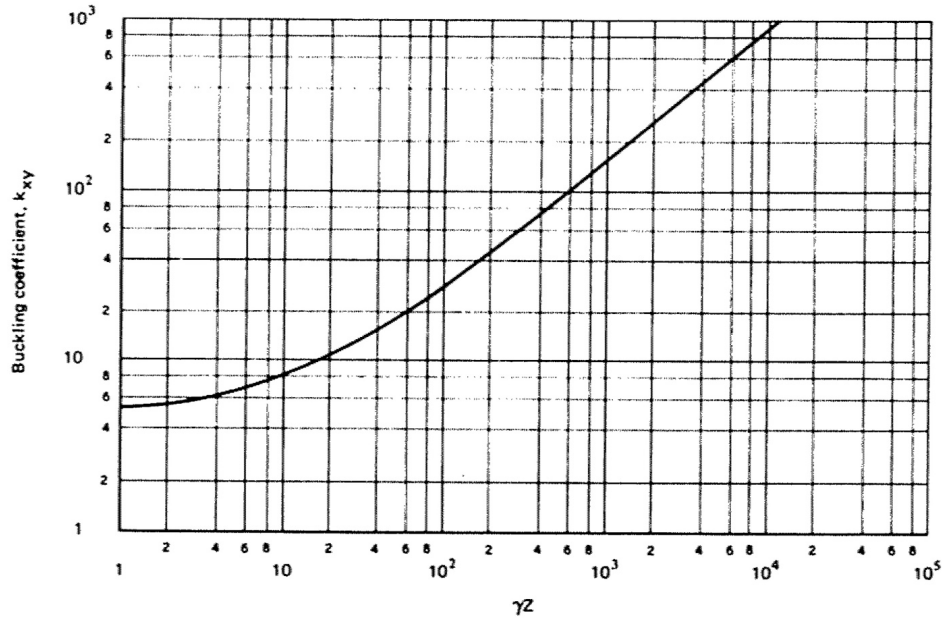


Figure 4.3 Buckling coefficients for simply supported isotropic circular cylinders subjected to torsion.

$N_{xy}$  is the applied torsion load per unit length around the circumference of the cylinder. The correlation factor  $\gamma$  has been included to account for the differences between theory and test. Eq. 25 can be expressed as torsion stress  $\tau_{xy}$

$$\tau_{xy} = \frac{N_{xy}}{t} = \frac{0.747\gamma^{\frac{3}{4}}E}{\left(\frac{R}{t}\right)^{\frac{5}{2}}\left(\frac{L}{R}\right)^{\frac{1}{2}}} \quad (33)$$

To approximate the lower bound to most buckling data provided in Ref. 90, the value

$$\gamma^{\frac{3}{4}} = 0.67 \quad (34)$$

is recommended for moderately long cylinders.

For very long cylinders,  $\gamma Z > 78\left(\frac{R}{t}\right)^2(1 - \nu^2)$ , the cylinder buckles into a mode shape with two circumferential waves ( $n = 2$ ). The critical buckling stress given by equation 11-27 in Ref. 98 is

$$\tau_{xy} = \frac{\gamma E}{3\sqrt{2} (1 - \nu^2)^{\frac{3}{4}}} \left(\frac{t}{R}\right)^{\frac{3}{2}} \quad (35)$$

and corresponds to a buckling coefficient

$$k_{xy} = \frac{2\sqrt{2} \gamma Z}{\pi^2 \left(\frac{R}{t}\right)^{\frac{1}{2}} (1 - \nu^2)^{\frac{1}{4}}} \quad (36)$$

where  $\gamma = 0.80$  is recommended for very long cylinders.

Plasticity may be taken into account by applying the plasticity factor from Ref. 102 in the above equations

$$\eta = \frac{E_{sec}}{E} \quad (37)$$

The quantity  $E_{sec}$  is obtained from a uniaxial stress-strain curve at a normal stress equal to twice the critical shear stress. Eq. 37 applies to cylinders of all lengths.

#### 4.2.5 Combined Loads

Typical load combinations encountered in practice are treated here. Generally, the recommended practice to account for combinations of two or more loading conditions that may cause buckling is to assume that the sum of the various critical load ratios is equal to unity. However, for some load cases, it has been shown theoretically and experimentally that this assumption can be somewhat conservative (e.g., combined compression and torsion and combined bending and torsion) [Refs. 20 and 91]. Alternate approaches used to account for the effects of combined loads can yield more accurate and less conservative buckling load estimates, however, it is advised that these alternate approaches be substantiated by test or validated buckling load predictions.

##### 4.2.5.1 Combined Axial Compression and Bending

The recommended interaction equation for combined axial compression and bending is

$$R_c + R_b = 1 \quad (38)$$

where the quantities  $R_c$  and  $R_b$  are the compressive and bending load or stress ratios given by

$$R_c = \frac{P}{P_{cr}} \quad (39)$$

and

$$R_b = \frac{M}{M_{cr}} \quad (40)$$

$P$  and  $M$  are the applied compressive load and applied bending load, respectively.  $P_{cr}$  and  $M_{cr}$  are the allowable loads or stresses derived from Eq. 1 for axial compression and Eq. 13 for cylinders in bending, respectively.

#### 4.2.5.2 Combined Axial Compression and External Pressure

The recommended interaction equation for combined axial compression and bending is

$$R_c + R_p = 1 \quad (41)$$

The quantities  $R_c$  and  $R_p$  are the compressive and hydrostatic- or lateral-pressure load or stress ratios.

$$R_p = \frac{p}{p_{cr}} \quad (42)$$

$p$  is the applied pressure load and  $p_{cr}$  is the allowable load given in Section 4.2.3 for cylinders subjected to external pressure.

#### 4.2.5.3 Combined Axial Compression and Torsion

For cylindrical shells subjected to combined axial compression and torsion, the analytical interaction curve is a function of  $Z$ . The experimental test data suggests the use of a straight-line interaction equation

$$R_c + R_t = 1 \quad (43)$$

The quantities  $R_c$  and  $R_t$  are the compressive and torsion load or stress ratios, respectively.

$$R_t = \frac{\tau}{\tau_{cr}} \quad (44)$$

$\tau$  is the applied torque load and  $\tau_{cr}$  is the allowable load or stress given in Section 4.2.4 for cylinders subjected to torsion.

#### 4.2.5.4 Combined Axial Compression and Internal Pressure

Buckling and collapse typically coincide for cylinders subjected to combined internal pressure and axial compression. The internal pressure increases the buckling load of the cylinder in the following ways:

1. The total axial compressive load must be greater than the tensile pressurization load in the shell wall  $p\pi R^2$  before buckling can occur.
2. The destabilizing effect of initial imperfections is reduced.
3. The circumferential tensile stress induced by the pressurization inhibits the formation of the classical diamond-shaped buckling pattern, and, at sufficiently high pressures, the cylinder buckles into the classical axisymmetric mode at approximately the classical buckling stress.

Lower bound curves giving the increase in buckling load as a function of internal pressure, based on the results for Mylar cylinders, are given in Ref. 103 for various radius-to-thickness ratios. Because these curves are unsubstantiated at present for other materials, the more conservative values given in Ref. 104 are recommended for design use. It is therefore recommended that the total load for buckling, unless substantiated by test, be obtained by the addition of the pressurization load  $p\pi R^2$ , the buckling load for the unpressurized cylinder [Eqs. (4) and (5)], and an increase in the buckling load cause by the pressurization; that is

$$P_{press} = 2\pi E t^2 \left( \frac{\gamma}{\sqrt{3(1-\nu^2)}} + \Delta\gamma \right) + p\pi R^2 \quad (45)$$

where  $\Delta\gamma$  is obtained from Fig. 4.4. For  $\nu = 0.3$ , Eq. (45) simplifies to

$$P_{press} = 2\pi Et^2 (0.6\gamma + \Delta\gamma) + p\pi R^2 \quad (46)$$

The  $\Delta\gamma$  curve provided in Fig. 4.4 should only be used with the equations presented here. Application of data from Fig. 4.4 to other untested cylinder configurations or use with other less conservative knockdown factors could result in unconservative designs.

#### 4.2.5.5 Combined Bending and Internal Pressure

For cylinders subjected to combined internal pressure and bending, collapse loads are considerably higher than buckling loads (Refs. 105 -107), with the increase being substantially more than the tension stress induced by the pressurization. For example, for the true membrane cylinder, i.e., a cylinder with very thin walls  $R/t = 6000$  (Ref. 108), the collapse load ( $M = p\pi R^3$ ) is twice the initial buckling load. The theoretical collapse load is, however, unattainable unless large undesirable deformations are present. It is therefore recommended that the collapse moment for pressurized cylinders be obtained by adding the moment-carrying capability of a pressurized membrane cylinder (taken for design purposes as 80% of the theoretical value), the collapse moment for the unpressurized cylinder [Eqs. (4) and (9)], and an increase in the critical moment caused by pressurization. Then

$$M_{press} = \pi REt^2 \left( \frac{\gamma}{\sqrt{3(1-\nu^2)}} + \Delta\gamma \right) + 0.8 p\pi R^3 \quad (47)$$

where  $\Delta\gamma$  is obtained from Fig. 4.4. For  $\nu = 0.3$ , Eq. 47 simplifies to

$$M_{press} = \pi R E t^2 (0.6\gamma + \Delta\gamma) + 0.8 p \pi R^3 \quad (48)$$

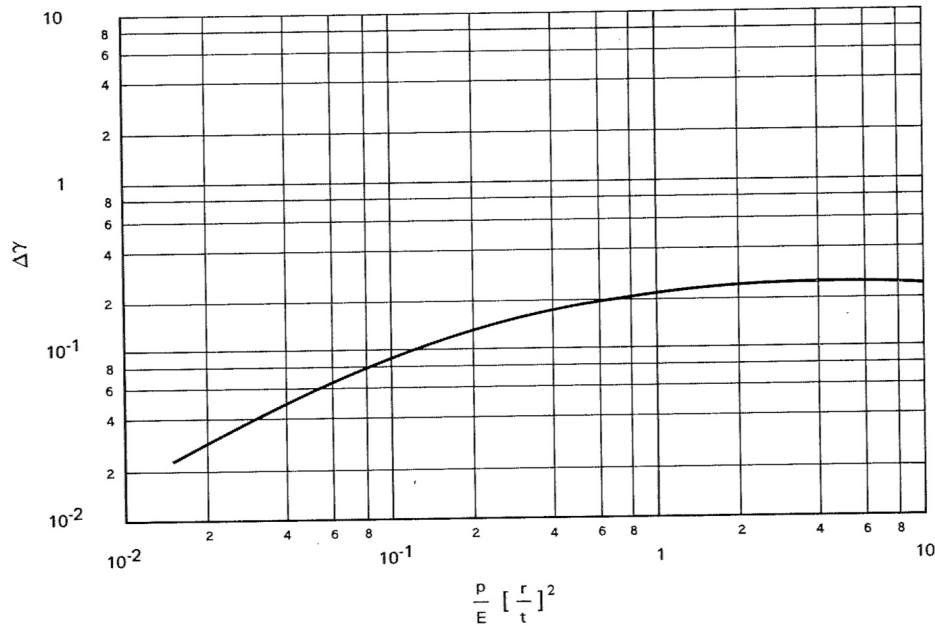


Figure 4.4 Increase in axial buckling knockdown factor (correlation coefficient) for cylinders due to internal pressure.

#### 4.2.5.6 Combined Axial Compression, Bending, and Internal Pressure

For internally pressurized cylinders subjected to combined axial compression and bending, Eq. (30) is recommended for use in combination with Eqs. (33) or (34) and (35) or (36)

### 4.3 Orthotropic Cylinders

The term *orthotropic cylinders* covers a wide variety of cylinder configurations. In the strictest sense, it denotes cylinders made of a single orthotropic material or of multiple orthotropic layers. It also denotes stiffened cylinders for which the stiffener geometry and spacing is such that the cylinder can be approximated by a fictitious layer whose orthotropic bending and extensional properties include those of the individual stiffening element averaged or *smear*d out over representative widths or areas. Generally the directions of the axes of orthotropy are taken to coincide with the longitudinal and circumferential directions of the cylinder.

The buckling behavior of various types of orthotropic cylinders may be described by a single theory, the elements of which are equations of equilibrium for the buckled structure, and stress-strain relations. For cylinders of a single orthotropic layer, it is generally permissible to neglect coupling between membrane stresses and bending strains, and between moment resultants and extensional strains. The theory is then

similar to that for isotropic cylinders. For stiffened cylinders or for cylinders having multiple orthotropic layers, however, the neglect of coupling terms can lead to significant errors.

For example, cylinders that have stiffeners on the inner surface or on the outer surface will exhibit bending-extension coupling due to the eccentricity of the stiffeners relative to the mid-surface of the cylinder wall. In addition, the character of the coupling will be different depending on the orientation of the stiffeners and if the stiffeners are on the inside or the outside, and can have a significant influence on the buckling response of the cylinder. [Refs. 109 - 113] In particular, the eccentricity effect is very pronounced for axially-stiffened cylinders in compression. Similarly, laminated composite cylinders can exhibit various types of elastic coupling even if the laminate is balanced and symmetric. [Ref. 114].

In stiffened cylinders, other failure modes should also be investigated including local skin buckling between stiffeners, as well as stiffener buckling and stiffener crippling. In addition, the adequacy of the smeared stiffener theory should be investigated if the spacing of the stiffeners becomes sufficiently large, or if geometrically nonlinear prebuckling deformations are anticipated. (Ref. 25 Sections 13.1.3-13.1.6)

#### 4.3.1 Axial Compression

An equation for the buckling of orthotropic cylinders in compression (Ref. 115) is given by:

$$N_x = \left(\frac{L}{m\pi}\right)^2 \frac{\begin{vmatrix} A_{11} & A_{12} & A_{13} \\ A_{21} & A_{22} & A_{23} \\ A_{31} & A_{32} & A_{33} \end{vmatrix}}{\begin{vmatrix} A_{11} & A_{12} \\ A_{21} & A_{22} \end{vmatrix}} \text{ for } n \geq 4 \quad (49)$$

or

$$N_x \left(\frac{m\pi}{L}\right)^2 = A_{33} + A_{23} \left(\frac{A_{13}A_{12} - A_{11}A_{23}}{A_{11}A_{22} - A_{12}^2}\right) + A_{13} \left(\frac{A_{12}A_{23} - A_{13}A_{22}}{A_{11}A_{22} - A_{12}^2}\right) \quad (50)$$

where

$$A_{11} = \bar{E}_x \left(\frac{m\pi}{L}\right)^2 + \bar{G}_{xy} \left(\frac{n}{R}\right)^2 \quad (51)$$

$$A_{22} = \bar{E}_y \left(\frac{n}{R}\right)^2 + \bar{G}_{xy} \left(\frac{m\pi}{L}\right)^2 \quad (52)$$

$$A_{33} = \bar{D}_x \left( \frac{m\pi}{L} \right)^4 + \bar{D}_{xy} \left( \frac{m\pi}{L} \right)^2 \left( \frac{n}{R} \right)^2 + \bar{D}_y \left( \frac{n}{R} \right)^4 + \frac{\bar{E}_y}{R^2} + \frac{2\bar{C}_y}{R} \left( \frac{n}{R} \right)^2 + \frac{2\bar{C}_{xy}}{R} \left( \frac{m\pi}{L} \right)^2 \quad (53)$$

$$A_{12} = A_{21} = (\bar{E}_{xy} + \bar{G}_{xy}) \frac{m\pi}{L} \frac{n}{R} \quad (54)$$

$$A_{23} = A_{32} = (\bar{C}_{xy} + 2\bar{K}_{xy}) \left( \frac{m\pi}{L} \right)^2 \frac{n}{R} + \frac{\bar{E}_y}{R} \frac{n}{R} + \bar{C}_y \left( \frac{n}{R} \right)^3 \quad (55)$$

$$A_{31} = A_{13} = \frac{\bar{E}_{xy}}{R} \frac{m\pi}{L} + \bar{C}_x \left( \frac{m\pi}{L} \right)^3 + (\bar{C}_{xy} + 2\bar{K}_{xy}) \frac{m\pi}{L} \left( \frac{n}{R} \right)^2 \quad (56)$$

Values of the stiffnesses  $\bar{E}_x$ ,  $\bar{E}_{xy}$ ,  $\bar{E}_y$ ,  $\bar{G}_{xy}$ ,  $\bar{D}_x$ ,  $\bar{D}_{xy}$ ,  $\bar{D}_y$ ,  $\bar{C}_x$ ,  $\bar{C}_{xy}$ ,  $\bar{C}_y$ , and  $\bar{K}_{xy}$ , for various types of construction are given in Section 4.3.6. Prebuckling deformations are not taken into account in the derivation of the equation. The cylinder edges are assumed to be simply supported, that is the displacements  $w = 0$  and the rotations about the tangent  $r_\nu = \text{free}$ . These conditions are assumed to be representative of rings that are rigid in their own plane but offer no resistance to rotation or bending out of their plane. For ring-stiffened corrugated cylinders, a similar but not identical theory is given in Refs. 66 and 116. For given cylinder and stiffener dimensions, the values of  $m$  and  $n$  (the number of axial halfwaves and circumferential full-waves, respectively) to be used are those which minimize the buckling load  $N_x$ .

The large number of parameters in Eq. (37) does not permit a complete treatment of results to be shown. However, some generalizations can be made and references provided. For combinations of parameters representative of stiffened shells, calculations indicate that external stiffening, whether rings or stringers or both, can be more effective than internally stiffened cylinders for axial compression. Generally, calculations neglecting stiffener eccentricity yield unconservative values of the buckling load of internally stiffened cylinders and conservative values of the buckling load for externally stiffened cylinders [Ref. 117]. In addition, boundary conditions and loading can have a significant effect on these trends [Ref. 118]. An extensive investigation of the variation of the buckling load with various stiffener parameters is reported in Refs. 78 and 109. In general, the experimental data [Refs. 66 to 73 and 118-123], for cylinders with closely spaced, moderately large stiffeners are in reasonably good agreement with the theoretical results for the range of parameters investigated.

However, some experimental buckling loads have been shown to be as low as 65% of the predicted classical buckling load. Thus, it is recommended that the buckling loads for a uniform cylinder with closely spaced, moderately large stiffeners calculated from Eq. 37 be multiplied by a factor of 0.65.<sup>2</sup>

---

<sup>2</sup> Note: NASA SP-8007, 1968 [Ref. 1] suggested a knockdown factor equal to 0.75, however, for conservatism a knockdown factor of 0.65 is recommended based on the results presented in Ref 5. Less conservative analysis-based factors can be derived based on an approach outlined in Sec 4.7

[Refs. 5 and 6] Correlation coefficients covering the transition from unstiffened cylinders to cylinders with closely spaced stiffeners have not been fully investigated and may require investigation via detailed analysis and/or experimental testing. While theory and experiment [Ref. 72] indicate that restraint against edge rotation and longitudinal movement can significantly increase the buckling load, not enough is known about the edge restraint of actual cylinders to warrant taking advantage of these effects unless substantiated by tests.

For layered or unstiffened orthotropic cylinders, the available test data has increased substantially since the previous version of the SP-8007 was written and the results indicate higher buckling loads as compared to older isotropic data and the lower bound design curve of Eq. 5. Filament-wound cylinders [Refs. 124-127], laminated composite cylinders [Refs. 10-11, 128-133], and stiffened composite cylinder [Ref. 134] However, due to the tremendous number of possible design variables and structural configurations, no new empirical guidelines have been developed based on this data. Thus, the correlation factor  $\gamma$  is taken to be of the same form as for the isotropic cylinders [Eq. 5] with the thickness  $t$  replaced by the geometric mean of the radii of gyration for the axial and circumferential directions. Thus

$$\gamma = 1 - 0.901(1 - e^{-\phi}) \quad (57)$$

where

$$\phi = \frac{1}{29.8} \left[ \frac{R}{\sqrt[4]{\frac{\bar{D}_x \bar{D}_y}{\bar{E}_x \bar{E}_y}}} \right]^{\frac{1}{2}} \quad (58)$$

As discussed in Section 4.2, more recent testing has produced buckling loads that are significantly higher than the lower bound design curve given by Eq. 5. It is not uncommon to obtain experimental buckling loads for uniform cylinders of 70-90% of the theoretical predictions. These higher loads are most likely a result of greater quality control associated with the fabrication and testing of these structures and thus minimizing the effects of initial geometric imperfections and loading nonuniformities. However, given the severe imperfection sensitivity of compression-loaded thin-walled cylinders, the design factors provided herein should be used unless alternate values can be justified. Alternate methods, including semi-empirical and high-fidelity analysis-based methods, for determining less conservative knockdown factors are presented in Sections 4.6 and 4.7.

### 4.3.2 Bending

Theoretical and experimental results for stiffened cylinders in bending can be found in (Refs. 74-76, 116, 136-139) The results indicate that the critical maximum load per unit circumference of a stiffened cylinder in bending can exceed the critical unit load in axial compression. However, in the absence of an extensive investigation, it is recommended that the critical maximum load per unit circumference of a uniform cylinder with closely spaced stiffeners be taken as equal to the critical load in axial compression, which is calculated from Eq. (37) multiplied by a factor  $\gamma = 0.72$ , which is slight greater than the factor for compression loaded cylinders due to the reduced imperfection sensitivity. In addition, as with compression-loaded stiffened cylinders, local skin buckling can also occur prior to global buckling as in the case of widely spaced stiffeners and should be checked.

For layered or unstiffened orthotropic cylinders, it is recommended that the correlation factor

$$\gamma = 1 - 0.731(1 - e^{-\phi}) \quad (59)$$

be used where

$$\phi = \frac{1}{29.8} \left[ \frac{R}{\sqrt[4]{\frac{\bar{D}_x \bar{D}_y}{\bar{E}_x \bar{E}_y}}} \right]^{\frac{1}{2}} \quad (60)$$

### 4.3.3 External Pressure

The counterpart of Eq. 37 for orthotropic cylinders under lateral pressure is given by

$$p = \frac{R}{n^2} \frac{\begin{vmatrix} A_{11} & A_{12} & A_{13} \\ A_{21} & A_{22} & A_{23} \\ A_{31} & A_{32} & A_{33} \end{vmatrix}}{\begin{vmatrix} A_{11} & A_{12} \\ A_{21} & A_{22} \end{vmatrix}} \quad (61)$$

For hydrostatic pressure, the quantity  $n^2$  in Eq. 61 is replaced by

$$n^2 + \frac{1}{2} \left( \frac{m\pi R}{L} \right)^2 \quad (62)$$

In the case of lateral pressure,  $m$  is equal to unity while  $n$  must be varied to yield a minimum value of the critical pressure, but not less than 2. In the case of hydrostatic pressure, the value of  $m$  should be varied along with  $n$ . For long cylinders, Eq. 61 is replaced by

$$p = \frac{3 \left( \bar{D}_y - \frac{\bar{C}_y^2}{\bar{E}_y} \right)}{R^3} \quad (63)$$

If the coupling coefficients can be neglected (i.e., are equal to or close to zero valued), the critical buckling pressure can be approximated by:

$$p \approx \frac{5.513}{LR^{\frac{3}{2}}} \left[ \frac{\bar{D}_y^3 (\bar{E}_x \bar{E}_y - \bar{E}_{xy}^2)}{\bar{E}_y} \right]^{\frac{1}{4}} \quad (64)$$

for the case of

$$\left(\frac{\bar{D}_y}{\bar{D}_x}\right)^{\frac{3}{2}} \left(\frac{\bar{E}_x \bar{E}_y - \bar{E}_{xy}^2}{12 \bar{E}_y \bar{D}_x}\right)^{\frac{1}{2}} \frac{L^2}{R} > 500 \quad (65)$$

Equation (61) has been investigated primarily for isotropic cylinders with ring stiffeners (Refs. 140 to 142). For closely spaced ring stiffening, Refs. 140 and 141 show that the effectiveness of inside or outside rings depends on the cylinder and ring geometries. Generally, for cylinders with values of  $Z$  less than 100, outside rings are more effective, while for value of  $Z$  greater than 500, the reverse is true. As the ring geometry varies, the effectiveness of the outside stiffening tends to increase as the stiffness of the rings relative to the cylinder increases. Somewhat lower buckling pressures are given by the more complex but more accurate theory of Ref. 143; however, the differences are not so significant as to warrant its use.

The experimental results for ring-stiffened cylinders described in Refs. 144-147 are in reasonably good agreement with the theoretical results of Eq. (49). For cylinders of all types, it is recommended that the buckling pressure calculated from Eq. 49 be multiplied by a factor of 0.75, as has been recommended for unstiffened isotropic cylinders of moderate length.

#### 4.3.4 Torsion

Buckling of orthotropic cylinders in torsion has been treated in Refs. 61, 148, and 149. If coupling effects are negligible, the critical torsion load for moderately long cylinders can be estimated based on the equations provided in Ref. 61. A more convenient form for the critical buckling torque can be derived for Ref. 61 and give by

$$T_{cr} \approx 21.75 \bar{D}_y^{\frac{5}{8}} \left(\frac{\bar{E}_x \bar{E}_y - \bar{E}_{xy}^2}{\bar{E}_y}\right)^{\frac{3}{8}} \frac{R^{\frac{5}{4}}}{L^{\frac{1}{2}}} \quad (66)$$

for the case of

$$\left(\frac{\bar{D}_y}{\bar{D}_x}\right)^{\frac{5}{6}} \left(\frac{\bar{E}_x \bar{E}_y - \bar{E}_{xy}^2}{12 \bar{E}_y \bar{D}_x}\right)^{\frac{1}{2}} \frac{L^2}{R} \gtrsim 500 \quad (67)$$

Reference 149, however, indicates that coupling effects can be quite important for cylinders stiffened with closely space rings. For long cylinders, internal rings are generally more effective than outside rings; for short cylinders, the reverse is true. In the absence of general formulas or graphs for the range of practical parameters, the equations in Ref. 147 should be solved for each specific case considered.

The limited test data of Ref. 150 for relatively short stiffeners, are in good agreement with theoretical predictions but are insufficient to provide an adequate test of the theory for more practical designs. It is therefore recommended that theoretical critical torsion load  $T_{cr}$  be multiplied by a factor of 0.67 for moderately long cylinders.

### 4.3.5 Combined Loads

On the basis of theory [Refs. 116, 135, and 139] and limited test data [Refs. 66 and 116], interaction equations found in Section 4.2.5 for isotropic cylinders are recommended.

However, as discussed in Section 4.2.5, it has been shown theoretically and experimentally that this assumption can be somewhat conservative (e.g., combined compression and torsion and combined bending and torsion) [Refs. 20, 91]. Alternate approaches used to account for the effects of combined loads can yield more accurate and less conservative buckling load estimates, however, it is advised that these alternate approaches be substantiated by test or validated buckling load predictions.

### 4.3.6 Elastic Constants

Equations for the elastic constants for commonly used cylinder wall constructions are provided in this section, including:

- Stiffened Multilayered Orthotropic Cylinders
- Isotropic Cylinders with Rings and Stringers
- Isotropic Isogrid-Stiffened Cylinders
- Ring-Stiffened Corrugated Cylinders

Equations for determining elastic constants for other stiffener patterns and structural configurations are presented in Nemeth, including Hexagonal stiffener pattern, Kagome stiffener pattern, and sandwich plates with nonidentical anisotropic facesheets. [Ref. 151]

#### 4.3.6.1 Stiffened Multilayered Orthotropic Cylinders

Commonly used expressions for the elastic constants for multilayered cylinders with isotropic rings and stringers are:

$$\bar{E}_x = \sum_{k=1}^N \left( \frac{E_x}{1 - \nu_x \nu_y} \right)_k t_k + \frac{E_s A_s}{b} \quad (68)$$

$$\bar{E}_y = \sum_{k=1}^N \left( \frac{E_y}{1 - \nu_x \nu_y} \right)_k t_k + \frac{E_r A_r}{d} \quad (69)$$

$$\bar{E}_{xy} = \sum_{k=1}^N \left( \frac{\nu_x E_y}{1 - \nu_x \nu_y} \right)_k t_k = \sum_{k=1}^N \left( \frac{\nu_y E_x}{1 - \nu_x \nu_y} \right)_k t_k \quad (70)$$

$$\bar{G}_{xy} = \sum_{k=1}^N (G_{xy})_k t_k \quad (71)$$

$$\bar{D}_x = \sum_{k=1}^N \left( \frac{E_x}{1 - \nu_x \nu_y} \right)_k \left( \frac{1}{12} t_k^3 + t_k \tilde{z}_k^2 \right) + \frac{E_s I_s}{b} + \tilde{z}_s^2 \frac{E_s A_s}{b} \quad (72)$$

$$\bar{D}_y = \sum_{k=1}^N \left( \frac{E_y}{1 - \nu_x \nu_y} \right)_k \left( \frac{1}{12} t_k^3 + t_k \tilde{z}_k^2 \right) + \frac{E_r I_r}{d} + \tilde{z}_r^2 \frac{E_r A_r}{d} \quad (73)$$

$$\bar{D}_{xy} = \sum_{k=1}^N \left( 4G_{xy} + \frac{\nu_x E_y}{1 - \nu_x \nu_y} + \frac{\nu_y E_x}{1 - \nu_x \nu_y} \right)_k \left( \frac{1}{12} t_k^3 + t_k \tilde{z}_k^2 \right) + \frac{G_s J_s}{b} + \frac{G_r J_r}{d} \quad (74)$$

$$\bar{C}_x = \sum_{k=1}^N \left( \frac{E_x}{1 - \nu_x \nu_y} \right)_k t_k \tilde{z}_k + \tilde{z}_s \frac{E_s A_s}{b} \quad (75)$$

$$\bar{C}_y = \sum_{k=1}^N \left( \frac{E_y}{1 - \nu_x \nu_y} \right)_k t_k \tilde{z}_k + \tilde{z}_r \frac{E_r A_r}{d} \quad (76)$$

$$\bar{C}_{xy} = \sum_{k=1}^N \left( \frac{\nu_y E_x}{1 - \nu_x \nu_y} \right)_k t_k \tilde{z}_k = \sum_{k=1}^N \left( \frac{\nu_x E_y}{1 - \nu_x \nu_y} \right)_k t_k \tilde{z}_k \quad (77)$$

$$\bar{K}_{xy} = \sum_{k=1}^N (G_{xy})_k t_k \tilde{z}_k \quad (78)$$

$E$ ,  $G$ ,  $\nu$ , denote the Young's modulus, shear modulus, and Poisson's ratio of the skin and stiffener materials. The subscripts  $x$  and  $y$  are associated with the skin properties and correspond to the axial and circumferential coordinates of the cylinder, and the subscripts  $s$  and  $r$  refer to the stringer and ring stiffeners. The subscript  $k$  refers to the  $k^{\text{th}}$  layer of an  $N$ -layer cylinder wall. The thickness of the  $k^{\text{th}}$  layer is denoted by  $t_k$  and the location of the layer midsurface relative to the wall reference surface is defined as  $\tilde{z}_k$ , and is positive valued for layers radially outside of the reference surface (see Fig. 4.5). The reference surface is typically taken to be associated with the mid-surface of the laminate, however, this is not a requirement. Individual stiffener area, and torsional moment of inertia are denoted by  $A$ ,  $I$ , and  $J$ . The moments of inertia of the axial and circumferential stiffeners are calculated relative to the reference-surface of the skin. Circumferential and axial stiffener spacing is denoted by  $b$  and  $d$ , respectively, and the corresponding stiffener eccentricities,  $\tilde{z}_r$ ,  $\tilde{z}_s$ , are defined as the distances between the shell-wall reference surface and the stiffener centroid, as shown in Fig. 4.6.

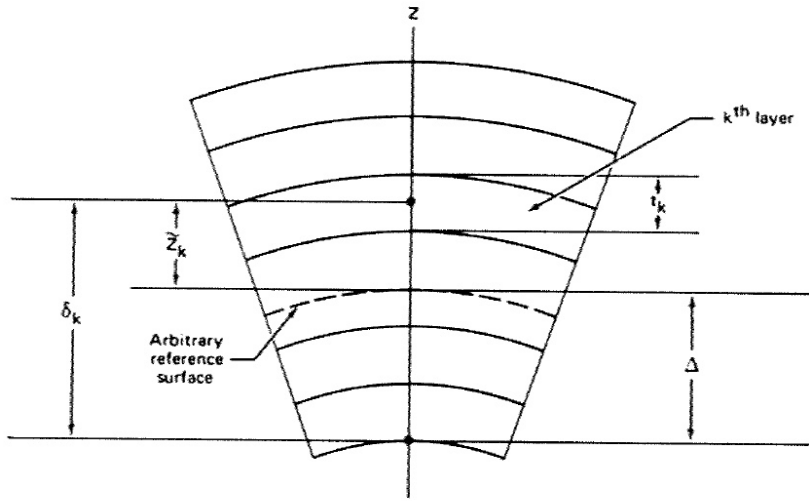


Figure 4.5. Multilayered orthotropic cylindrical shell wall geometry.

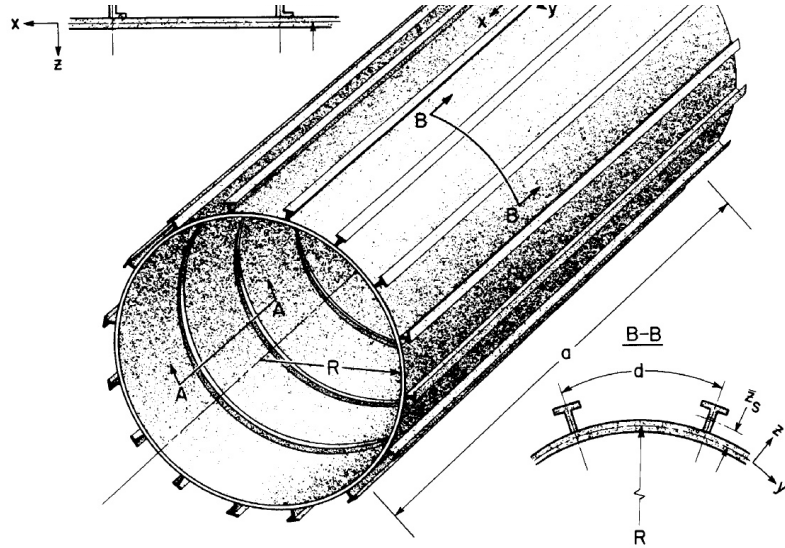


Figure 4.6. Ring and stringer stiffened shell wall geometry.

#### 4.3.6.2 Isotropic Cylinders with Rings and Stringers

For an isotropic cylinder with rings and stringers and a reference surface at the mid-surface of the skin, Eqs. 56 to 66 reduce to

$$\bar{E}_x = \frac{E t}{1 - \nu^2} + \frac{E_s A_s}{b_s} \quad (79)$$

$$\bar{E}_y = \frac{E t}{1 - \nu^2} + \frac{E_r A_r}{b_r} \quad (80)$$

$$\bar{E}_{xy} = \frac{\nu E t}{1 - \nu^2} \quad (81)$$

$$\bar{G}_{xy} = \frac{E t}{2(1 + \nu)} \quad (82)$$

$$\bar{C}_x = \bar{z}_s \frac{E_s A_s}{b_s} \quad (83)$$

$$\bar{C}_y = \bar{z}_r \frac{E_r A_r}{b_r} \quad (84)$$

$$\bar{C}_{xy} = \bar{K}_{xy} = 0 \quad (85)$$

$$\bar{D}_x = \frac{E t^3}{12(1 - \nu^2)} + \frac{E_s I_s}{b_s} \quad (86)$$

$$\bar{D}_y = \frac{E t^3}{12(1 - \nu^2)} + \frac{E_r I_r}{b_r} \quad (87)$$

$$\bar{D}_{xy} = \frac{\nu E t^3}{6(1-\nu^2)} + \frac{E t^3}{6(1+\nu)} + \frac{G_s J_s}{b_s} + \frac{G_r J_r}{b_r} \quad (88)$$

#### 4.3.6.3 Isotropic Isogrid-Stiffened Cylinders

A derivation of stiffness parameters for a general orthogonal stiffener pattern with diagonal stiffener elements is presented in Ref. 151. From that, stiffness parameters for the traditional waffle grid pattern can be derived. In addition, a common stiffener pattern, somewhat related to the waffle pattern, consisting of equilateral triangle pattern, commonly referred to as an isogrid stiffener pattern can also be derived as shown in Fig. 4.7.

The stiffnesses for isogrid-stiffened isotropic cylinders are given by

$$\bar{E}_x = \bar{E}_y = \frac{E t}{1-\nu^2} + \frac{3\sqrt{3} E A_s}{4 a} \quad (89)$$

$$\bar{E}_{xy} = \frac{\nu E t}{1-\nu^2} + \frac{\sqrt{3} E A_s}{4 a} \quad (90)$$

$$\bar{G}_{xy} = \frac{E t}{2(1+\nu)} + \frac{\sqrt{3} E A_s}{4 a} \quad (91)$$

$$\bar{C}_x = \bar{C}_y = \bar{z}_s \frac{3\sqrt{3} E A_s}{4 a} \quad (92)$$

$$\bar{C}_{xy} = \bar{K}_{xy} = \bar{z}_s \frac{\sqrt{3} E A_s}{4 a} \quad (93)$$

$$\bar{D}_x = \bar{D}_y = \frac{E t^3}{12(1-\nu^2)} + \frac{3\sqrt{3} E I_s}{4 a} + \frac{\sqrt{3} G J_s}{4 a} \quad (94)$$

$$\bar{D}_{xy} = \frac{\nu E t^3}{6(1-\nu^2)} + \frac{E t^3}{6(1+\nu)} + \frac{3\sqrt{3}}{2a} E I_s + \frac{\sqrt{3}}{2a} G J_s \quad (95)$$

where  $a$  is the stiffener length

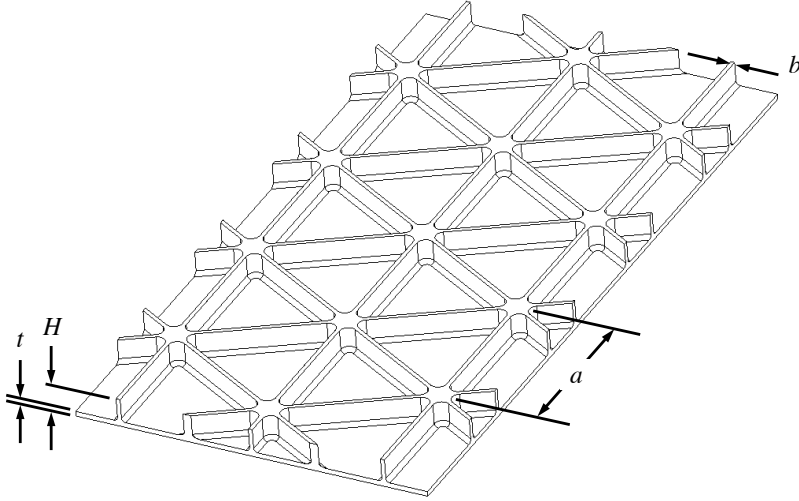


Figure 4.7. Isogrid geometry definition. (Note: The figure shows fillet details commonly found in integrally stiffened metallic designs. The effects of the fillets are neglected in these stiffness calculations)

#### 4.3.6.4 Ring-Stiffened Corrugated Cylinders

The following equations are commonly used to calculate the elastic constants for ring-stiffened corrugated cylinders. [Ref. 75] These properties assume that each segment of the corrugation has the length  $p$ . The corrugated shell geometry definition is given in Fig. 4.8.

$$\bar{E}_x = E\bar{t} \quad (96)$$

$$\bar{t} = \frac{2 t_c}{1 + \cos \theta} \quad (97)$$

$$\bar{E}_y = \frac{E_r A_r}{b_r} \quad (98)$$

$$\bar{G}_{xy} = G t_c \left( \frac{t_c}{\bar{t}} \right) \quad (99)$$

$$\bar{D}_x = E\bar{I} \quad (100)$$

$$\bar{I} = \frac{t_c p^2}{3} \left( \frac{\sin^2 \theta}{1 + \cos \theta} \right) \quad (101)$$

$$\bar{D}_y = \frac{E_r I_r}{b_r} + \bar{z}_r^2 \frac{E_r A_r}{b_r} \quad (102)$$

$$\bar{D}_{xy} = \frac{G_r J_r}{b_r} \quad (103)$$

$$\bar{C}_y = \bar{z}_r \frac{E_r A_r}{b_r} \quad (104)$$

$$\bar{E}_{xy} = \bar{C}_y = \bar{C}_{xy} = \bar{K}_{xy} = 0 \quad (105)$$

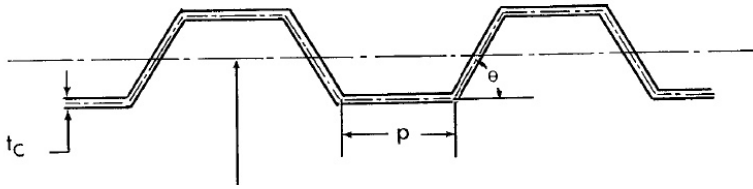


Figure 4.8. Corrugated shell geometry definition.

#### 4.3.7 Integrally-Stiffened Cylinders with Axial Welds

Analysis-based buckling knockdown factors were generated for selected orthogrid-stiffened and isogrid-stiffened metallic cylinders with axial welds. The cylinder designs considered were representative of large-scale cylinders for a specific range of design parameters. The cylinder design details and KDF development assumptions are presented in the subsections that follow. The information provided will help guide the appropriate application of the KDFs and design recommendations and identify their limitations. Extension of the KDFs and design recommendations to other cylinders, outside the range for which these KDFs were originally intended, may be possible if sufficient technical rationale is developed through additional detailed analyses and testing to show applicability. The knockdown factor development approach used to generate the KDFs is described in Section 4.7.

##### *Cylinder configuration*

The cylinder configuration used to develop the KDFs was limited to a single diameter, length, and fabrication approach that was representative of a large-scale launch vehicle cylinder section. The following cylinder dimensions and design and modeling assumptions were used in the development of the KDF data (the cylinder configuration is illustrated in Fig. 9) :

1. OML diameter  $D = 330$  in.
2. Cylinder length  $L = 330$  in., ( $L/D = 1.0$ ).
3. The cylinder is composed of eight (8) integrally-stiffened, 48-in-radius curved-panel segments that were joined together along axial weld lands
  - a. Orthogrid (Fig. 10) and isogrid (Fig. 11) stiffener patterns
  - b. Internal stiffeners with rectangular cross-section
4. The cylinder is supported by a stiff ring-frame at the upper and lower end that constrained radial and tangential displacements at the ends and can be approximated by assuming simply-supported boundary conditions in the KDF calculations.
5. The material is isotropic and linear-elastic.
6. The cylinder is subjected to axial compression load or combined axial compression and internal pressure.

The orthogrid and isogrid stiffener patterns and design variables are shown in Figs. 4.10 and 4.11 and the range of parameter values considered are provided in Tables 4.1 and 4.2. The cylinder radius to effective thickness ratio  $R/t_{eff}$  and *stiffener efficiency parameter*,  $t_{eff}/t_a$  are also presented.  $t_{eff}/t_a = 1.0$  corresponds to an unstiffened monocoque cylinder. The effective thickness,  $t_{eff}$ , and the effective membrane thickness  $t_a$ , are defined as

$$t_{eff} = \sqrt[4]{\frac{144D_{11}D_{22}}{A_{11}A_{22}}} \quad (106)$$

$$t_a = \frac{\sqrt{(A_{11}A_{22} - A_{12}^2)(1 - \nu^2)}}{E} \quad (107)$$

where  $A_{11}$ ,  $A_{12}$ ,  $A_{22}$  are orthotropic membrane stiffnesses,  $D_{11}$  and  $D_{22}$  are orthotropic bending stiffnesses,  $E$  is Young's modulus, and  $\nu$  is Poisson's ratio.

Two different weld land designs were considered. The first design includes a transition region in which the axial and circumferential stiffeners gradually taper down into the monocoque weld land region and the skin thickness is increased from  $t$  to  $t_s$ , shown in Fig. 4.12a. The value of  $t_s$  is midway between the skin thickness  $t$  and the weld land thickness  $t_w$ . This type of design is referred to as a *tapered stiffener* design. The second weld land and transition regions have many of the same features as the first, however, the circumferential stiffeners in the second design do not gradually taper down into the monocoque weld land region, rather the stiffeners terminate at an axial stiffener adjacent to the weld land shown in Fig. 4.12b. This type of design is referred to as a *picture frame* design. Minimum and maximum values of the weld land design variables are listed in Table 4.3.

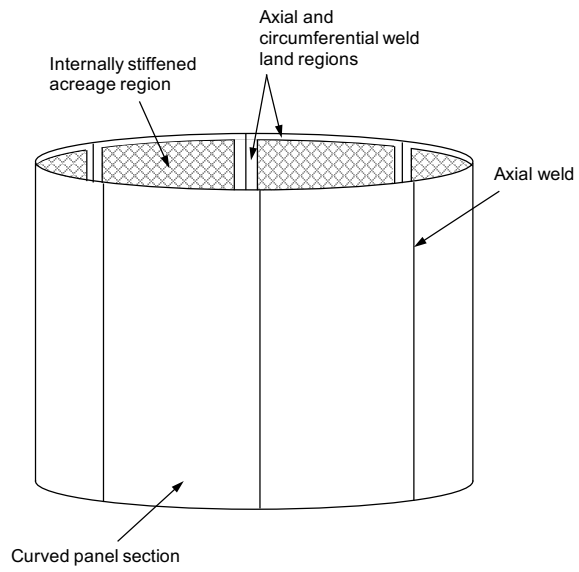


Figure 4.9. Cylinder configuration.

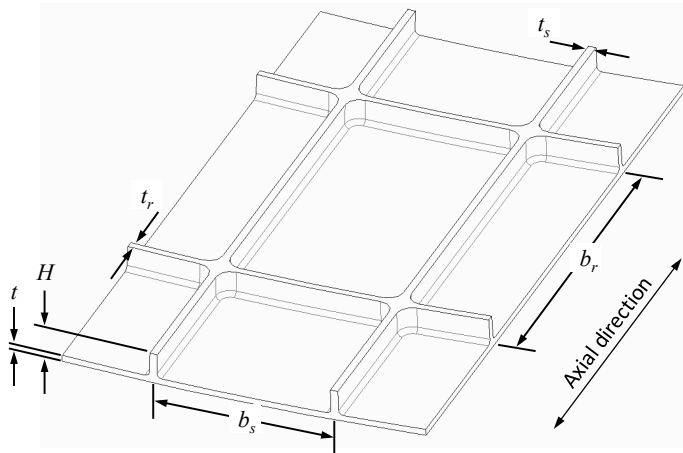


Figure 4.10. Orthogrid geometry definition.

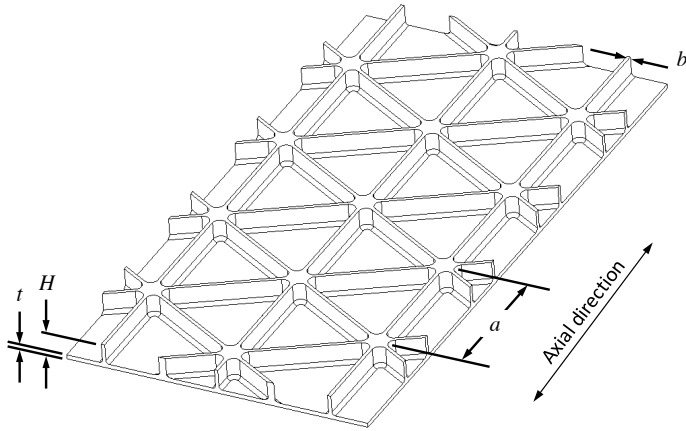


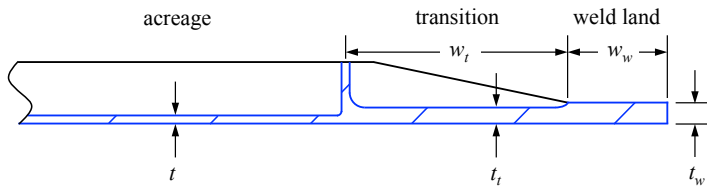
Figure 4.11. Isogrid geometry definition.

**Table 4.1. Orthogrid design parameters – minimum and maximum values**

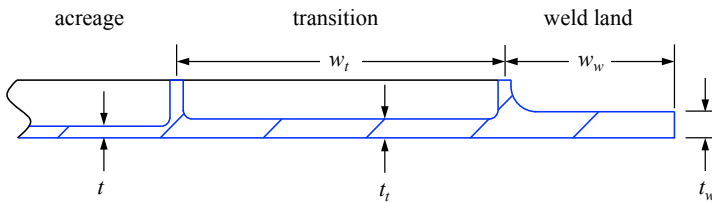
Design variable	Minimum value in.	Maximum value in.
$t$	0.100	0.375
$H$	1.115	3.695
$b_r$	12.00	18.11
$t_r$	0.125	0.340
$b_s$	5.00	9.00
$t_s$	0.125	0.400
$R/t_{eff}$	46.0	335.0
$t_{eff}/t_a$	2.12	12.72

**Table 4.2. Isogrid design parameters – minimum and maximum values**

Design variable	Minimum value in.	Maximum value in.
$t$	0.100	0.300
$H$	1.100	2.700
$a$	7.5	16.5
$b$	0.110	0.300
$R/t_{eff}$	72.8	199.25
$t_{eff}/t_a$	5.63	10.14



a) Typical acreeage and weld land design with a tapered stiffener transition.



b) Typical acreeage and weld land design with a “picture frame” stiffener transition.

Figure 4.12. Weld land geometry definition (shown in shown in the flat condition used for machining).

**Table 4.3. Weld land design variables**

Design variable	Values
$w_w$	2.000 in. - 2.500 in.
$t_w$	0.350 in. - 0.650 in.
	1.115 in. – 3.750 in. (orthogrid/taperd)
	5.0 in. – 9.0 in. (orthogrid/picture frame)
$w_t$	0.800 in. – 2.600 in. (isogrid/tapered)
	6.495 in. – 14.289 in. (isogrid/picture frame)
$t_t$	$\frac{t_w + t}{2}$

***KDF Assumptions***

Initial shell-wall geometric imperfections and nonuniform loading due to interface/loading surface irregularities (referred to herein as loading imperfections) can have a significant effect on the buckling of thin-walled compression-loaded cylinders. In addition, axial welds and weld land features used to construct large-scale cylinders, can lead to as much as a 30% reduction in the buckling load of the cylinder and cause undesirable large-magnitude prebuckling radial deformations in the cylinder wall. [Ref. 56] Similarly, local skin pockets and stiffener flexibility can interact with global deformations and lead to lower buckling loads. With these and other affects in mind, the following KDF assumptions are defined:

1. *Geometric imperfections:*
  - a. It is assumed that the initial geometric imperfections have the same overall character and amplitude (or better) as those defined by the imperfection signature given in Figs. 4.13 and 4.14.
  - b. This imperfection signature is specific to cylinders manufactured by welding multiple curve panels sections together using a conventional friction-stir welding process which reduces the severity of local distortions and residual stresses.
  - c. It is assumed that well-established aerospace-quality panel machining, forming, and welding procedures are used and will produce the same or better imperfection distributions and amplitudes. This should be verified before use.
2. *Nonuniform loading due to interface tolerances (loading imperfection):*
  - a. It is assumed that state-of-the-art manufacturing and assembly processes will result in limited geometric nonuniformities at the interfaces between the cylinder and adjacent structure that can result in nonuniform loading in the cylinder.
  - b. It is assumed (based on previous measurements) that the geometric nonuniformities at each end of the cylinder exhibit a smoothly-varying periodic distribution as shown in Fig. 4.15; have arbitrary circumferential orientation; and have an amplitude  $\delta \leq 0.1 \Delta_{cr}$ , where  $\Delta_{cr}$  is the critical end-shortening displacement of the cylinder predicted from a linear buckling analysis.

- c. It is assumed that aerospace-quality machining and assembly procedures (e.g., shimming) will produce the same or better imperfection distributions and amplitudes. This should be verified before use.
3. Axial weld lands:
    - a. Two different weld land designs with different dimensions are considered as described previously (see Fig. 4.12 and Table 4.3)
    - b. It is assumed that these weld land designs will result in the largest reduction in buckling load as they do not include local stiffness tailoring that is often added to help mitigate buckling at the weld land.
  4. Skin pocket and stiffener details:
    - a. It is assumed that skin pocket buckling and stiffener buckling/crippling failure modes will be addressed by using separate failure mode calculations
    - b. The effects of skin and stiffener flexibility and local skin buckling on the global buckling response is accounted for in the KDF formulation
    - c. The effects of radius fillets between the skin and stiffeners are neglected (e.g., see Figs. 4.10 and 4.11)
    - d. It is assumed that the skin pocket thickness adjacent to the axial and circumferential weld lands follow the geometry definitions given in Fig. 4.12.
  5. Stiffener pattern:
    - a. Different orthogrid and isogrid stiffener patterns are considered.
    - b. It is assumed that the stiffener patterns are uniform throughout each panel section and uniform from panel to panel
    - c. Different KDFs are provided for orthogrid-stiffened and isogrid-stiffened cylinders
  6. Residual stresses:
    - a. Residual stresses due to panel machining, forming and panel friction stir welding are neglected.
      - i. Assumed that the panels have undergone stress-relief procedures including heat treating and artificial aging to minimize residual stresses.
      - ii. Limited parametric studies indicate that potential residual stresses due to panel forming and friction stir welding have a negligible effect on the predicted global buckling load and buckling mode for large-scale cylinders considered here. The applicability of these results and assumptions to other cylinder configurations and manufacturing processes should be verified.
    - b. Stresses that result from joining the cylinder with adjacent structure during assembly, via bolted joints, are accounted for in nonuniform loading as described in item 2.
  7. Thickness variations:
    - a. Thickness variations due to manufacturing tolerances are not accounted for in the KDFs
    - b. It is assumed that machined panel geometries have relatively uniform dimensions, i.e., thickness, height, and width only vary slightly and do not result in abrupt thickness changes that could cause local bending deformations due to a load path eccentricity.
    - c. Thickness tolerances can be accounted for by assuming design minimum values in all buckling load calculations, including classical calculations and FE-based calculations, unless actual measured thickness values are available. However, if actual as-built thickness measurements are available, then an average thickness can be used.
  8. Material property variations:
    - a. Material property variations are not accounted for in the KDFs.
    - b. Material property variations shall be accounted for by assuming design minimum values in all buckling load calculations, including classical calculations and FE-based calculations, unless actual material value properties are available.

9. Uncertainty in applied loads:
  - a. Uncertainty in applied loads are not accounted for in the KDFs.
  - b. Load uncertainty shall be accounted for by using appropriate design safety factors for limit and ultimate loads as defined by program requirements.
10. Cylinder length and boundary conditions:
  - a. The cylinder design of interest may be a single cylinder or may consist of multiple cylinders attached together with intermediate ring-frames to create a longer cylinder. However, cylinder buckling and column buckling interaction should be checked for long cylinders (e.g.,  $L/D > 4.0$ ).
  - b. If stiff ring-frames are not used between adjacent cylinder sections, the effects of the unstiffened circumferential joint should be investigated.<sup>152, 153</sup>
  - c. The KDFs developed should be conservative for shorter cylinders  $L/D < 1.0$  since cylinders typically become less imperfection sensitive as they become shorter and approach the solution for a compression-loaded infinitely-long flat plate.

### Characteristic Imperfections

The KDFs are applicable if all the KDF assumptions are met including the characteristic imperfections. The imperfections are defined next.

Shell-wall geometric imperfection: An imperfection signature for a large-scale 330-in.-diameter, 265-in.-long metallic launch vehicle tank cylinder section is presented in Fig. 4.13. This cylinder was constructed from 8 curved panels that were welded together using a conventional friction stir welding process to form a complete cylinder. It is assumed that well-established aerospace-quality panel machining, forming, stress-relieving, and welding procedures are used and will produce the same or better imperfection distributions and amplitudes. This should be verified before use.

The axial weld locations are marked with dashed vertical lines in the contour plot. The imperfection signature is characterized by distinct inward radial imperfections at the axial weld lands of approximately -0.90 inches and smaller magnitude variations in the acreage of the cylinder.

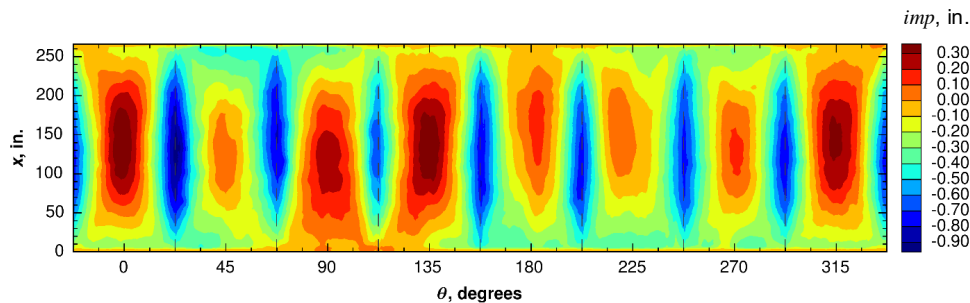


Figure 4.13. Imperfection signature for a full-scale metallic cylinder with eight axial weld lands.

The imperfection signature can be represented by a two-dimensional Fourier series given by

$$imp = \sum_{m=0}^{20} \sum_{n=0}^{40} \cos\left(\frac{m\pi x}{L}\right) [A_{mn} \cos(n\pi\theta) + B_{mn} \sin(n\pi\theta)] \quad (108)$$

where  $L$  is the cylinder length;  $x$  and  $\theta$  are the axial and circumferential coordinates; and  $m$  and  $n$  are integers corresponding to the number of axial half-waves and circumferential full-waves, respectively. The coefficient distribution for the imperfection signature shown in Fig. 4.13 is presented in Fig. 4.14. The largest magnitude component of the imperfection is associated with the  $m = 0, n = 8$ , coefficients and correspond to the large magnitude inward imperfection at the eight weld lands. In addition, noticeable contributions to the imperfection are associated with  $n$  equal to integer multiples of eight,  $n = 16, 24, 32,$  and  $40$ . Other contributions to the imperfection are associated with long-wave-length circumferential modes,  $n = 2$  and  $3$  (i.e., ovalization and triovalization, respectively). Axial half-waves of  $m > 4$  were omitted from the plot for clarity but are relatively small magnitude, i.e.,  $X_{mn} < 0.01$ .

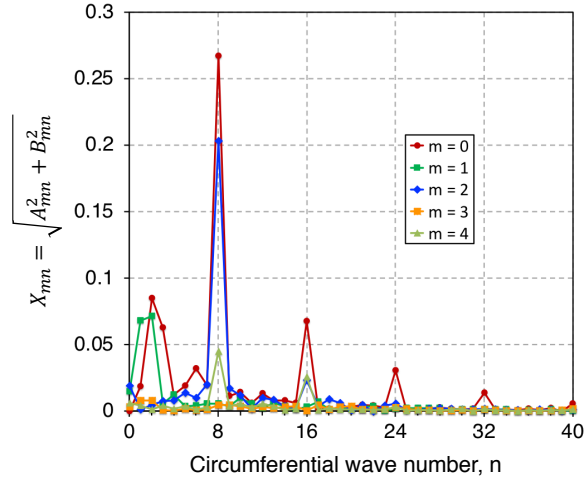


Figure 4.14. Fourier series coefficient distribution for imperfection signature given in Fig. 13.

Loading imperfection: Measured interface surface geometry of large-scale cylinders (i.e.,  $R \geq 48$  ft.) exhibit a periodic variation around the circumference and is approximated by a sine function. Most measurements indicate a 2-full-wave imperfection shape (see blue curve in Fig. 4.15). However, some imperfections include an additional shorter wave-length component which can be approximated by assuming a 3-full-wave imperfection shape as given by the red curve in Fig. 4.15. The alignment (i.e., the phase shift) of the imperfection shape on the top end relative to the bottom end of the cylinder is assumed to be random, but is likely a characteristic of a particular machining facility. It is further assumed that the top and bottom imperfection can either consist of 2 full waves or 3 full waves. The amplitude of the measured imperfections obtained from numerous large-scale cylinders with metallic interface rings are consistently  $\delta < 0.010$  in.

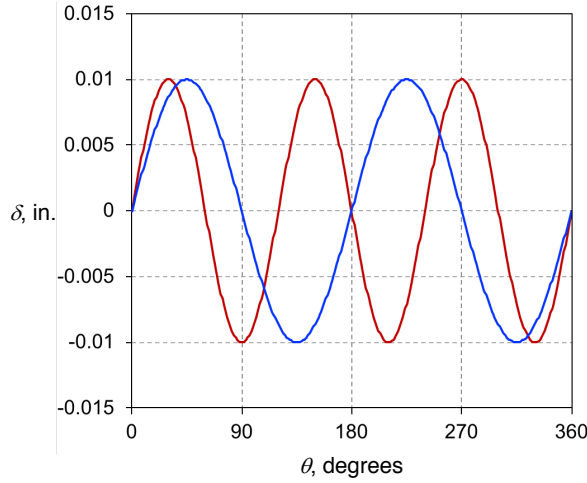


Figure 4.15. Assumed loading surface imperfection shapes.

#### 4.3.7.1 Design recommendations for orthogrid-stiffened cylinders subjected to uniform axial compression

A design buckling load  $\widehat{P}_{cr}$  can be calculated for preliminary or detailed design using the following relationships:

For conceptual or preliminary design in which the classical buckling load  $P_{cl}$  is used,

$$\widehat{P}_{cr} = \Gamma_1 \Gamma_2 P_{cl} \quad (109)$$

and for detailed design in which an FEM-based eigenvalue load  $P_{bif}$  is used,

$$\widehat{P}_{cr} = \Gamma_2 P_{bif} \quad (110)$$

$P_{cl}$  is the buckling load predicted from a classical linear bifurcation buckling analyses of an idealized geometrically perfect orthogrid-stiffened cylinder such as that given in Section 4.3, or equivalent.  $P_{bif}$  is predicted linear bifurcation buckling load (eigen load) from a detailed FE model that includes all structural details including discrete stiffeners, weld lands (see Section 4.7.1 on model development)

The factor  $\Gamma_1$  is represented by the tri-linear curve and provides a good approximation to the predicted buckling load data  $P_{bif}/P_{cl}$  as a function of a *stiffener efficiency parameter*,  $t_{eff}/t_a$ , in Figure 4.16 (predicted data represented by the blue data points).  $t_{eff}/t_a = 1.0$  corresponds to an unstiffened monocoque cylinder.

The data in Fig. 4.16 indicate that the buckling loads of the cylinders decrease as the stiffener efficiency increases, and is divided into three distinct regions. For  $1 \leq t_{eff}/t_a \leq 3.2$ ,  $\Gamma_1 = 1.0$  and corresponds to designs with essentially no sensitivity to the as-modeled discrete weld land and stiffener features when

compared to the classical solution. Buckling in these cylinders is characterized by uniform global buckling that can initiate in the weld lands or in the stiffened acreage. As the stiffener efficiency increases from 3.2 to 8.75,  $\Gamma_1$  monotonically decreases to an approximate lower-bound of 0.78. In this region of the design space, the axial weld lands have an increasingly larger influence on the buckling load of the cylinder. In addition, local pocket buckling and stiffener flexibility also begin to influence the prebuckling and buckling response for  $7.0 < t_{eff}/t_a < 8.75$ . Finally, for  $t_{eff}/t_a > 8.75$ ,  $\Gamma_1$  is assumed to have a constant value of 0.78. The buckling response for this range of  $t_{eff}/t_a$  is characterized by widespread skin buckling prior to buckling of the weld lands.

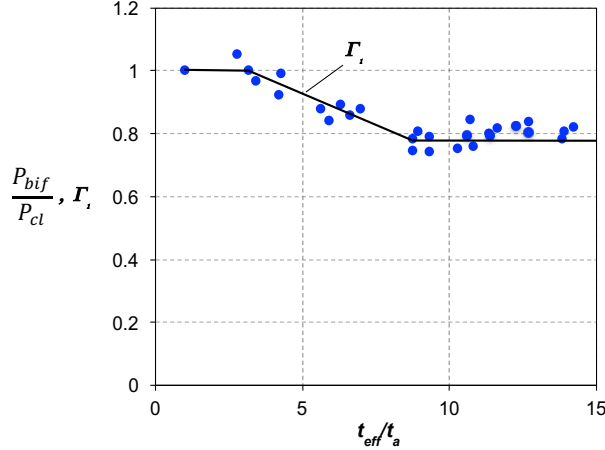


Figure 4.16.  $\frac{P_{bif}}{P_{cl}}$  and  $\Gamma_1$  versus  $t_{eff}/t_a$  for orthogrid-stiffened cylinders with axial weld lands.

The following equations define  $\Gamma_1$  as a function of  $t_{eff}/t_a$

$$\Gamma_1 = 1.0 \quad 1 \leq t_{eff}/t_a \leq 3.2 \quad (111a)$$

$$\Gamma_1 = 1 - 0.0396 t_{eff}/t_a \quad 3.2 \leq t_{eff}/t_a \leq 8.75 \quad (111b)$$

$$\Gamma_1 = 0.78 \quad t_{eff}/t_a > 8.75 \quad (111c)$$

The factor  $\Gamma_2$  defined for this particular class of cylinder is composed of two factors  $\Gamma_2(g)$  and  $\Gamma_2(l)$  that account for the effects of geometric imperfections (denoted by  $(g)$ ) and loading imperfections (denoted by  $(l)$ ), respectively, and is expressed as

$$\Gamma_2 = \Gamma_2(g) \Gamma_2(l) \quad (112)$$

A series of recommended design curves for  $\Gamma_2(g)$  are presented in Fig. 4.17. The curves provide an approximate relationship for the predicted normalized buckling load data  $P_{cr}(g)/P_{bif}$  as a function of

cylinder radius-to-effective-thickness ratio  $R/t_{eff}$  for three different classes of initial geometric imperfections, Class I – Class III. The *Class III* imperfection was based on the imperfection signature from a previous generation cylinder manufacturing process, corresponding to the data shown in Fig. 4.13, and has the largest imperfection amplitude. The *Class II* and *Class I* imperfections are assumed to have the same characteristic shape as the Class III imperfection signature but with successively smaller amplitudes of 75% and 50% of the Class III amplitude, respectively. The Class I imperfection is representative of imperfections that have been demonstrated from current state-of-the-art manufacturing process.

Heavily stiffened cylinders (i.e., cylinders with  $R/t_{eff}$  of approximately 43 to 66) are primarily weld land buckling sensitive and are relatively insensitive to imperfection amplitude. The buckling response is strongly influenced by large-magnitude prebuckling radial deformations of the weld lands that lead to the overall buckling of the cylinder. This region of the design space can be approximated by the solid black line for all classes of imperfection. As  $R/t_{eff}$  increases, the cylinders become more sensitive to the initial geometric imperfections and the imperfection amplitude, as indicated by the three different curves for the three classes of imperfection.

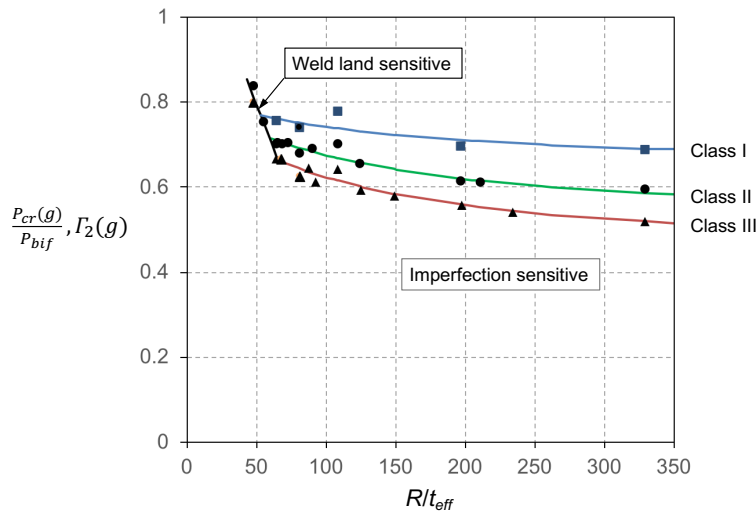


Figure 4.17.  $\frac{P_{cr}(g)}{P_{bif}}$  (data points) and  $\Gamma_2(g)$  (curves) versus  $R/t_{eff}$  for orthogrid-stiffened cylinders with axial weld lands.

The equations for  $\Gamma_2(g)$  follow

$R/t_{eff}$	Equation	Imperfection class	
43 - 66	$\Gamma_2(g) = 1.215 - 0.0084 \frac{R}{t_{eff}}$	All	(113a)
53.2 - 350	$\Gamma_2(g) = 0.867 - 0.0159 \sqrt{\frac{R}{t_{eff}}} + 0.000340 \frac{R}{t_{eff}}$	Class I	(113b)
60.6 - 350	$\Gamma_2(g) = 0.899 - 0.0286 \sqrt{\frac{R}{t_{eff}}} + 0.000623 \frac{R}{t_{eff}}$	Class II	(113c)
66 - 350	$\Gamma_2(g) = 0.898 - 0.0355 \sqrt{\frac{R}{t_{eff}}} + 0.000806 \frac{R}{t_{eff}}$	Class III	(113d)

A design curve for  $\Gamma_2(l)$  is presented in Fig. 4.18. The curve provides an approximate relationship for the predicted normalized buckling load data  $P_{cr}(g,l)/P_{cr}(g)$ , denoted by the blue circle symbols, as a function of normalized end-imperfection amplitude  $\delta/\Delta_{cr}$ .

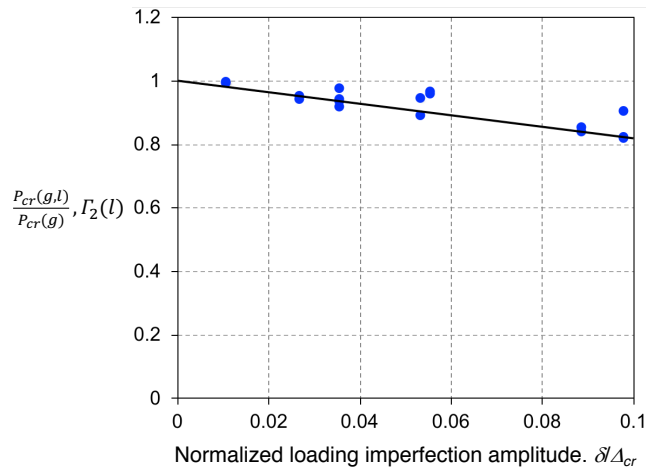


Figure 4.18.  $\frac{P_{cr}(g,l)}{P_{cr}(g)}$  (data points) and  $\Gamma_2(l)$  (curve) versus  $\delta/\Delta_{cr}$  for orthogrid-stiffened cylinders with axial weld lands.

The equation for  $\Gamma_2(l)$  is given by

$$\Gamma_2(l) = 1 - \#ends * 0.9 \frac{\delta}{\Delta_{cr}} \quad (114)$$

where  $\#ends$  is the number of loading/interface surfaces on the cylinder that can have loading imperfections.  $\#ends = 0, 1, 2$ . For example, a single cylinder with interfaces at both ends,  $\#ends = 2$ . For a two-cylinder stack with an intermediate ring frame separating the two cylinders, each cylinder will have  $\#ends = 1$ . For a cylinder in the interior of a multi-cylinder stack (a stack of three cylinders or more),  $\#ends = 0$ . It is recommended that values  $\delta/\Delta_{cr} > 0.1$  be avoided as they have been shown to induce large localized prebuckling deformations that can cause significant reductions in buckling load.

#### 4.3.7.2 Combined axial compression and internal pressure

Internal pressure can reduce the imperfection sensitivity of compression-loaded thin-walled cylinders. A factor has been derived for orthogrid-stiffened cylinders that accounts for the reduced imperfection sensitivity due to internal pressure. Analysis results indicated that  $\Gamma_1$  was relatively insensitive to the effects of internal pressure for the cylinder designs and pressure levels considered, and thus  $\Gamma_1$  remained unaltered. In contrast, the analysis results showed that  $\Gamma_2$  was very sensitive to internal pressures. Thus, an additional term  $\Delta\Gamma$  is added to Eq. 109 to account for the change in  $\Gamma_2$  due to the internal pressure load and gives a preliminary design equation

$$\widehat{P}_{cr} = \Gamma_1(\Gamma_2 + \Delta\Gamma(1 - \Gamma_2))P_{cl}^{press} \quad (115)$$

Similarly, for the detailed design of cylinders with internal pressure, Eq. 110 becomes

$$\widehat{P}_{cr} = (\Gamma_2 + \Delta\Gamma(1 - \Gamma_2))P_{bif}^{press} \quad (116)$$

Predicted  $\Delta\Gamma$  data is plotted as a function of  $R/t_{eff}$  along with approximate design curves for four different internal pressure levels in Fig. 4.19. The limited numerical results appear independent of the class of imperfection, i.e., imperfection amplitude, and are only dependent on the internal pressure load for  $R/t_{eff} > 105$ . This result is illustrated in Fig. 117 for cylinders with an internal pressure of 2 psi where the red data is associated with a Class III imperfection and the blue data is associated with a Class I imperfection. An approximate relationship for  $\Delta\Gamma$  as a function of internal pressure for this range of  $R/t_{eff}$  is given by

$$\Delta\Gamma = 0.829 - 0.810e^{(-0.327p)} \quad (117)$$

Equation 117 approaches an maximum value of 0.829 based on the data available in Fig. 4.19. However, it is expected that the true maximum is closer to 1.0. For  $48 < R/t_{eff} < 105$ ,  $\Delta\Gamma$  is dependent on the internal pressure level and  $R/t_{eff}$ . A functional relationship between  $\Delta\Gamma$ ,  $R/t_{eff}$ , and internal pressure has not been identified for this range of  $R/t_{eff}$ .

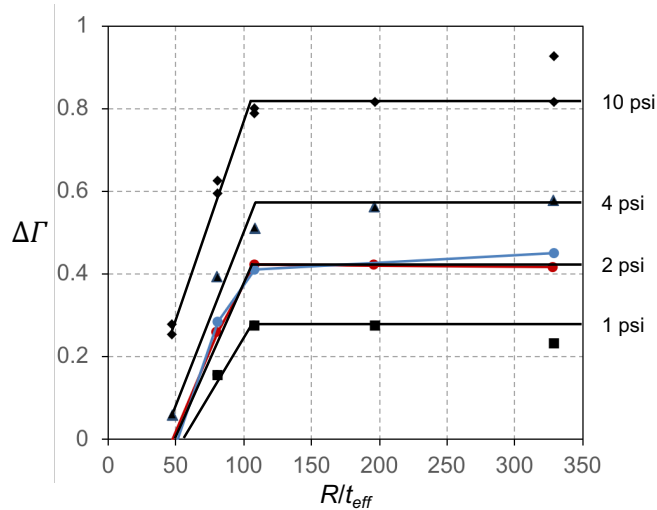


Figure 4.19.  $\Delta\Gamma$  (bi-linear curves) and analysis data versus  $R/t_{eff}$  for 1 psi, 2 psi, 4 psi, and 10 psi internal pressure.

#### 4.3.7.3 Isogrid cylinders subjected to uniform axial compression

A design buckling load  $\widehat{P}_{cr}$  can be calculated for isogrid-stiffened cylinders with axial weld lands by using the same approach defined for orthogrid-stiffened cylinders in Section 4.3.7.1, Eqs. 109 and 110.

Predicted  $P_{bif}/P_{cl}$  data for selected isogrid configurations indicated similar behavior as that exhibited by the orthogrid-stiffened cylinders presented in Section 4.3.7.1. Thus, the same factor  $F_1$  represented by the tri-linear curve in Fig. 4.16 is recommended. However, only data for isogrid stiffened cylinders with  $5.63 < t_{eff}/t_a < 10.14$  was produced.

A series of recommended design curves for  $F_2(g)$  are presented in Fig. 4.20 for isogrid-stiffened cylinders. The curves provide an approximate relationship for the predicted normalized buckling load data  $P_{cr}(g)/P_{bif}$  as a function of cylinder radius-to-effective-thickness ratio,  $R/t_{eff}$  for three different classes of initial geometric imperfections, Class I – Class III. The *Class III* imperfection was based on the imperfection signature from a previous generation cylinder manufacturing process, corresponding to the data shown in Fig. 4.13, and has the largest imperfection amplitude. The *Class II* and *Class I* imperfections are assumed to have the same characteristics as the Class III imperfection signature but with successively smaller amplitudes of 75% and 50% of the Class III amplitude, respectively. The Class I imperfection is representative of imperfections that result from the current state-of-the-art manufacturing process.

The response of heavily stiffened cylinders (i.e., cylinders with  $R/t_{eff}$  of approximately 74 to 86) are primarily associated with weld land buckling and exhibit some imperfection sensitivity. As  $R/t_{eff}$  increases, the cylinders become more sensitive to the initial geometric imperfections and buckling can initiate at the weld lands or in the acreage.

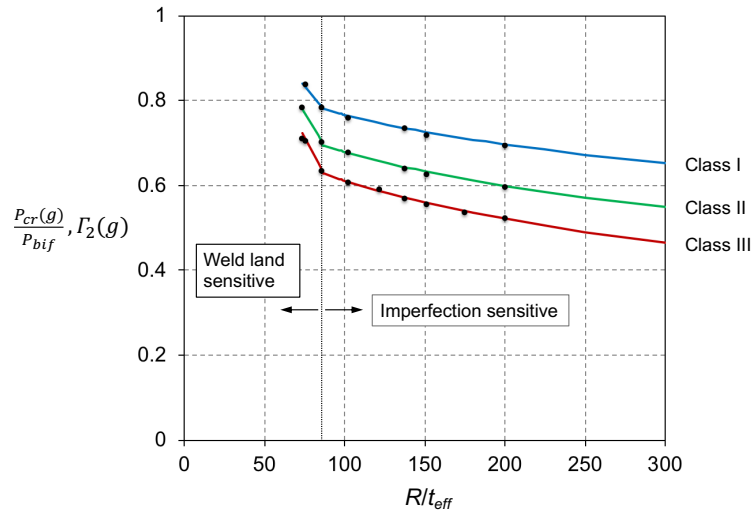


Figure 4.20.  $\frac{P_{cr}}{P_{bif}}$  (data points) and  $\Gamma_2(g)$  (curves) versus  $R/t_{eff}$  for isogrid-stiffened cylinders with axial weld lands.

The equations for  $\Gamma_2(g)$  for the curves in Fig. 4.20 follow

$R/t_{eff}$	Equation	Imperfection class	
74 - 87	$\Gamma_2(g) = 1.27 - 0.0074 \frac{R}{t_{eff}}$		(118a)
87 - 300	$\Gamma_2(g) = 0.95 - 0.75 \left( 1 - e^{-0.06 \sqrt{\frac{R}{t_{eff}}}} \right)$	Class III	(118b)
74 - 87	$\Gamma_2(g) = 1.26 - 0.0065 \frac{R}{t_{eff}}$		(118c)
87 - 300	$\Gamma_2(g) = 0.98 - 0.667 \left( 1 - e^{-0.06 \sqrt{\frac{R}{t_{eff}}}} \right)$	Class II	(118d)
74 - 87	$\Gamma_2(g) = 1.188 - 0.0047 \frac{R}{t_{eff}}$		(118e)
87 - 300	$\Gamma_2(g) = 1.03 - 0.583 \left( 1 - e^{-0.06 \sqrt{\frac{R}{t_{eff}}}} \right)$	Class I	(118f)

Analysis results for isogrid-stiffened cylinders indicate similar sensitivity to loading imperfections as was observed for the orthogrid-stiffened cylinders presented in Section 4.3.7.1. Thus,  $\Gamma_2(l)$  given in Fig. 4.18 and Eq. 114 are recommended for isogrid-stiffened cylinders along with the same design recommendations.

### 4.3.8 Other design considerations

#### 4.3.8.1 Local skin buckling

In some stiffened cylinder designs, the skin may buckle before the global buckling and collapse of the cylinder. A buckled skin is less stiff than an unbuckled skin. The decreased stiffness can be calculated by methods similar to those presented in Refs. 69, 76, and 152 and incorporated in the global buckling calculation. In some designs, local bending associated with the bending boundary layer response at the end of the cylinder or local bending near stiffness discontinuities can cause premature skin buckling. This type of local skin buckling is typically identified in the detailed design phase by using geometrically nonlinear analyses of detailed finite-element models. Mass allowances typically cover any additional reinforcement required to mitigate this buckling response if necessary. In other cases, local skin buckling may be intentionally allowed so that skin thicknesses may be reduced in an effort to reduce weight. The

effects of skin buckling have been included in the knockdown factor calculations, thus, no additional design factor is required.

#### 4.3.8.2 Effects of the smeared stiffener approximation

In general, the smeared stiffener theory is often adequate in the preliminary design of cylinders, that is the discreteness of the stiffeners usually have a negligible effect on the predicted linear bifurcation buckling load if the stiffeners are closely spaced. However, some cases have been identified where the stiffeners can exhibit large-magnitude out-of-plane deformations (i.e., rolling) and loss of stiffness when the cylinder undergoes large radial displacements. Such situations may arise in the prebuckling range of loading of the cylinder near cutouts, joints, or other stiffness discontinuities in the cylinder. The loss of effective stiffness of the stiffener can then lead to an overall and significant loss of stiffness in the cylinder at lower applied load levels. Thus the effects of discrete stiffeners on the buckling response must be assessed. (See Section 13.1.6 of Ref. 25.

### 4.4 Isotropic Sandwich Cylinders

The term isotropic sandwich designates a layered construction formed by two thin face sheets separated by a thicker core. Generally, the thin face sheets provide the majority of the bending stiffness of the construction. The core separates the face sheets and provides the transverse shear stiffness of the sandwich construction.

Sandwich construction should be checked for two possible modes of instability failure: (1) general instability i.e., global buckling, where the shell fails with the core and face sheets acting together, and (2) local instability failure taking the form of face sheet dimpling or wrinkling. See Fig. 4.21.

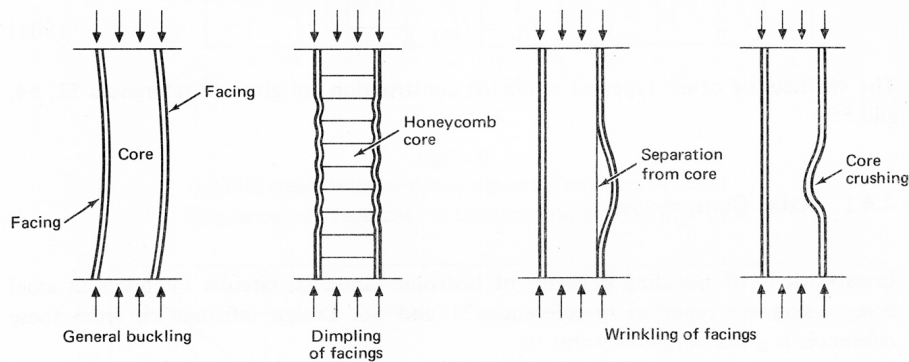


Figure 4.21 Types of failure in sandwich shells.

If the isotropic sandwich cylinder has thin face sheets, and the core has relatively low bending stiffness, then for unequal thickness face sheets, the bending stiffness is given by

$$D_1 = \frac{Et_1t_2h^2}{(1-\nu^2)(t_1+t_2)} \quad (119)$$

and for equal thickness face sheets by

$$D_1 = \frac{Et_f h^2}{2(1-\nu^2)} \quad (120)$$

The extensional stiffness for unequal thickness face sheets is given by

$$B_1 = \frac{E}{(1-\nu^2)}(t_1+t_2) \quad (121)$$

And for equal thickness face sheets

$$B_1 = \frac{2Et_f}{(1-\nu^2)} \quad (122)$$

The transverse shear stiffness for an isotropic core and unequal thickness face sheets is given by

$$D_q = G_{xy} \frac{h^2}{h - \frac{(t_1+t_2)}{2}} \quad (123)$$

and for equal thickness face sheets by

$$D_q = G_{xy} \frac{h^2}{h - t_f} \quad (124)$$

The stiffnesses of other types of sandwich construction are given in Refs. 151, and 153-155.

#### 4.4.1 Axial Compression

Investigations of buckling behavior of isotropic sandwich cylinders in axial compression are reported in Ref. 156 and 157. Design information from these references are given in Figs. 4.22 and 4.23. Figure 4.22 is the more convenient of the two figures; it is applicable to all but very short cylinders  $\gamma Z < \pi^2/(1 + R)$ . R is the shear flexibility coefficient given by

$$R = \frac{\pi^2 D_1}{L^2 D_q} \quad (124)$$

Figures 4.22 and 4.23 are based on the small-deflection buckling theory and should be used in conjunction with the knockdown factor of Fig. 4.24 to calculate buckling loads. Figure 4.24 is based on Eq. 57, given for orthotropic cylinders. For the present application, the parameter  $\phi$  becomes

$$\phi = \frac{\sqrt{2}}{29.8} \sqrt{\frac{R}{h}} \quad (125)$$

This procedure is consistent with the procedures given earlier for other types of construction when shearing of the core does not contribute significantly to the buckling deformations; that is, when  $N_o/D_q$  of Fig. 4.23 is small. As shearing deformations become more pronounced, the correction resulting from

the application of the factor  $\gamma$ , as prescribed above, decreases and becomes zero corresponding to buckling from a weak core  $[(N_o/D_q) > 2]$ .

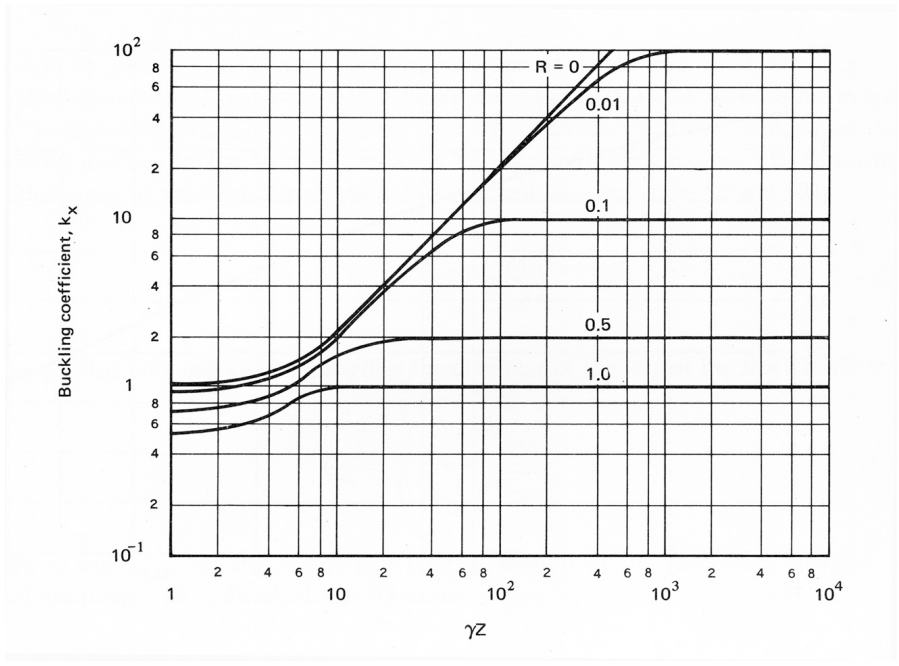


Figure 4.22 Buckling coefficients for simply supported isotropic sandwich circular cylinders subjected to axial compression,  $G_{xz}/G_{yz} = 1.0$ .

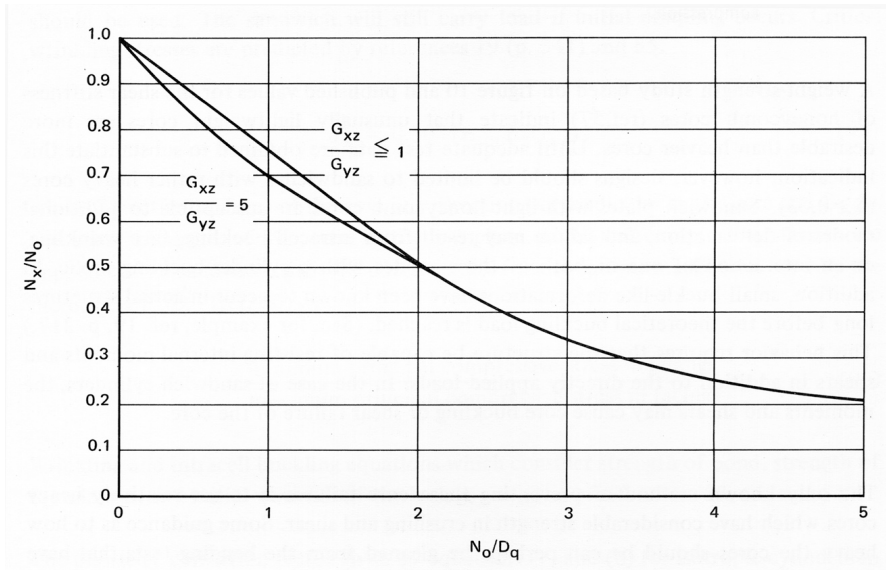


Figure 4.23 (fig 10) Buckling of moderately long, simply supported, isotropic sandwich circular cylinders subjected to axial compression.

Figure 4.24 (fig 11) Knockdown factors for isotropic sandwich circular cylinders subjected to axial compression.

A weight-strength study based on Fig. 4.23 and published values for shear stiffness of honeycomb cores [Ref. 158] indicate that unusually lightweight cores are more desirable than heavier cores. Until adequate test data are obtained to substantiate this, designs should be limited to sandwiches with heavy cores ( $\delta > 0.03$ ). Sandwich plates with light honeycomb cores are susceptible to additional modes of deformation, and failure may result from intracell buckling, face-sheet wrinkling, or an interaction of one or both of these modes with a global cylinder buckling mode. In addition, small buckle-like deformations have been known to occur in actual structures long before the theoretical buckling load is reached. (See, for example, Ref. 108, p. 217) This behavior requires that the structure be capable of resisting internal moments and shears in addition to the directly applied loads. In the case of sandwich cylinders, the moments and shears may cause buckling or shear failure of the core.

The only known method for preventing these core failures is to use a relatively heavy core which have considerable strength in crushing and shear. Some guidance as to how heavy the cores should be can perhaps be gleaned from the bending tests that have been made on multi-web beams. The internal structure of these beams is subjected to the same types of loads as the cores of loaded sandwich plates. Reference 159 indicates that honeycomb cores with a density ratio of  $\delta = 0.03$  should be adequate to prevent core failure. Large margins against failure in intracell buckling and wrinkling can be obtained with rather heavy cores ( $\delta > 0.03$ ) with little or no weight penalty. Moreover, when heavy cores are used, approximate equations are adequate for predicting failures in the intracell buckling and face-sheet wrinkling modes. The following may be used for this purpose. For intercell buckling (Refs. 155 and 160):

$$\sigma_x = 2.5E_R \left(\frac{t}{S}\right)^2 \quad (126)$$

where  $S$  is the core cell size and characterized as the diameter of the largest inscribed circle

$$E_R = \frac{4EE_{tan}}{(\sqrt{E} + \sqrt{E_{tan}})^2} \quad (127)$$

$E$  and  $E_{tan}$  are the elastic and tangent moduli of the face-sheet material. If initial face-sheet dimpling is to be checked, the following equation should be used:

$$\sigma_x = 2.2E_R \left(\frac{t}{S}\right)^2 \quad (128)$$

The sandwich will still carry the load if initial dimpling occurs. Critical wrinkling stresses are predicted by Refs. 108 and 155.

$$\sigma_x = 0.50(E_{sec}E_zG_{xz})^{1/3} \quad (129)$$

where  $E_z$  is the modulus of the core in the direction perpendicular to the core and  $G_{xz}$  is the transverse shear modulus of the core in the  $x$ - $z$  plane. If biaxial compressive stresses are applied to the sandwich, then the coefficients of the equations must be reduced by the factor  $(1 + f^3)^{-1/3}$  [Ref. 161] where

$$f = \frac{\text{minimum principal compressive strain in face-sheets}}{\text{maximum principal compressive strain in face-sheets}} \quad (130)$$

Wrinkling and intracell buckling equations which consider strength of bond, strength of foundation, and initial waviness of the face-sheets are given in Refs. 155, 162, and 163.

The plasticity correction factor given in Eqs. 11 and 12 for isotropic cylinders in axial compression may also be applied to isotropic sandwich cylinders. The factor is applicable to sandwich cylinders with stiff cores and becomes somewhat conservative as the shear stiffness of the core is decreased (Ref. 159).

#### 4.4.2 Bending

The buckling equations given in Section 4.2.1 for circular cylinders in axial compression may be used for cylinders in bending, provided the knockdown factor  $\gamma$  is taken from Fig. 4.25. The knockdown factor curve in Figure 4.25 is based on Eq. 59, given earlier for orthotropic cylinders in bending.

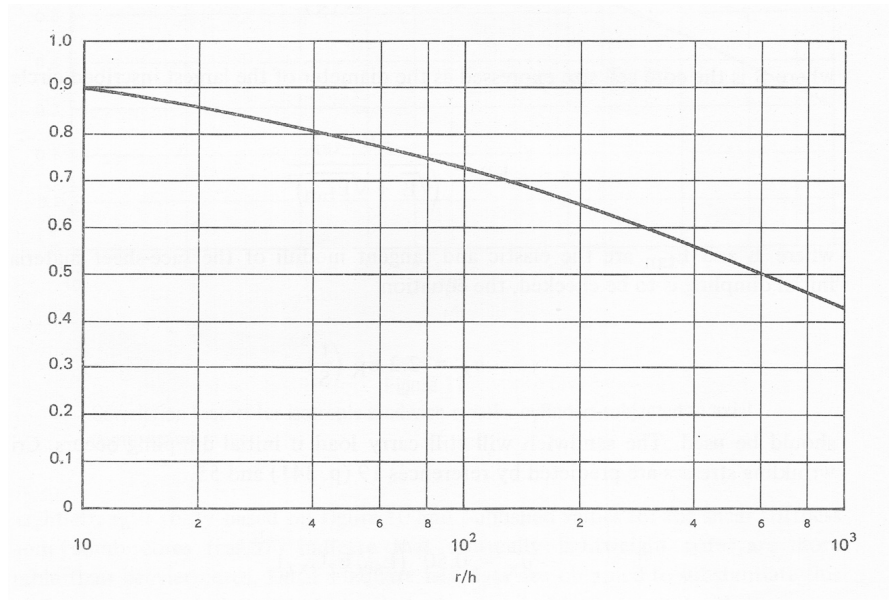


Figure 4.25. Knockdown factors for isotropic sandwich cylindrical shell subjected to bending.

#### 4.4.3 Lateral Pressure

A plot of buckling coefficient  $k_y$  as a function of  $\gamma Z$ , based on data given in Ref. 164, is given in Fig. 4.26. The straight-line portion of the curve in Fig 4.26 for a sandwich cylinder with rigid core ( $R = 0$ ) is given by the equation

$$k_y = \frac{N_y L^2}{\pi^2 D_1} = 0.56 \sqrt{\gamma Z} \quad (131)$$

There are no experimental data to substantiate Fig. 4.26; experience with isotropic cylinders, however, suggests that a knockdown factor  $\gamma = 0.56$  should be used with this figure.

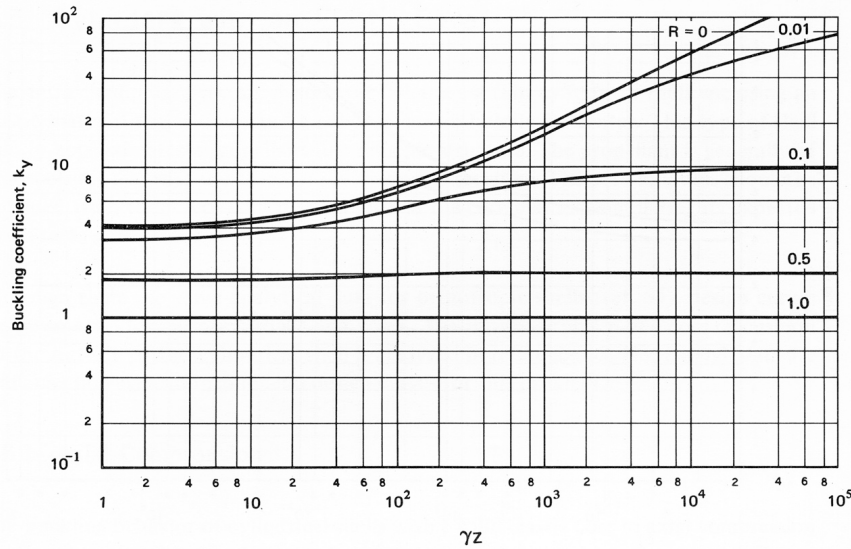


Figure 4.26. Buckling coefficients for isotropic sandwich circular cylinders subjected to lateral pressure and  $G_{xz}/G_{yz} = 1.0$ .

Here, as with sandwich cylinders in axial compression or bending, designs should be limited to sandwich cylinders for which the density ratio  $\delta > 0.03$  or greater, unless the design is substantiated by tests.

The plasticity factors for isotropic cylinders subjected to external pressure, expressed by Eqs. 29-31, may be used for isotropic sandwich cylinders subjected to lateral pressure.

#### 4.4.4 Torsion

Isotropic sandwich cylinders in torsion have not received the same attention as cylinders in compression. Rigid- and weak-core cases are reasonably well defined. While the transition between rigid and weak core is not well defined, it is probably sufficient for design purposes. Information on the transition region is given in Refs. 153 and 164, the latter of which was used to construct the plot shown in Fig. 4.27, which applies to sandwich cylinders with core exhibiting isotropic shear behavior  $G_{xz}/G_{yz} = 1.0$ . The curves in this figure are discontinuous at the value of  $\gamma Z$  where the buckling coefficient  $k_{xy}$  become equal to  $1/R$ , associated with a

change in buckling mode at that point. Reference 153 does not support this observation, but it does not cover a sufficiently wide range of geometric proportions necessary in the construction of the curves in Fig. 4.27. In addition, Ref. 153 indicates that there was some scatter in the calculated results used to construct the charts in that reference. In the ranges where comparisons between the data of Ref. 156 and 164 could be made, only relatively small discrepancies were noticed. The straight-line portion of the curve in Fig. 4.27 for a rigid core ( $R = 0$ ) is given by the equation

$$k_{xy} = \frac{N_{xy}L^2}{\pi^2 D_1} = 0.34(\gamma Z)^{3/4} \quad (132)$$

Experimental data are not available to substantiate Fig 14 for most sandwich cylinders. Experience with isotropic cylinders suggests that a knockdown factor  $\gamma = 0.586$  should be used with this figure. Here, as with sandwich cylinders in axial compression or bending, designs should be limited to sandwich cylinders for which the density ratio  $\delta > 0.03$  or greater, unless the design is substantiated by tests.

The plasticity factor for isotropic cylinders subjected to torsion, expressed by Eq 37, may be used for isotropic sandwich cylinders subjected to torsion.

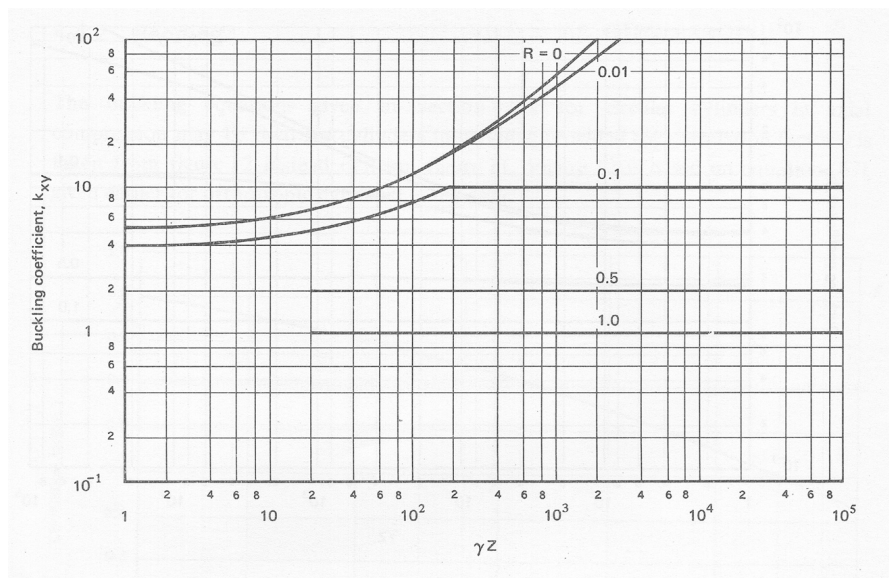


Figure 4.27. Buckling coefficients for isotropic sandwich circular cylinders subjected to torsion and  $G_{xz}/G_{yz} = 1.0$ .

## 4.5 Cylinders with an Elastic Core

The term *cylinder with an elastic core* refers to a thin-walled cylindrical shell that encloses an elastic material that can be either solid or have a hole in its center. This type of cylinder closely approximates a propellant-filled missile or solid rocket motor. The propellant is typically of a viscoelastic material and therefore is strain-rate sensitive. The core modulus should be obtained from tension or compression test of the core material simulating its expected strain rate.

Although there are some analytical data for orthotropic shells (Ref. 165), design curves are given only for isotropic shells and cores. He inverts problem of a cushion or foam material on the outside of the cylinder is analyzed in Ref. 166. Not enough data are available, however, to recommend design curves for this problem.

### 4.5.1 Axial Compression

The buckling of cylindrical shells with an elastic core in axial compression is presented in Ref. 167. Analytical results obtained from this reference are shown graphically in Fig 4.28. For small values of  $\phi_1$

$$\frac{\sigma_p}{\sigma_c} \approx 1 + \phi_1 \quad (133)$$

where

$$\sigma_c = \frac{\gamma E}{\sqrt{3(1 - \nu^2)}} \quad (134)$$

and

$$\phi_1 = \frac{\sqrt[4]{12(1 - \nu^2)}}{4(1 - \nu_c^2)} \frac{E_c}{E} \left(\frac{R}{t}\right)^{\frac{3}{2}} \quad (135)$$

This approximation is accurate for  $\phi_1 < \frac{1}{2}$ . For larger values of  $\phi_1$ , say  $\phi_1 > 3$ ,

$$\frac{\sigma_p}{\sigma_c} \approx \frac{3}{2} (\phi_1)^{\frac{2}{3}} \quad (136)$$

The experimental data provided in Ref. 167 suggest that the correlation factor  $\gamma$  in Eq. 134 can be taken as that for isotropic cylinders in compression

$$\gamma = 1 - 0.901(1 - e^{-\phi}) \quad (137)$$

where

$$\phi = \frac{1}{16} \sqrt{\frac{R}{t}} \quad (\text{for } \frac{R}{t} < 1500) \quad (138)$$

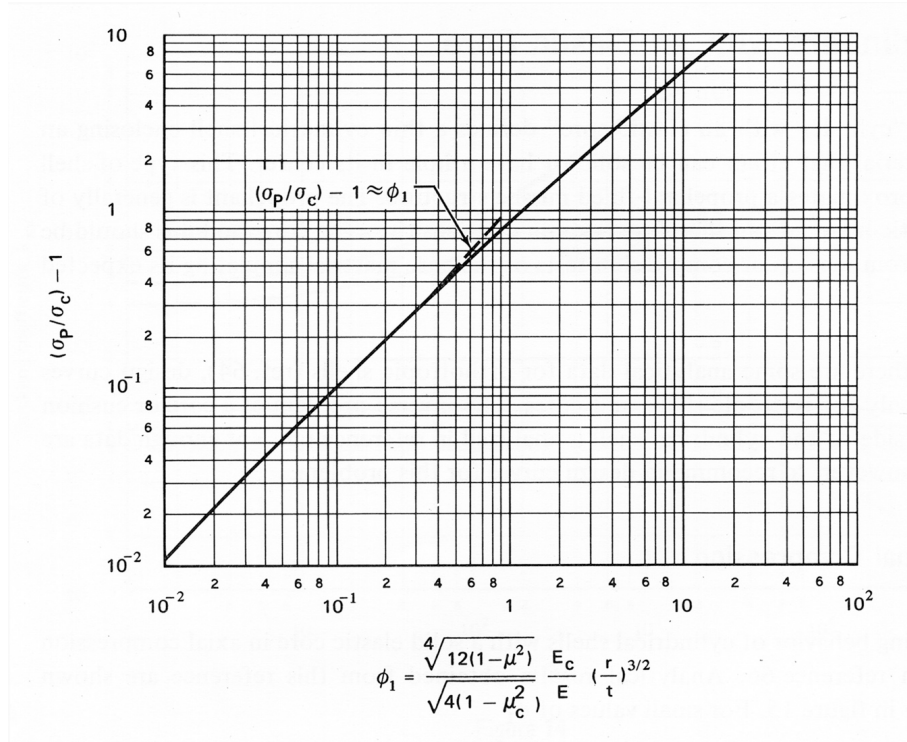


Figure 4.28. Compressive buckling stress versus core stiffness parameter.

#### 4.5.2 External Pressure

Analytical curves for lateral pressure are presented in Ref. 167. A plot of  $k_{pc}$  versus  $\pi R/L$  for  $R/t = 100, 200, 500,$  and  $1000$  is shown graphically in Fig. 4.29. The parameter  $k_{pc}$  is expressed by

$$k_{pc} = \frac{pR^3}{D} \quad (139)$$

These curves are to be used for finite length cylinders loaded by lateral pressure. However, some cylinders are long enough for the critical pressure to be independent of length (Fig. 4.29); the single curve

shown in Fig 4.30 can then be used. The straight-line portion of the curve can be approximated by the equation

$$\frac{k_{pc}}{1 + \frac{E_c R}{Et(1 - \nu_c)}} = 3(\phi_2)^{\frac{2}{3}} \quad (140)$$

where

$$\phi_2 = \frac{3(1 - \nu^2) E_c}{1 - \nu_c^2} \frac{E_c}{E} \left(\frac{R}{t}\right)^3 \quad (141)$$

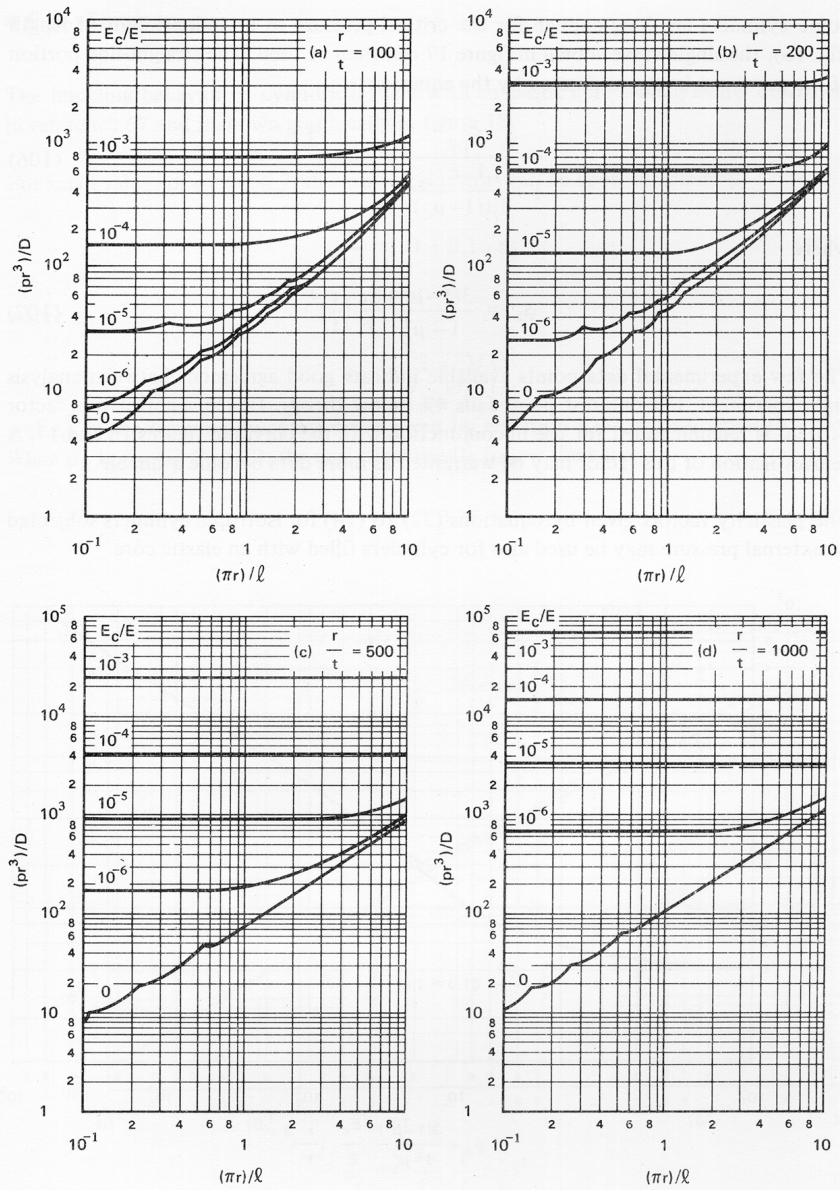


Figure 4.29. Variation of buckling pressure coefficient with length and modulus ratio ( $\nu = 0.3, \nu_c = 0.5$ ).

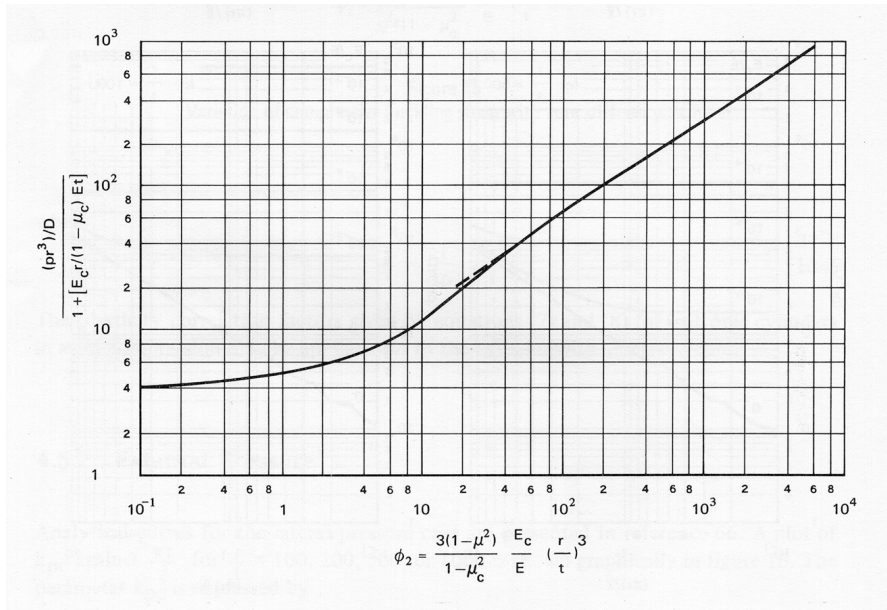


Figure 4.30. Buckling pressure coefficients for long cylinder with a solid core.

### 4.5.3 Torsion

The buckling behavior of cylindrical shells with an elastic core subjected to a torsion load is presented in Ref. 168 and is shown graphically in Fig. 4.31.

For small values for  $\phi_3$ ,  $\phi_3 < 7$ , the analytical results can be approximated by

$$\frac{\tau}{\tau_{cr}} = 1 + 0.16 \phi_3 \quad (142)$$

where

$$\phi_3 = \frac{E_c}{E} \left(\frac{L}{R}\right) \left(\frac{R}{t}\right)^2 \quad (143)$$

And  $\tau_{cr}$  is torsional buckling stress given by Eq. 33, with the correlation factor  $\gamma$  equal to unity. When  $\phi_3$  is  $> 10$ , the analytical results follow the curve

$$\frac{\tau}{\tau_{cr}} = 1 + 0.25 \phi_3^{\frac{3}{4}} \quad (144)$$

Experimental data are not available for this loading condition. The experimental points obtained for cylinders with elastic core for axial compression and external pressure, however, show better correlation with theory than the corresponding hollow cylinders. Hence, conservative design curves can be obtained by calculating  $\tau_{cr}$  in Eqs. 108 and 110 with the correlation and plasticity factors for isotropic cylinders of equations 28 and 29.

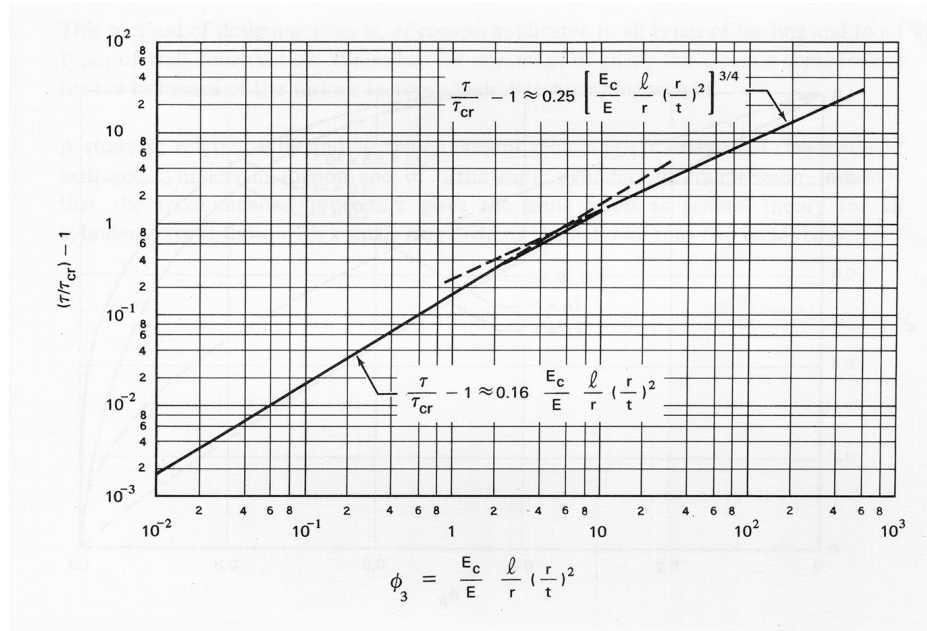


Figure 4.31. Torsional buckling coefficients for cylinders with an elastic core.

#### 4.5.4 Combined Axial Compression and External Pressure

Interaction curves for cylinders with an elastic core subjected to combined axial compression and lateral pressure are shown in Fig. 4.32. These curves were obtained analytically in Ref 167 and indicate that for sufficiently stiff core, the critical axial stress is insensitive to the lateral pressure and, similarly, the critical lateral pressure is insensitive to the axial compression. However, until more experimental data become available, the use of a straight-line interaction curve is recommended for conservative design.

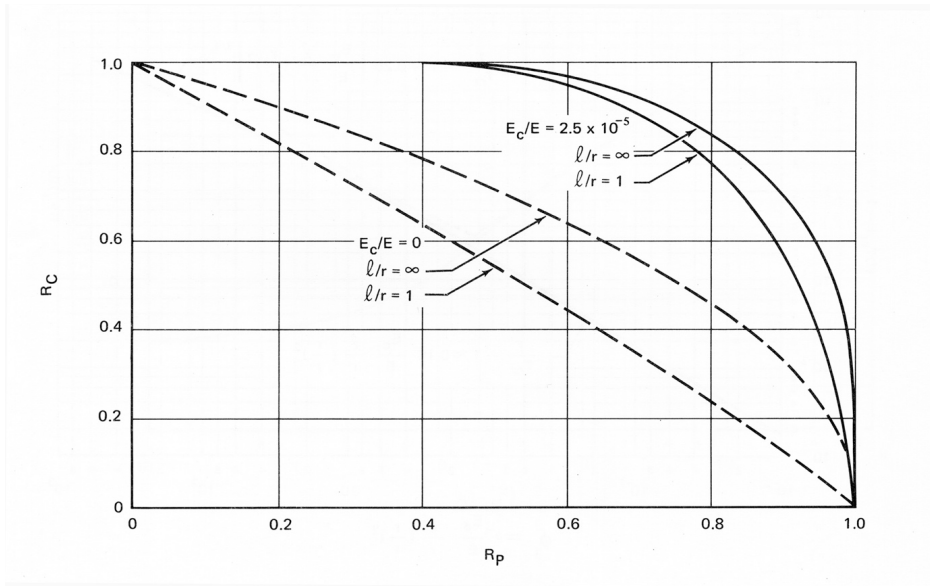


Figure 4.32. Interaction curves for cylinders with an elastic core ( $R/t = 300$ ).

## 4.5.5 Other Design Features

### 4.5.5.1 Joints

Little information is available in the open literature on the design of joints in buckling-critical cylinders. However, a detailed study on the effects of axial weld lands, and to a lesser extent, circumferential weld lands have been conducted for large-scale cylinders such as those discussed in Section 4.3.7. [Refs. 56, 169, 170]. Results in Ref. 56 indicate that axial weld lands in large-scale compression-loaded orthogrid-stiffened cylinders, such as those shown in Figs. 4.12, can lead to a significant reduction in the buckling load, on the order of 25% or more. The general conclusion from the study was that the weld land region has relatively high membrane stiffness compared to the stiffened acreage, typically composed of thin skin and tall stiffeners. However, with very low bending resistance, the weld land buckles at much lower load levels than the stiffened acreage. In addition, more recent results indicate that the weld lands exhibit large magnitude radially inward prebuckling displacements that further exacerbate the weld land buckling response. If possible, a stiffness-neutral joint design should be sought. Local bending stiffness can be increased by adding additional stiffeners adjacent to the weld land. Increasing the weld land thickness typically does not help improve the buckling load, and in fact, has been shown to reduce the buckling load further.

### 4.5.5.2 Cutouts – TBD

It is common for cylindrical shell structures to have one or more cutouts to allow access to the interior of the shell. Cutouts can have a significant influence on the buckling response of the shell depending on the size and shape of the cutout and the type of cutout reinforcement implemented. [Refs. 50-55] Experimental results from Refs. 50, 52 indicate that sufficiently small unreinforced cutouts will have a minimal effect on the buckling response and that other

imperfections in the shell govern the global buckling response in the shell. However, for larger unreinforced cutouts, large-magnitude bending deformations occur near the edges of the cutout which leads to a local reduction in effective stiffness and cause stresses to be redistributed away from the cutout. This load redistribution and local stiffness reduction can result in a stable local buckling response around the cutout or initiate a global collapse, depending on the design. For most practical applications, however, some type of reinforcement is typically applied around the cutout to control local stresses and deformations. If done correctly, the reinforcement should restore the shell to its full load carrying capacity. However, work by Toda and Hilburger suggest that local reinforcement concepts can cause buckling to occur adjacent to the reinforcement if an abrupt stiffness change exists between the area and the reinforcement [Refs. 51, 54, 55]. In addition, the prebuckling displacements and stresses in shells with unreinforced or reinforced cutouts grow nonlinearly with increasing load which can result in internal load redistribution and can cause the shell to buckle long before the load reaches the classical buckling load value, as described in a previous section. Thus, linear bifurcation analyses may not always produce a conservative buckling load estimate.

#### **4.5.5.3 Design of Rings**

Little information is available in the open literature on the design of rings for cylinders not intended to be subject to general instability failures. The criterion from Ref. 171 is frequently cited as applicable to cylinders subjected to bending or compression loads. Unfortunately, this criterion is empirical and is based on data from test cylinders with configurations that may not be relevant to the design of modern vehicles. A few checks made on cylinders in use have indicated that the criterion is usually conservative, but this may not be so in certain cases. See Refs. 116 and 172.

A less direct procedure for designing rings may be used. It consists of calculating the global buckling response (i.e., general instability), which involves failure of the rings and cylinder, as well as calculation of the buckling response of the cylinder between the rings (inter-ring buckling). Both calculations are made for several ring configurations. The buckling loads are then plotted against ring weight, and the ring design and weight necessary to produce the desired mode can be determined. It is likely that there may be some interaction between failure modes; thus, somewhat heavier rings than those indicated by the calculations should be used. These interactions should be assessed by using a geometrically nonlinear analysis and validated through suitable testing as necessary.

This method of designing rings is, of course, applicable to all types of loading and to all types of wall construction. It also has the advantage of giving the designer some feeling for the influence of the various factors which determine the ring weight.

A review of Refs. 172 and 173, which present general linear analyses of ring-stiffened isotropic cylinders in torsion and of orthotropic cylinders in compression, indicates that the recommended procedure gives the same result as general theory for all cylinders except those with a single ring dividing the cylinder into two equal-length bays.

## **4.6 Semi-Empirical Design Approach**

In 1970, Almroth et al. proposed a semi-empirical design approach for compression-loaded cylindrical shells in an attempt to incorporate new knowledge, that had been acquired from the 1940's - 1960's, into the design process.[Ref. 12] In particular, Almroth and others had acknowledged that research efforts in that time period had led to a good understanding of the basic reasons for the poor correlation between the theoretical buckling loads and the corresponding test loads but that results from that research had "not been utilized to devise better methods for practical analysis." Furthermore, for orthotropic/composite

shells, stiffened shells, and other practical cylinder configurations, the number of design parameters becomes so large that a purely empirical design approach becomes infeasible. Thus, a semi-empirical design approach was developed by Almroth et. al based on Koiter's theory in combination with a wide-column buckling analysis by Peterson and Dow[Ref. 174]. This approach has been used successfully in the design of several launch vehicles over the years. A brief summary of this semi-empirical design approach is presented in this section.

#### **Assumptions**

This semi-empirical design approach assumes that initial geometric imperfections in the shell wall are the primary reason for the discrepancy between theory and test and that the initial imperfection is axisymmetric (and often results in the largest reduction in buckling load). Additionally, it is assumed that both the Koiter method and the wide-column buckling approach produce conservative estimates of the buckling load and that the higher of the two predictions is to be used as the design buckling load.

#### **Approach**

For a given cylindrical shell, an equivalent monocoque cylinder is defined in terms of an effective radius-to-thickness ratio,  $(R/t)_e$ , where

$$\left(\frac{R}{t}\right)_e = 256 \phi^2 \quad (145)$$

where  $\phi$  is defined in Eq. 58.

Next, the empirical knockdown factor that corresponds to the  $(R/t)_e$  can be calculated using Eq. 9 or Eq. 14 for cylinders subjected to axial compression or bending, respectively. The amplitude  $\mu$  of an axisymmetric imperfection that would result in this knockdown factor  $\gamma$  can then be determined based on the curve presented by Koiter[9], see the lowest curve shown in Fig. 4.32. An equation for  $\mu$  as a function of  $\gamma$  is given by

$$\begin{aligned} \mu = & 8.232 - 84.988\gamma + 400.897\gamma^2 - 1060.739\gamma^3 + 1665.240\gamma^4 \\ & - 1539.817\gamma^5 + 774.762\gamma^6 - 163.586\gamma^7 \end{aligned} \quad (146)$$

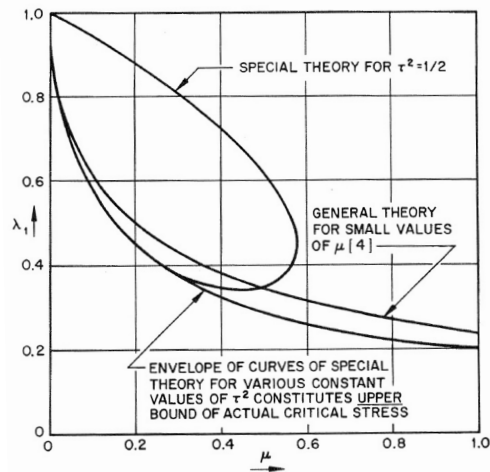


Figure 4.32.

It is then assumed that the given cylinder under consideration has the same imperfection amplitude  $\mu$  and the corresponding buckling load can be found analytically, as is done in Almroth et. al.

Almroth found however, that this approach had limitations (was overly conservative) when applied to core-filled cylinders and short stringer-stiffened (i.e., axially stiff) cylinders and that the wide-column buckling load predictions as proposed by Peterson and Dow were more applicable. Thus, it is recommended that the wide column buckling load also be calculated and compared to the semi-empirical approach, with the larger of the two values being used as the design buckling load.

#### 4.7 Analysis-Based Design

Analysis-based KDFs can be a viable replacement for some of the empirical and semi-empirical KDFs defined in Sections 4.2 through 4.6, (for example see Section 4.3.7). Improved nonlinear structural analysis tools, improved theories of elastic stability and imperfection sensitivity in shell structures, and advanced testing and measurement technologies are enabling the development and validation of high-fidelity buckling predictions of thin-walled shell structures. If suitably developed, these buckling predictions can be used in place of physical tests and provide a more accurate and less conservative estimate of the actual buckling load. However, thorough model development and validation is required to ensure that the model adequately and correctly represents the physics of the structural response, and can be a significant effort. Recommended procedures and considerations for developing and validating finite-element-based high-fidelity models and design factors are presented in this section. These recommended procedures are not a replacement for sound engineering judgement and experience. These recommended procedures can be modified as needed if supported by technical rational and/or by physical testing.

NOTE: It is assumed, herein, that the finite-element method is to be used to develop the high-fidelity models, and thus all discussion is related to the development, validation, and implementation of models based on the finite-element method. However, this does not preclude the use of other modeling techniques if they provide similar levels of fidelity.

#### 4.7.1 Model Development

It is assumed that the state of the art finite-element modeling approach is to be used in the development of high-fidelity models and buckling load predictions. However, this is not a strict requirement. Other analysis methods are permitted as long as they produce similar levels of prediction fidelity as described in this section.

##### 4.7.1.1 Objectives

To develop a high-fidelity model of the buckling response of a thin-walled cylinder subjected to combined mechanical, pressure and thermal loads. The model shall accurately predict all relevant structural response characteristics up to and including the buckling of the cylinder. For example, effective stiffness (i.e., load versus end-displacement response), prebuckling and buckling displacement and strain response, buckling mode, and the buckling load.

The accuracy of the model is naturally limited by how well the structural details are known, e.g., geometry, material properties, and loading and boundary conditions, and how well the details are represented in the model. Thus, the development of a high-fidelity model will require a substantial amount of information on the cylinder and thorough model development and validation. The model development is presented in the following subsections. Suggested model validation methods and metrics are discussed in Section 4.7.2.

##### 4.7.1.2 Structural idealization

Structural idealization is the process of converting the physical design into a mathematical representation. Details that can significantly influence the buckling response, stiffness, loads and load paths, and local and global deformations should be assessed carefully. Some examples of common modeling details and considerations are listed here.

- For the majority of thin-walled unstiffened and stiffened cylinders considered in this monograph, 2D shell elements are sufficient to accurately model the elastic cylinder buckling response.
- It is almost always required that discrete stiffeners and other flexible structural components that contribute to or influence the overall structural behavior need to be modeled explicitly.
  - Smear stiffener theory is often not adequate for the development of a high-fidelity model as the flexibility of the individual stiffener and skin elements can significantly influence the prebuckling and buckling response.
  - Modeling stiffeners and other detail features explicitly enable accurate predictions of the interaction between local and global effects
  - Local detail features such as fillets are often ignored in lower-fidelity design-level models, however, they may contribute additional stiffness necessary to accurately model local or global displacement and stiffness responses, especially if the fillet radius is large relative to other structural element dimensions. See examples and modeling strategies in Ref. 44.
- Material overlap at 2D shell element intersections should be minimized as it adds additional local stiffness and mass.
- Shell wall mid-surface offsets should be incorporated into the model to represent any mid-surface eccentricities such as those associated with local reinforcements or thickness changes.
  - Can cause local bending, load redistribution, and premature buckling
- Stiffness discontinuities such as cutouts, structural joints, or large load-bearing secondary structures should be modeled.

- Proper modeling of joint stiffness may require additional subcomponent test or detailed models to assess the adequacy of modeling approach especially for bolted joints, attachments, and interfaces.
- Bolted or riveted connections can be modeled as smeared or discrete connections. However, if used, the adequacy of the smeared modeling approach should be assessed and may require detailed subcomponent models or tests if inter-rivet or inter-bolt buckling, flexibility, or movement is expected.
- Adjacent structure can be simulated using lower fidelity models as long as they produce an adequate representation of load paths and interface flexibility, including membrane and bending flexibility.

It is recommended that a hierarchical approach be taken in the model development. A basic uniform cylinder should be modeled and analyzed first, and the results compared to known closed-form solutions. From here, additional structural details can be added knowing that the foundational model is adequate and the analyst has some basis for comparison when more complex details and loading conditions are added to the model. If there is some uncertainty in the structural details, then it is strongly recommended that a sensitivity study be conducted to determine the effects of these uncertainties and provide bounds to the predicted response.

#### 4.7.1.3 Discretization

Discretization refers to the finite-element meshing. The discretization process includes choosing element type, element shape, element distribution, etc. A list of common discretization considerations are as follows

- The majority of thin-walled cylinder buckling problems can be treated using standard linear or quadratic quadrilateral shell elements.
  - Elements with transverse shear capability are often necessary for sandwich cylinders or cylinders that may exhibit localized out-of-plane deformations, for example, short wave length displacement responses near cutouts and other significant stiffness discontinuities or cylinders with discrete stiffeners that may exhibit local rotations relative to the cylinder skin.
  - Triangular shell elements may also be used but in the past have been shown to possess some undesirable characteristics due to shear locking. In particular, higher-order triangular elements can be used to minimize the effects of shear locking.
- For sandwich cylinders with relatively thick core and a high degree of transverse shear flexibility, standard 2D shell elements with transverse shear flexibility might not be adequate.
  - These models may require the use of other element types such as special-purpose sandwich elements, or a combination of 2D and 3D elements to model face sheets and core material.

Ultimately, the choice of elements and spatial distribution necessary for a high-fidelity buckling simulation should be determined and justified through a systematic study. Closed-form solutions should be used in the early stages of model development when possible. Additionally, it should be understood that a large-scale detailed finite element model does not equate to a *high-fidelity* finite element model. The former implies a large number of finite elements. The latter implies that the mathematical model adequately and correctly represents the physics of the systems for its intended purpose.

#### 4.7.1.4 Material properties

The material properties and material model selected is a function of the material form and the anticipated structural response of the cylinder. The basis of the material model, the required material data for input, and the limitations of the material model need to be understood.

For elastic buckling simulations of metallic cylinders, linear elastic isotropic material properties are often assumed and are typically adequate. However, there are certain high-performance alloys that exhibit bi-modulus properties, that is, different tension and compression moduli. The effects of bi-modulus materials on the buckling response will be a function of the loading conditions and the relative difference between the tension and compression moduli. If the prebuckling response of the cylinder results in local stresses that approach the yield strength of the material, then an elastoplastic or elastic perfectly plastic material model may be required to account for local material yielding and load redistribution.

Cylinders constructed from laminated composite materials such as graphite-epoxy have been shown to exhibit nonlinear elastic prebuckling stiffness behavior. The nonlinearity can be a result of matrix nonlinearity, as seen in angle-ply laminates, or fiber nonlinearity.[Refs. 175, 176] These nonlinearities can be accounted for by using a nonlinear elastic material model with data determined from coupon testing. Laminated composite structures can also possess orthotropic or anisotropic stiffness properties that depend on the laminate stacking sequence and can be particularly important to the buckling and imperfection sensitivity of thin-walled cylinders, as described in Section 4.6.

High-fidelity model development will typically require coupon test data obtained from witness panels or tag-ends from the tested cylinder in order to provide the most accurate set of material properties and to verify the adequacy of the material model. If this data is not available, then a sensitivity study should be conducted to bound the predicted response characteristics.

#### 4.7.1.5 Boundary conditions

In general, models will either assume an analytical definition of the boundary conditions (e.g., classical clamped or simple support) or explicit modeling of the interface/boundary conditions and adjacent structure. In a design setting, conservative analytical boundary conditions are often utilized and are appropriate. However, for most high-fidelity buckling simulations such as those used for the development of analysis-based design factors, the modeling of the actual adjacent structure is often necessary to properly account for structure to structure interactions that may influence load introduction, interface flexibility (e.g., bolted, bonded, or potted joints), and overall system kinematics. [Ref. 44] In addition, modeling approaches that can simulate nonuniform loading due to geometric imperfections at the interfaces (i.e., interface surface geometry variations due to manufacturing tolerances that results in gaps between the interfaces) may need to be implemented. It is also conceivable that joints that have contacting surfaces that can open and close as a function of loading may also require the use of contact elements. Nonuniform loading due to loading surface imperfections will be discussed in more detail in a later in Section 4.7.1.7.

#### 4.7.1.6 Loading conditions

Modeling test loading conditions are typically straightforward as long as the test interfaces and loading structure are understood, characterized, and modeled adequately. As discussed previously, most high-fidelity models will include models of the boundary conditions and adjacent structure, and in the case of a structural test, representations of the load fixtures and discrete load application points should be available for load application. However, if additional secondary loads are applied directly to the cylinder, e.g., lateral loads to simulate internal payloads, or external booster loads, then the representation of these point loads and local effects should be addressed.

Modeling complex flight loading conditions that include vehicle accelerations, aerodynamic pressure, thermal loads, and cryogenic fuel slosh loads are altogether different as they are associated with surface load distributions and body forces. As such, care must be taken in applying these distributed loads onto a discretized model.[Ref. 40]

In both cases, test loading conditions and flight loading conditions, problems involving load sequencing for combined loads, deformation dependent loading (follower loads), and quasi-static versus transient-dynamic and time-dependent loading, may also arise.

#### **4.7.1.7 Initial imperfections and loading nonuniformities**

Initial geometric and thickness imperfections (i.e., manufacturing-process-induced variations in the geometry) and loading nonuniformities due to interface surface geometry variations can have a significant influence on the buckling response of thin-walled cylinders. Efforts have been made to characterize these imperfections and nonuniformities in order to establish characteristic imperfection signatures that are associated with different cylinder manufacturing processes. With this information established, high-fidelity buckling analyses and robust design criteria can be developed. Several important imperfection types are described next.

##### Initial geometric and thickness imperfections

The outer mold line (OML) and inner mold line (IML) geometry of cylinder can be measured routinely by using commercially available geometry measurement systems such as structured light scanners, laser trackers, or coordinate measurement machines (CMM). These data can then be used to characterize the as-built geometric imperfection and thickness imperfection of the cylinder. The geometric imperfection corresponds to the difference between the measured OML or IML surface geometry and an ideal circular cylinder. Similarly, the as-built thickness is obtained by subtracting the measured IML radius from the measured OML radius.

A typical measured geometric imperfection of a large-scale metallic launch vehicle tank cylinder section is presented as a contour plot in Fig. 4.33. The color contours indicate the difference between the as-built geometry and the idealized perfect circular cylinder. Inward radial imperfections are denoted by negative contour values and outward radial imperfections are denoted by positive contour values. This cylinder was constructed from 8 curved panels that were friction stir welded together to form a complete cylinder. The axial welds are marked with dashed vertical lines in the contour plot. The measured imperfection exhibits distinct inward imperfections at the axial weld lands of approximately -0.90 inches and smaller magnitude variations in the acreage of the cylinder.

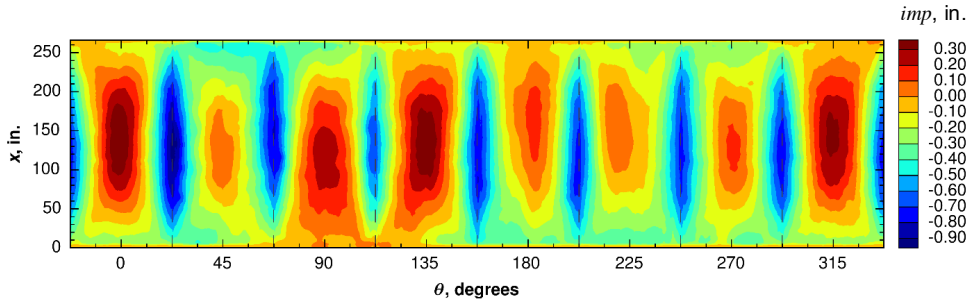


Figure 4.33. Geometric imperfection for a large-scale metallic cylinder with eight axial weld lands.

The measured imperfection data can be represented by a two-dimensional Fourier series given by

$$imp = \sum_{m=0}^N \sum_{n=0}^N \cos\left(\frac{m\pi x}{L}\right) [A_{mn} \cos(n\pi\theta) + B_{mn} \sin(n\pi\theta)] \quad (147)$$

where  $L$  is the cylinder length;  $x$  and  $\theta$  are the axial and circumferential coordinates; and  $m$  and  $n$  are integers corresponding to the number of axial half-waves and circumferential full-waves, respectively. Using a representation of this type enables convenient analysis and comparison of imperfection distributions from different cylinders and different manufacturing processes. For example, the coefficient distribution for the measured imperfection shape from Fig. 4.33 is presented in Fig. 4.34. The largest magnitude component of the imperfection is associated with the  $m = 0$ ,  $n = 8$ , coefficients and correspond to the large magnitude inward imperfection at the eight weld lands. In addition, noticeable contributions to the imperfection are associated with  $n$  equal to integer multiples of eight,  $n = 16, 24, 32$ , and  $40$ . Other contributions to the imperfection are associated with long-wave-length circumferential modes,  $n = 2$  and  $n = 3$ . Axial half-waves of  $m > 4$  were omitted from the plot for clarity. Other mathematical representations can be used as needed.

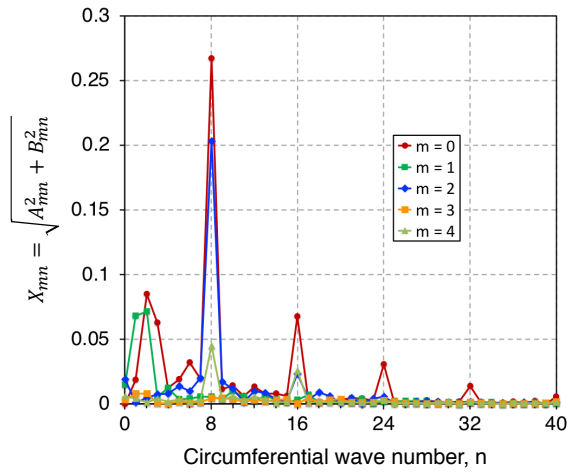


Figure 4.34. Coefficient distribution of Fourier series representation of measured imperfection given in Fig. 17.

OML and IML geometry measurements for a large-scale sandwich cylinder test article were obtained and used to calculate the as-built thickness distribution for the cylinder. [Ref. 176] In Fig. 4.35, it is seen that the top and bottom of the cylinder have the greatest thickness and are associated with structural padups on each end, indicated by the orange and red contours. The global thickness-variation pattern in the acreage of the cylinder, indicated by the blue/green contours appears to be correlated primarily to the core layout, and the use of rectangular core sheets with slightly different thicknesses. In addition, horizontal, vertical, and angled features appear in the contour pattern and are likely associated with gaps and overlaps between adjacent lamina plies that can occur during the manufacturing process. Similarly, measured thickness of laboratory-scale laminated composite cylinders can also be found in Refs. 11 and 49.

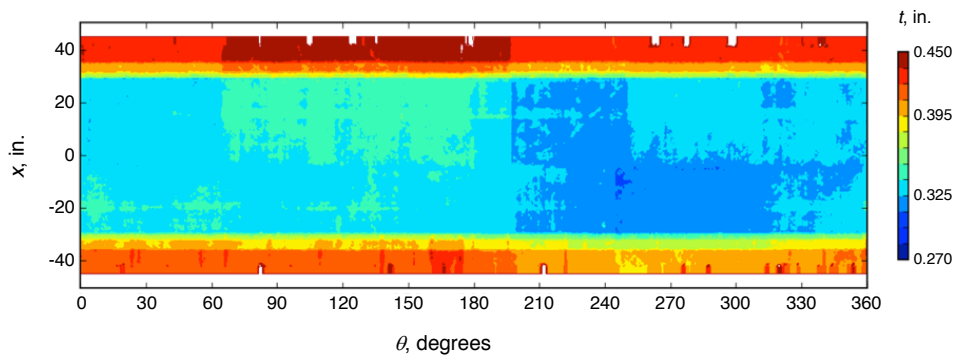
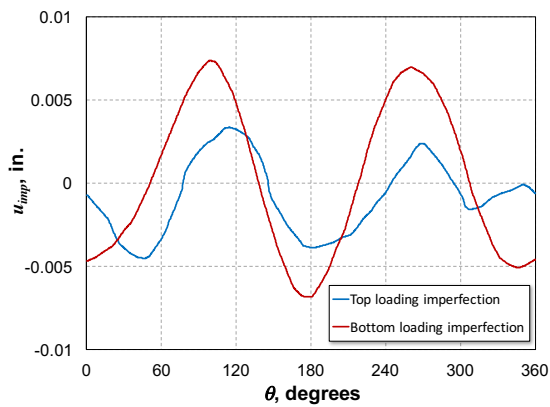
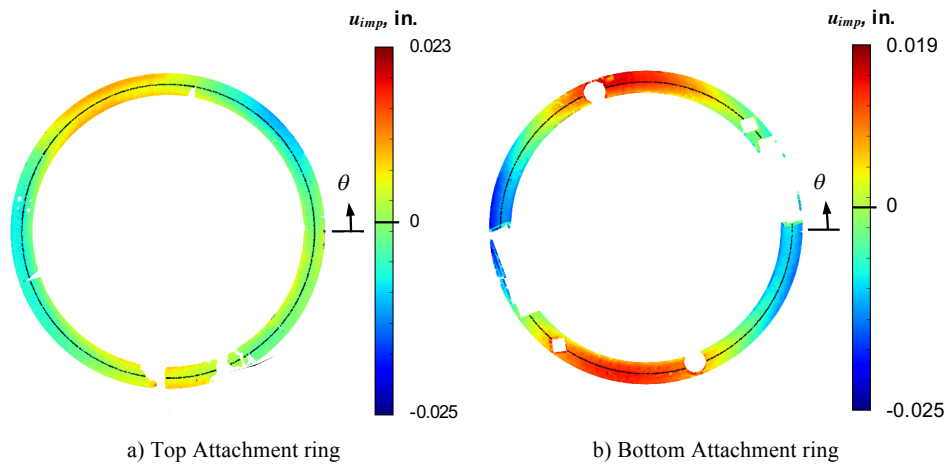


Figure 4.35. measured thickness distribution of a sandwich cylinder test article.

Loading surface/interface surface imperfections

Loading surface imperfections can lead to loading nonuniformities, changes in behavior, and reduce the buckling load of thin-walled cylinders. [Refs. 11, 44 and 49]. Loading surface or interface surface geometry should be characterized through detailed measurement. Example loading surface geometry measurement results are presented in Fig. 4.36 for an 8-ft-diameter cylinder test article. Fig. 4.36a and 4.36b show contours of top and bottom attachment ring interface surface imperfections, deviations of the measured geometry from best-fit planes  $u_{imp}$ . Data traces are extracted from the contour data at a fixed radius of 48.0 inches and are shown in Fig. 4.36c. The results indicate long-wavelength imperfections around the circumference of the cylinder, with two full waves on the bottom ring and approximately three full waves on the top ring. These results appear to be typical for cylinders that are machined using a rotating turn-table type machining approach.



c) Extracted top and bottom attachment ring imperfection data (curve-fitting was used to fill in missing data from imperfection measurement)

Figure 4.36. Measured attachment ring interface surface imperfections.

#### 4.7.1.8 Analysis Approach

A sequence of analyses is recommended when first developing a model. First, a linear elastic stress analysis of the finite element model should be performed to verify the overall performance and quality of the model, including stiffness, displacement response, and internal stress and strain distributions. Next, a linear bifurcation buckling analysis of the cylinder should be conducted. The solution for the bifurcation buckling of cylinders is typically characterized by the existence of multiple buckling or eigen-modes at or in the vicinity of the critical buckling load value. Thus, it is suggested that multiple eigen-modes be obtained during the analysis as there may be a variety of different local and global modes shapes. In addition, this clustering of eigen modes can lead to numerical solution difficulties and thus convergence

of the solution should be carefully assessed and solution convergence tolerances may need to be adjusted. Eigenvalue analyses can provide additional insight into the state of the finite element model even when an eigenvalue analysis is not required. The eigenvectors (or mode shapes) can give an indication of the anticipated deformation patterns that may be expected and the adequacy of the finite element mesh to represent those patterns. Consideration should be given to these items:

- Convergence criteria for the eigenvalue analysis
- Solution procedure for extracting the eigenpairs (is the solution space sufficiently spanned to represent the deformation states?)
- Influence of finite element meshing (can short-wavelength mode shapes be represented by the given finite element mesh?)

Finally, because cylinder buckling is inherently a highly nonlinear response problem, a geometrically nonlinear quasi-static and/or transient dynamic analyses should be performed to obtain a high-fidelity prediction of the buckling response of the cylinder. Further mesh refinement study maybe necessary at this point if the predicted deformations and stresses are significantly different from those predicted by the linear static and linear eigenvalue analyses. Typically, the prebuckling response is quasi-linear up to the buckling load and a quasi-static Newton-Raphson or Riks arc-length procedure can be used. The transient buckling response and initial post-buckling response is best predicted by using transient dynamic analysis solution routine. This dynamic analysis can be either explicit or implicit. Quasi-static Newton-Raphson or Riks arc-length methods typically fail in predicting the buckling response of the cylinder due to the highly complex transient mode jumping phenomena that accompanies the buckling response [Ref. 177].

Specific solution controls for nonlinear solution procedures include:

- Convergence metrics (change in residuals, change in displacement increments, change in energy)
- Specified convergence tolerance – too small and no solution is obtained; too large and the solution will “drift” from solution equilibrium
- Solution control procedure (load control, displacement control, arc-length control)
- Solution damping (too much solution damping may produce unrealistic erroneous predictions)
- Nonlinear solution algorithm (Newton-Raphson procedure, modified Newton-Raphson procedure, quasi-Newton procedures)
- Number of negative roots in the tangent stiffness matrix decomposition (more than the number of Lagrange-multiplier constraints?)

Default values for these and other solution parameters should be assessed and solution sensitivities should be understood.

Note: In some cylinder buckling analyses (e.g., symmetric, geometrically perfect cylinder model that exhibit minimal prebuckling nonlinear behavior), it is not uncommon for the quasi-static solution to obtain equilibrium solutions on the primary equilibrium path at load levels above the critical buckling load. These solutions are mathematically feasible but physically unstable. An unstable equilibrium solution can be identified when negative roots appear in the tangent stiffness matrix (or the number of negative roots becomes great than the number of Lagrange constraints). In other instances, erroneous solutions can be obtained when using default solution parameters and specifically, artificial solution damping, common to commercial codes, used to help traverse unstable equilibrium paths. One should be skeptical of any global buckling solution that is obtained when artificial damping is used in the solution procedure.

#### 4.7.1.9 Identify and quantify sources of error and uncertainty

Sources of uncertainty and assumptions should be identified to help determine the limitations and risks associated with the modeling and analysis results. Common sources of uncertainty include geometry, material properties, part-to-part variability in material properties and geometry due to manufacturing processes variability, statistical basis of material properties, distribution and magnitude of mechanical and/or thermal loading, and boundary conditions.

Similarly, assumptions are made in the process of developing the model based on the known information and modeling needs. Sensitivity studies should be conducted to assess the effects uncertainties and modeling assumptions. Understanding the response sensitivities can help guide testing requirements and data collection and identify model development and refinement needs.

#### 4.7.2 Model Validation

In general, model validation requirements are dictated by modeling needs. For the development of high-fidelity cylinder buckling predictions, key response characteristics and metrics include:

- Prebuckling stiffness, characterized by axial load versus end-displacement, moment versus end-rotation, etc. (characteristic global displacement versus applied load)
- Prebuckling and buckling displacement response (axial, circumferential, radial)
  - Load versus point displacements
  - Full-field displacement distributions
- Prebuckling strains (axial and circumferential)
  - Load versus point strain
  - Full-field strain distributions
- Buckling load

Required accuracy of the analysis predictions is determined by individual project needs. High-fidelity models have been shown to routinely produce results to within  $\pm 5\%$  of measured. Prebuckling stiffnesses and prebuckling displacement response are expected to correlate with experimental measurements reasonably well (e.g.,  $\pm 2\%$ ). Overall character of the full-field prebuckling and buckling displacement response should also correlate well. In particular, the character and location of the initiation of buckling should be similar to that observed in test, thus, indicating that the physics of the buckling response is well represented. Because of cylinders extreme sensitivity to variations in geometry, load distribution, and boundary conditions, slight variations in the as-tested cylinder configuration can and often will shift the buckling initiation location. Thus, an analysis-based sensitivity study can be used to bound the test results and provide additional confidence in the analysis model. Local or point strain measurements are often the most difficult to correlate due to local gradients that can result from local bending, slight variations in loading, and variations in the as-built versus as-modeled geometry and material properties. Thus, the overall character of the strain response amplitudes should be assessed for correlation.

Validation testing and data requirements follow directly from the model validation needs, such as those listed above. Comprehensive instrumentation and measurement techniques will be necessary during validation testing in order to obtain required data to correlate with analysis predictions. A combination of displacement and strains sensors should be used to measure displacements and strains at key locations on the cylinder test article and any adjacent load introduction structure. In addition, full-field digital image correlation (DIC) type techniques are needed to characterize prebuckling and buckling displacement response over as much of the cylinder as possible. Other instrumentation such as fiber-optic strain sensors and acoustic emissions sensors can also be used. Several successful validation test programs on the

buckling of large-scale integrally-stiffened metallic cylinders are documented in Refs. 44 and 178 and include detailed information on the testing approach.

Typical measured data needed for high-fidelity model validation and measurement considerations include:

- Effective stiffness characterized by load versus displacement response curves.
  - Obtain displacement measurements directly from cylinder.
  - Do not rely solely on load actuator displacement measurements as they may be influenced by flexibility of the attachments and adjacent loading structure.
- Prebuckling and buckling displacement response
  - Point measurements by using DCDTs/LVDT type instrumentation or equivalent; provides data for direct correlation to predicted results; provides data to verify accuracy of 3-D DIC-based measurements
  - 3-D DIC techniques to measure full-field displacement response; low-speed systems used to characterize quasi-static response, high-speed systems used to characterize buckling initiation and transient collapse response
- Load introduction - characterize uniformity of load
  - back-to-back strain sensors applied to cylinder test article near ends to characterize load introduction, membrane and bending response
  - back-to-back strain sensors in adjacent load introduction structure to characterize behavior
  - 3-D DIC measurements of cylinder interface region characterize load introduction and identify any anomalous behavior
- Boundary flexibility
  - all degrees of freedom at the boundary may need to be monitored
  - can be characterized by using a combination of displacement and strain sensors and 3-D DIC, including sensors used for load introduction characterization
- As-built vs. as-installed /as-tested geometry and interface conditions
  - installation of test article into test facility may result in slight change in geometry and induce an initial pre-stress due to fit-up tolerances
    - mis-match in radius and circularity
    - interface surface flatness
  - characterize change in geometry by using 3-D DIC or other high-resolution geometry measurement techniques
  - characterize pre-stress by recording strain data during installation process and changes in test article geometry via 3-D DIC
- Manufacturing
  - residual stresses and variations in material properties may occur during manufacturing. The extent of these manufacturing effects and their importance should be assessed as part of the manufacturing process development. Analysis-based sensitivity studies should be used to determine their importance on the buckling of the cylinder

#### 4.7.3 Knockdown Factor Development Approach

A typical vehicle design approach includes several phases, the *conceptual/preliminary* design phase and the *detailed* design phase. Other design approaches may be used, but it is assumed that all will follow a similar multi-phased approach that also includes increasing levels of analysis model and design fidelity. The conceptual/preliminary design phase is performed in the beginning of the design process to determine overall structural sizing and mass estimates, and to perform basic material and configuration trades.

Buckling load predictions are based on classical closed-form buckling analyses of idealized geometrically perfect cylinders with smeared stiffener properties (i.e., the stiffener properties are approximated by a fictitious layer with properties based on the bending and extensional properties of the individual stiffeners averaged out over the representative stiffener spacing). The detailed design phase begins after some of the basic design decisions have been made such as structural concept, material type, manufacturing approach, and geometry. In this phase, the buckling load predictions are often based on detailed finite-element models of a geometrically-perfect structure and will begin to include many of the relevant detail features such as stiffeners, joints, cutouts, attachments, and skin thickness tailoring. In both phases of the design, however, it is assumed that a buckling knockdown factor (KDF) is needed to account for the differences between the predicted buckling load results (classical solution or idealized FE model) and the expected buckling load of the as-built cylinder.

### ***Development Approach***

An approach for developing analysis-based KDFs for thin-walled cylinders is described next. The KDFs development approach will lead to a hierarchical set of factors that can account for a variety of individual effects such as initial geometric imperfections, nonuniform loading/interface tolerances, joints, internal pressure, stiffeners, geometric nonlinearities, etc. Thus, since the different effects can be treated individually, different KDFs can be chosen based on the fidelity of the analysis used in the design process (e.g., classical solution versus FE-based linear eigen analysis), the quality of the cylinder (i.e., imperfection amplitude), loading conditions, and structural details present.

Following from the traditional KDF definition found in Sections 4.2-4.6, an analysis-based KDF,  $\Gamma$ , is defined as

$$\Gamma = \frac{P_{cr}}{P_{cl}} \quad (148)$$

where  $P_{cr}$  is the predicted buckling load from an experimentally-validated, high-fidelity finite-element model, as described in Section 4.7.1, and represents the *expected buckling load* for an as-built cylinder design of interest.  $P_{cl}$  is the buckling load predicted from a classical linear bifurcation buckling analyses of an idealized geometrically perfect cylinder such as that given in Sections 4.2-4.6.

It is convenient to rewrite the KDF defined in Eqs. 148 as

$$\Gamma = \Gamma_1 \Gamma_2 \quad (149)$$

where

$$\Gamma_1 = \frac{P_{bif}}{P_{cl}} \quad (150)$$

and

$$\Gamma_2 = \frac{P_{cr}}{P_{bif}} \quad (151)$$

$P_{bif}$  is predicted using a linear bifurcation buckling analysis from a detailed FE model. The FE model used in this analysis should be based on an idealized version of the high-fidelity model used to predict  $P_{cr}$ , i.e., geometrically perfect, uniform loading, classical simply-supported boundary conditions.

The definition of  $\Gamma_1$  given by Eq. 150 is relatively straightforward and can be regarded as a first-order approximation of the effects of structural details on the buckling load of the cylinder. A series of design data or curves can be generated that account for the effects of a variety of structural details of interest such as cutouts, joints, or discrete stiffeners (e.g., see Fig. 4.16). Similarly,  $\Gamma_2$  given by Eq. 151, is used to account for the effects of geometrically and materially nonlinear behavior as well as geometric imperfections, nonuniform loading, elastic boundary conditions, and other structural details and behavioral characteristics that are included in the high-fidelity buckling load prediction,  $P_{cr}$ .

$\Gamma_1$  and  $\Gamma_2$  can be further subdivided as necessary to characterize the effects of individual features and response characteristics, as long as mathematical consistency is maintained or conservatism is demonstrated. For example, it may be advantageous to define  $\Gamma_2$  as follows:

$$\Gamma_2 = \frac{P_{cr}(g) P_{cr}(g, l)}{P_{bif} P_{cr}(g)} \quad (152)$$

where  $P_{cr}(g)$  corresponds to the buckling load of cylinder with only geometric imperfections, indicated by the  $(g)$ , and  $P_{cr}(g, l)$  corresponds to the buckling load of a cylinder with geometric and loading imperfections indicated by  $(g, l)$ . Equation 152 can be rewritten as

$$\Gamma_2 = \Gamma_2(g)\Gamma_2(l) \quad (153)$$

where

$$\Gamma_2(g) = \frac{P_{cr}(g)}{P_{bif}} \quad (154)$$

and

$$\Gamma_2(l) = \frac{P_{cr}(g, l)}{P_{cr}(g)} \quad (155)$$

In this way, a hierarchical set of KDFs can be defined that can be implemented in a mathematically consistent manner as the fidelity of the design process and corresponding analysis models improve. In addition, different effects can be separated into different factors that can be added or removed from the design process as needed. Thus, a design buckling load  $\widehat{P}_{cr}$  can be calculated for preliminary and detailed design using the following relationships:

For conceptual/preliminary design where  $P_{cl}$  is calculated,

$$\widehat{P}_{cr} = \Gamma_1 \Gamma_2 P_{cl} \quad (156)$$

and for detailed design where  $P_{bif}$  is calculated,

$$\widehat{P}_{cr} = \Gamma_2 P_{bif} \quad (157)$$

where  $\Gamma_1$  and  $\Gamma_2$  are developed for a specific structural configuration.

## 5.0 References

1. Peterson, J. P., Weingarten, V. I., Seide, P., "Buckling of Thin-Walled Circular Cylinders," NASA Space Vehicle Design Criteria, NASA SP-8007, September 1965 (Revised August 1968).
2. Peterson, J. P., Weingarten, V. I., Seide, P., "Buckling of Thin-Walled Truncated Cones," NASA Space Vehicle Design Criteria, NASA SP-8019, September 1968.
3. Peterson, J. P., Weingarten, V. I., Seide, P., "Buckling of Thin-Walled Doubly Curved Shells," NASA Space Vehicle Design Criteria, NASA SP-8032, August 1969.
4. Anon., "Buckling Strength of Structural Plates," NASA Space Vehicle Design Criteria, NASA SP-8068, June 1971.
5. Peterson, J. P., "Buckling of Stiffened Cylinders in Axial Compression and Bending – A Review of Test Data," NASA TN D-5561, 1969.
6. McDonnell-Douglas Astronautics Company, "Isogrid Design Handbook," NASA CR-124075, February 1973.
7. von Karman, T. and Tsien, H.-S., "The Buckling of Thin Cylindrical Shells Under Axial Compression," *Journal of the Aeronautical Sciences*, Vol. 8, No. 8, 1941, pp. 303-312.
8. Donnell, L. H., Wan, C. C., "Effect of Imperfections on Buckling of Thin Cylinders and Columns Under Axial Compression," *Journal of Applied Mechanics*, Vol. 17, March 1950, p. 73.
9. Koiter, W. T., "On the Stability of Elastic Equilibrium," Ph. D. Thesis (in Dutch), University of Delft, 1945. Also available in English translation as NASA TT F-10833, 1967 and AFFDL-TR-70-25, 1970.
10. Hilburger, M. W., and Starnes, J. H., Jr., "Effects of Imperfections on the Buckling Response of Compression-Loaded Composite Shells," *International Journal of Non-Linear Mechanics*, Vol. 37, 2002, pp 623-643.
11. Hilburger, M. W., and Starnes, J. H., Jr., "Effects of Imperfections of the Buckling Response of Composite Shells," *Thin-Walled Structures*, Vol. 42, 2004, pp. 369-397.
12. Almroth, B. O., Burns, A. B. and Pittner, E. V., "Design Criteria for Axially Loaded Cylindrical Shells," *Journal of Spacecraft and Rockets*, Vol. 7 No. 6, 1970, pp. 714-720.
13. Hilburger, M. W., Nemeth, M. P., and Starnes, J. H. Jr., "Shell Buckling Design Criteria Based on Manufacturing Imperfection Signatures," *AIAA Journal*, Vol. 44, No. 3, pp. 654-663.
14. Arbocz, J. and Hilburger, M. W., "Towards a Probabilistic Preliminary Design Criterion for Buckling Critical Composite Shells," 44th AIAA/ASME/ASCE/AHS Structures, Structural Dynamics, and Materials Conference, Norfolk, Virginia, 2003, paper # AIAA-2003-1842.
15. Budiansky, B. and Hutchinson, J. W., "A Survey of Some Bucking Problems," *AIAA Journal*, Vol. 4, No. 9, 1966, pp. 1505-1510.
16. Hoff, N., "The Perplexing Behavior of Thin Circular Cylindrical Shells in Axial Compression," *Israel Journal of Technology*, Vol. 4, No. 1, 1966, pp. 1-28.
17. Stein, M., "Some Recent Advances in the Investigation of Shell Buckling," *AIAA Journal*, Vol. 6, No. 12, 1968, pp. 2339-2345.
18. Hutchinson, J. W. and Koiter, W. T., "Postbuckling Theory," *Applied Mechanics Review*, Vol. 23, No. 12, 1970, pp. 1353-1366.

19. Babcock, C. D., "Shell Stability," *ASME Journal of Applied Mechanics*, Vol. 50, 1983, pp. 935-940.
20. Yamaki, N., *Elastic Stability of Circular Cylindrical Shells*, North-Holland, Amsterdam, 1984.
21. Bushnell, D., *Computerized Analysis of Shells*, Martinus Nijhoff Publishers, Kluwer Academic, Norwell, ME, 1985.
22. Simitzes, G. J., "Buckling and Postbuckling of Imperfect Cylindrical Shells: A Review," *ASME Applied Mechanics Review*, Vol. 39, No. 10, 1986, pp. 1517-1524.
23. Teng, J. G., "Buckling of Thin Shells: Recent Advances and Trends," *Applied Mechanics Reviews*, Vol. 49, No. 4, 1996, pp.263-274.
24. Knight, N. F. and Starnes, J. H., Jr., "Developments in Cylindrical Shell Stability Analysis," 38th AIAA/ASME/ASCE/AHS Structures, Structural Dynamics, and Materials Conference, Kissimmee, Florida, 1997, paper # AIAA-1997-1076.
25. Singer, J., Arboez, J. and Weller, T., *Buckling Experiments - Experimental Methods in Buckling of Thin-Walled Structures*, John Wiley & Sons, Chichester, UK and New York, Vol. 1 and Vol. 2, 1997 and 2001.
26. Arboez, J., "The Effect of Initial Imperfections on Shell Stability," *Thin-Shell Structures: Theory, Experiment, and Design*, Y. C. Fung and E. E. Sechler (editors), Prentice-Hall, Englewood Cliffs, New Jersey, 1974, pp. 205-245.
27. Babcock, C. D., "Experiments in Shell Buckling," *Thin-Shell Structures: Theory, Experiment, and Design*, Y. C. Fung and E. E. Sechler (editors), Prentice-Hall, Englewood Cliffs, New Jersey, 1974, pp. 345-369.
28. Haynie, W. T., and Hilburger, M. W., "Comparison of Methods to Predict Lower Bound Buckling Loads of Cylinders Under Axial Compression," AIAA Paper No. 2010-2532.
29. Arboez, J., and Williams, J. G., "Imperfection Survey on a 10-ft Diameter Shell Structure, AIAA Journal, Vol. 15, No. 7, July 1977, 949-956.
30. Arboez, J., "Imperfection Data Bank, a Means to Obtain Realistic Buckling Loads", *Buckling of Shells*, Proceedings of the State-of- the-Art Colloquium, Universitat Stuttgart, Germany, 1982. E. Ramm, Ed., Springer-Verlag, Berlin, Heidelberg, 1982, pp. 535-567.
31. Ricardo, O. G., "An Experimental Investigation of the Radial Displacements of a Thin-Walled Circular Cylinder," NASA Research Grant No. NsG-18-59, SM 67-7, Guggenheim Aeronautical Laboratory, California Institute of Technology, Pasadena CA, 1967.
32. Okubo, S., Wilson, P. E., Whittier, J.S., "Influence of Concentrated Lateral Loads on the Elastic Stability of Cylinders in Bending," *Experimental Mechanics*, Vol. 10, No. 9, pp 384-389, 1970.
33. Stein, M., "The Effect on the Buckling of Perfect Cylinders of Prebuckling Deformations and Stresses Induced by Edge Support," *Collected Papers on Instability of Shell Structures*, NASA TN D-1510, 1962, pp. 217-227.
34. Stein, M., "The Influence of Prebuckling Deformations and Stresses on the Buckling of Perfect Cylinders," NASA TR R-190, 1964.
35. Nachbar, W. and Hoff, N. J. "On Edge Buckling of Axially Compressed Circular Cylindrical Shells," *Quarterly of Applied Mathematics*, Vol. 20, No. 3, 1962, pp 267-277.
36. Almroth, B. O., and Brogan, F. A., "Bifurcation Buckling as an Approximation of the Collapse Load for General Shells," AIAA Journal, Vol. 10, No. 4, pp 463-467, April 1972.

37. Thornburgh, R. P. and Hilburger, M. W., "A Numerical and Experimental Study of Compression-Loaded Composite Panels with Cutouts," 47th AIAA/ASME/ASCE/AHS/ASC Structures, Structural Dynamics, and Materials Conference, Newport, Rhode Island, 2006. Paper # AIAA-2006-2004.
38. Arboez, J. And Hol, J. M. A. M. "On the Reliability of Buckling Load Predictions," 35th AIAA/ASME/ASCE/AHS/ASC Structures, Structural Dynamics, and Materials Conference, Hilton Head, South Carolina, 1994. Paper # AIAA-1994-1371.
39. Sridharan, S. and Alberts, J., "Numerical Modeling of Buckling of Ring-Stiffened Cylinders," *AIAA Journal*, Vol. 35, No. 1, 1997, pp. 187-195.
40. Nemeth, M. P., Britt, V. O., Collins, T. J. and Starnes, J. H., Jr., "Nonlinear Analysis of the Space Shuttle Superlightweight External Fuel Tank," NASA TP-3616, 1996.
41. Ohira, H., "Local Buckling Theory of Axially Compressed Cylinders," Proceedings of the 11<sup>th</sup> Japan National Congress of Applied Mechanics, Tokyo, 1961, pp. 37-40.
42. Simitzes, G. J., Shaw, D., and Sheinman, I., "Imperfection Sensitivity of Fiber-Reinforced Composite Thin Cylinders," *Composites Science and Technology*, Vol. 22, 1985, pp. 259-276.
43. Hilburger, M. W., and Starnes, J. H., Jr., "Parametric Study on the Response of Compression-Loaded Composite Shells with Geometric and Material Imperfections," NASA/TM-2004-212676, September 2004.
44. Hilburger TA
45. Geier, B., Klein, H., and Zimmermann, R., "Experiments on Buckling of CFRP Cylindrical Shells Under Non-Uniform Axial Load," *Proceedings of the International Conference on Composite Engineering (ICCE/1)*, D. Hui, ed., August 28-31, 1991, 1043-1044.
46. Zimmermann, R., "Buckling Research for Imperfection Tolerant Fiber Composite Structures," *Proceedings of the Conference on Spacecraft Structures, Materials, and Mechanical Testing*, Noordwijk, The Netherlands, March 27-29, 1996 (EAS SP-3856, June 1996), 411-416.
47. Huhne, C., Rolfes, R., Breitbach, E., and Teßmer, J., "Robust Design of Composite Cylinder Shells Under Axial Compression – Simulation and Validation," *Thin-Walled Structures*, 46(7-9), pp 947-962
48. Kriegesmann, B., Hilburger, M. W., Rolfes, R., "Effects of Geometric and Loading Imperfections on the response and Lower-Bound Buckling Load of a Compression-Loaded Cylindrical Shell," AIAA Paper No. 2012-1864.
49. Hilburger, M. W., and Starnes, J. H., Jr., "The Effects of Imperfections on the Buckling Response of Compression-Loaded Composite Shells," Proceedings of the 41st AIAA/ASME/ASCE/AHS/ASC Structures, Structural Dynamics, and Materials Conference, Atlanta, GA, 2000, AIAA Paper No. 2000-1387.
50. Starnes, J. H. Jr., "The Effects of Cutouts on the Buckling of Thin Shells," *Thin-Shell Structures: Theory, Experiment, and Design*, Y. C. Fung and E. E. Sechler (editors), Prentice-Hall, Englewood Cliffs, New Jersey, 1974, pp. 289-304.
51. Toda, S., "Buckling of Cylindrical Shells with Cutouts Under Axial Compression," *Experimental Mechanics*, Vol. 23, No. 4, December 1983, pp 414-417.
52. Julien, J. F., and Limam, A., "Effects of Openings on the Buckling of Cylindrical Shells Subjected to Axial Compression," *Thin-Walled Structures*, Vol. 31, , 1998, pp 187-202.

53. Hilburger, M. W., Starnes, J. H. Jr., and Waas, A., M., "A Numerical and Experimental Study of the Response of Selected Compression-Loaded Composite Shells with Cutouts," *Proceedings from 39<sup>th</sup> AIAA/ASME/ASCE/AHS/ASC Structures, Structural Dynamics and Materials Conference*, Long Beach CA, April 20-23, 1998, pp 2338-2351, AIAA Paper 98-1998.
54. Hilburger, M. W., and Starnes, J. H. Jr., "Buckling Behavior of Compression-Loaded Composite Cylindrical Shells with Reinforced Cutouts," *Proceedings from 43rd AIAA/ASME/ASCE/AHS/ASC Structures, Structural Dynamics and Materials Conference*, AIAA Paper 2002-1516.
55. Hilburger, M. W., and Nemeth, M. P., "Buckling and Failure of Compression-Loaded Composite Cylindrical Shells with Reinforced Cutouts," *Proceedings from 46rd AIAA/ASME/ASCE/AHS/ASC Structures, Structural Dynamics and Materials Conference*, AIAA Paper 2005-2370.
56. Thornburgh, R., P., and Hilburger, M. W., "Longitudinal Weld Land Buckling in Compression-Loaded Orthogrid Cylinders," NASA/TM-2010-216876, ARL-TR-5121, December 2010.
57. Arboez, J. and Hilburger, M. W., "Towards a Probabilistic Preliminary Design Criterion for Buckling Critical Composite Shells," *44th AIAA/ASME/ASCE/AHS Structures, Structural Dynamics, and Materials Conference*, Norfolk, Virginia, 2003, paper # AIAA-2003-1842.
58. Brush, D. O., and Almroth, B. O., *Buckling of Bars, Plates, and Shells*, McGraw-Hill Book Company, New York, 1975.
59. Donnell, L. H., "A New Theory for the Buckling of Thin Cylinders Under Axial Compression and Bending," *ASME Transactions*, Vol. 56, No. 11, 1934, pp. 795-806.
60. Batdorf, S. B., "A Simplified Method of Elastic-Stability Analysis for Thin Cylindrical Shells, NACA TR-874, 1947.
61. Becker, H., and Gerard, G., "Elastic Stability of Orthotropic Shells," *Journal of the Aeronautical Sciences*, Vol. 29, No. 5., 1962, pp 505-520.
62. Liang, K., Abdalla, M., M., and Sun, Q., "A Modified Newton-Type Koiter-Newton Method for Tracing the Geometrically Nonlinear Response of Structures," *Numerical Methods in Engineering*, Vol. 113, No 10, March 2018, pp 1541-1560.
63. Barut, A., and Madenci, E., "Postbuckling of Composite Panels with Isogrid Siffeners," *Proceedings from 49th AIAA/ASME/ASCE/AHS/ASC Structures, Structural Dynamics and Materials Conference*, April 7-10 2008, Schaumburg IL, AIAA Paper 2008-2274.
64. Barut, A., Madenci, E., and Nemeth, M. P., "Stress and Buckling Analyses of Laminates with a Cutout Using a {3, 0}-Plate Theory," *Journal of Mechanics of Materials and Structures*, Vol. 6, No. 6, 2001, pp 827-868.
65. Weingarten, V. I., Morgan, E. J. and Seide, P., "Elastic Stability of Thin-Walled Cylindrical and Conical Shells Under Axial Compression," *AIAA Journal*, Vol. 3, No. 3, 1965, pp. 500-505.
66. Dickson, J. N. and Broliar, R. H., "The General Instability of Ring-Stiffened Corrugated Cylinders Under Axial Compression," NASA TN D-3089, 1966.
67. Meyer, R. R., "Buckling of 45° Eccentric-Stiffened Waffle Cylinders," *Journal of the Royal Aeronautics Society (Tech. Notes)*, Vol. 71, No. 679, 1967, pp. 516-520.
68. Peterson, J. P. and Dow, M. B., "Compression Tests on Circular Cylinders Stiffened Longitudinally by Closely Spaced Z Section Stringers," NASA Memo 2-12-59L, 1959.
69. Peterson, J. P., Whitley, R. O., and Deaton, J. W., "Structural Behavior and Compressive Strength of Circular Cylinders with Longitudinal Stiffening," NASA TN D-1251, 1962.

70. Becket, H., Gerard, G. and Winter, R., "Experiments on Axial Compressive General Instability of Monolithic Ring-Stiffened Cylinders," *AIAA Journal*, Vol. 1, No. 7, 1963, pp. 1614-1618.
71. Card, M. F. and Jones, R. M., "Experimental and Theoretical Results for Buckling of Eccentrically Stiffened Cylinders," NASA TN D-3639, 1966.
72. Milligan, R., Gerard, G. and Lakshminantham, C. "General Instability of Orthotropically Stiffened Cylinders Under Axial Compression," *AIAA Journal*, Vol. 4, No. 11, 1966, pp. 1906-1913.
73. Singer, J. "The Influence of Stiffener Geometry and Spacing on the Buckling of Axially Compressed Cylindrical and Conical Shells," *Theory of Thin Shells*, F. I. Niordson, ed., Springer-Verlag, 1969, pp. 234-263.
74. Peterson, J. P. and Anderson, J. K., "Bending Tests of Large-Diameter Ring-Stiffened Corrugated Cylinders," NASA TN D-3336, 1966.
75. Anderson, J. K., "Bending Tests of Two Large-Diameter Corrugated Cylinders With Eccentric Ring Stiffeners," NASA TN D-3702, 1966.
76. Card, M. F., "Bending Tests of Large-Diameter Stiffened Cylinders Susceptible to General Instability," NASA TN D-2200, 1964.
77. Singer, J., "Buckling of Integrally Stiffened Cylindrical Shells-A Review of Experiment and theory," in: *Contributions to the theory of aircraft Structures*, Delft University Press, Rotterdam, 1972, pp 325-357.
78. Sendelbeck, R., S., and Hoff, N. J., "Loading Rig in which Axially Compressed Thin Cylindrical Shells Buckle Near Theoretical Values," *Experimental Mechanics*, Vol. 12, No. 8, 1972, pp 372-376.
79. Almroth, B. O., Burns, A. B. and Pittner, E. V., "Design Criteria for Axially Loaded Cylindrical Shells," *Journal of Spacecraft and Rockets*, Vol. 7 No. 6, 1970, pp. 714-720.
80. Tennyson, R. C., Muggerridge, D. B., and Caswell, R. D., "New Design Criteria for Predicting Buckling of Cylindrical Shells Under Axial Compression," *Journal of Spacecraft*, Vol. 8, No. 10, October 1972, pp 1062-1067.
81. Karr, D. G., Bushnell, D. and Skogh, J., "STAGS Analysis of the Space Shuttle External LH 2 Tank (LWT)," Martin Marietta Aerospace/Lockheed Missiles and Space Co. Report, August 1983.
82. Torres, W. and Karr, D. G., "Stability Analysis - Space Shuttle Liquid Hydrogen Tank", AIAA GNOS 84-002, New Orleans, LA., October 1984.
83. Nemeth, M. P., Young, R. D., Collins, T. J. and Starnes, J. H., Jr., "Effects of Welding-Induced Initial Geometric Imperfections on the Nonlinear Behavior of the Space Shuttle Superlightweight LO2 Tank," 39th AIAA/ASME/ASCE/AHS Structures, Structural Dynamics, and Materials Conference, Long Beach, California, 1998, paper # AIAA-98-1840.
84. Ayala, S., "Super-Lightweight Intertank Independent Stability Analysis," Sverdrup Technology, Inc. Report No. 621-017-03-001, June 1996.
85. Nemeth, M. P., Britt, V. O., Collins, T. J. and Starnes, J. H., Jr., "Nonlinear Analysis of the Space Shuttle Superlightweight External Fuel Tank," NASA TP-3616, 1996.
86. Nemeth, M. P. and Starnes, J. H., Jr., "The NASA Monographs on Shell Stability Design Recommendations. A Review and Suggested Improvements," NASA TP-1998-206290, 1998.
87. Almroth, B. O., "Influence of Edge Conditions on the Stability of Axially Compressed Cylindrical Shells," NASA CR-161, February 1965.

88. Hoff, N. J., and Soong, T. C., "Buckling of Circular Cylindrical Shells in Axial Compression," *International Journal of Mechanical Sciences*, Vol. 7, 1965, pp 489-520.
89. Hoff, N., and Rehfield, L. W., "Buckling of axially Compressed Circular Cylindrical Shells at Stresses Lower than the Classical Value," *Journal of Applied Mechanics*, vol. 32, no. 3, September 1965, pp 533-537.
90. Batdorf, S. B., "A Simplified Method of Elastic Stability Analysis for Thin Cylindrical Shells," NACA Rept. 874, 1947.
91. Gerard, G., and Becker, H., Handbook of Structural Stability Part III, Buckling of Curved Plates and Shells," NACA TN 3783, 1957.
92. Nemeth, M. P., "Buckling Analysis for Stiffened Anisotropic Circular Cylinders Based on Sanders Nonlinear Shell Theory," NASA TM-2014-218176, March 2014.
93. Krivitsky, A., "Plasticity Coefficients for Plastic Buckling of Plates and Shells," *Journal of Aeronautical Sciences* (Reader's Forum), vol. 22, no. 6, June 1955, pp 432-435.
94. Stowell, E. Z., "A Unified Theory of Plastic Buckling of Columns and Plates," NACA Rept. 898, 1948.
95. Seide, P., and Weingarten, V. I., "On the Buckling of Circular Cylindrical Shells Under Pure Bending," *Journal of Applied Mechanics*, vol. 28, no. 1, March 1961, pp 112-116.
96. Seide, P., Weingarten, V. I., and Morgan, E. J., "The Development of Design Criteria for Elastic Stability of Thin Shell Structures, STL/TR-60-0000-19425 (AFBMD/TR-61-7), Space Technology Laboratory, Inc. December, 1960.
97. Stephans, W. B., Starnes, J. H., and Almroth, B. O., "Collapse of Long Cylindrical Shells under Combined Bending and Pressure Loads," *AIAA Journal*, vol. 13, no. 1, January 1975, pp 20-25.
98. Timoshenko, S., and Gere, J. M., *Theory of Elastic Stability. Second ed.*, McGraw-Hill Book Co., Inc., 1961.
99. Sobel, L. H., "Effects of Boundary Conditions on the Stability of Cylinders Subject to Lateral and Axial Pressures," *AIAA Journal*, vol. 2, no. 8, August 1964, pp 1437-1440.
100. Singer, J., "The Effects of Axial Constraint on the Instability of Thin Cylindrical Shells under External Pressure," *Journal of Applied Mechanics*, vol. 27, no. 4, 1960, pp 737-739.
101. Weingarten, V. I., and Seide, P., "Elastic Stability of Thin-Walled Cylindrical and Conical Shells Under Combined External Pressure and Axial Compression," *AIAA Journal*, vol. 3, no. 5, May 1965, pp 913-920.
102. Gerard, G., Handbook of Structural Stability, Supplement to Part III, Buckling of Curved Plates and Shells," NACA TN D-163, 1959.
103. Harris, L. A., Suer, H. S., Skene, W. T., and Benjamin, R., J., "The Stability of Thin-Walled Unstiffened Circular Cylinders Under Axial Compression Including the Effects of Internal Pressure," *Journal of Aeronautical Sciences*, vol. 24, no. 8, August 1957, pp 587-596.
104. Leonard, R. W., McComb, H. G., Zender, G. W., and Stroud, W. J., "Analysis of Inflated Reentry and Space Structures," Proceedings from Recovery of Space Vehicles Symposium, August-September 1960, Institute of Aeronautical Sciences, New York.
105. Leonard, R. W., Brooks, G. W., and McComb, H. G., "Structural Considerations of Inflatable Reentry Vehicles," NASA TN D-457, 1960.

106. Sein, M., and Hedgepeth, J. M., "Analysis of Partly Wrinkled Membranes," NASA TN D-813, 1961.
107. *Collected Papers on Instability of Shell Structures*, NASA TN D-1510, 1962, pp. 229-237.
108. Singer, J., Baruch, M., and Harari, O., "On the Stability of Eccentrically Stiffened Cylindrical Shells Under Axial Compression," *International Journal of Solids and Structures*, vol. 3, no. 4, July 1967, pp 445-470.
109. Singer, J., and Baruch, M., "Recent Studies on Optimisation of Elastic Stability of Cylindrical and Conical Shells," in *Aerospace Proceedings*, 1966, Proceedings of the 5<sup>th</sup> International Congress of the Aeronautical Sciences, London, September 1966, pp 751-782.
110. Singer, J., Baruch, M., and Harari, O., "Inversion of the Eccentricity Effect in Stiffened Cylindrical Shells Buckling Under External Pressure," *Journal of Mechanical Engineering Science* (England), vol. 8, no. 4, December, 1966, pp 363-373.
111. Burns, A. B., "Structural Optimization on Axially Compressed Cylinders, Considering Ring-Stringer Eccentricity Effects," *Journal of Spacecraft and Rockets*, vol. 3, no. 8, August 1966, pp 1263-1268.
112. Bushnell, D., Almroth, B. O., and Sobel, L. H., "Buckling of Shells of Revolution with various Wall Constructions," NASA CR's 1049, 1050, 1051, 1968.
113. Hyer, M. W., *Stress Analysis of Fiber-Reinforced Composite Materials*, McGraw-Hill Book Co., Inc., 1998.
114. Jones, R. M., "Buckling of Circular Cylindrical Shells with Multiple Orthotropic Layers and Eccentric Stiffeners," *ALAA Journal*, vol. 6, no. 12, December 1968, pp 2301-2305.
115. Meyer, R. R., "Buckling of Ring-Stiffened Corrugated Cylinders Subjected to Uniform Axial Load and Bending," Rept. DAC-60698, Douglas Aircraft Co., July 1967.
116. Block, D. L., Card, M. F., and Mikulas, M. M., Jr., "Buckling of Eccentrically Stiffened Orthotropic Cylinders," NASA TN D-2960, August, 1965.
117. Singer, J., and Rosen, A., "Influence of Boundary Conditions on the Buckling of Stiffened Cylindrical Shells," in *Buckling of Structures*, Proceedings of IUTAM Symposium, Harvard University, Cambridge, MA, June 17-21 1974, B. Budiansky, ed., Springer-Verlag, Berlin, 1976, pp 227-250.
118. Singer, J., and Rosen, A., "A Design Criteria for Buckling and Vibration of Imperfect Stiffened Cylindrical Shells," in *ICAS Proceedings 1974*, Proceedings of the 9<sup>th</sup> Congress of the International Council of the Aeronautical Sciences, Haifa, August 1974, R. R. Dexter and J. Singer, eds., Weizmann Science Press of Israel, Jerusalem, 1974, pp 495-517.
119. Weller, T., and Singer, J., "Further Experimental Studies on Buckling of Integrally Ring-Stiffened Cylindrical Shells under Axial Compression," *Experimental Mechanics*, vol. 14, no. 7, July 1974, pp 268-273.
120. Weller, T., Singer, J., and Nachmani, S., "Recent Experimental Studies on the Buckling of Stringer-Stiffened Cylindrical Shells," TAE Report 100, Department of Aeronautical Engineering, Technion, Haifa, Israel, April 1970.
121. Weller, T., and Singer, J., "Experimental Studies on Buckling of 7075-T6 Aluminum Alloy Integrally Stringer-Stiffened Shells," TAE Report 135, Department of Aeronautical Engineering, Technion, Haifa, Israel, October 1971.

122. Abramovich, H., Singer, J., and Weller, T., "The Influence of Initial Imperfections on the Buckling of Stiffened Cylindrical Shells under Combined Loading," in *Buckling of Shells Structures, on Land, in the Sea, and in the Air*, J. F. Julien, ed., Elsevier Applied Science, London, 1991, pp 1-10.
123. Jenson, D. W., and Hipp, P. A., "Compressive Testing of Filament-Wound Cylinders, Composites, in *Proceedings of the 8<sup>th</sup> International Conference on Composite Materials (ICCM/8)*, Honolulu, Hawaii, July 15-19, 1991, 35-F-1—35-F-9.
124. Card, M. F., "Experiments to Determine the Strength of Filament Wound Cylinders Loaded in Axial Compression," NASA TN D-3522, August, 1966.
125. Tsai, J. Feldman, A., and Stang, D. A., "The Buckling Strength of Filament Wound Cylinders under Axial Compression," NASA CR-266, July 1965.
126. Hahn, H. T., Jensen, D. W., Claus, S. J., and Hipp, P. A., "Structural Design Criteria for Filament Wound Composite Shells," NASA CR-195125, January 1994.
127. Tennyson, R. C., Chan, K. H., and Muggeridge, D. B., "The Effect of Axisymmetric Shape Imperfections on the Buckling of Laminated Anisotropic Circular Cylinders," *Transactions of the Canadian Aeronautics and Space Institute*, vol. 4, no. 2, September 1971.
128. Tennyson, R. C., Muggeridge, D. B., Chan, K. H., and Khot, N. S., "Buckling of Fiber-Reinforced Circular Cylinders under Axial Compression, TR-72-102, Air Force Flight Dynamics Laboratory, Wright-Patterson Air Force base, August 1972.
129. Geier, B., Klein, H., and Zimmermann, R., "Buckling Tests with Axially Compressed Unstiffened Cylindrical Shells Made from CFRP," in *Buckling of Shell Structures on Land, in the Sea and in the Air*, Proceedings International Conference, J. F. Jullien, ed., INSA Lyon, September 17-19, Elsevier Applied Science, London, New York, 1991, 498-507.
130. Giavotto, V., Poggi, C., Castano, D., Guzzetti, D., and Fezzani, M., "Buckling Behavior of Composite Shells under Combined Loading," in *Proceedings, 17<sup>th</sup> European Rotorcraft Forum*, Berlin, September 1991, pp 84-1 – 84-13.
131. Poggi, C., Taliercio, A., and Capsoni, A., "Fiber Orientation Effects on the Buckling Behavior of Imperfect Composite Cylinders," in *Proceedings, International Colloquium on Buckling of Shell Structures on Land, in the Sea and in the Air*," Lyon, France, September 17-19, 1991, J. F. Jullien, ed., pp 114-123.
132. Bisagni, C., "Buckling and Postbuckling Behavior of Composite Cylindrical Shells," in *Proceedings, ICAS 1996, 20<sup>th</sup> Congress of the International Council of the Aeronautical Sciences*, Sorrento, Naples, Italy, September 8-13, 1996, vol. 1, pp1148-1155.
133. Davis, R. C., "Buckling Test of 3-Meter-Diameter Corrugated Graphite-Epoxy Ring-Stiffened Cylinder," NASA TP-2032, July 1982.
134. Hedgepeth, J. M., and Hall, D. B., "Stability of Stiffened Cylinders," *AIAA Journal*, vol.3 no. 12, December 1965, pp 2275-2286.
135. Peterson, J. P., "Bending tests of Ring-Stiffened Circular Cylinders," NACA TN 3735, July 1956.
136. Anderson, J. K., and Peterson, J. P., "Buckling Tests of Two Integrally Stiffened Cylinders Subjected to Bending," NASA TN D-6271, June 1971.
137. Dow, M. B., and Paterson, J. P., "Bending and Compression Tests of Pressurized Ring-Stiffened Cylinders, NASA TN D-360, April 1960.

138. Bodner, S. R., "General Instability of a Ring-Stiffened Circular Cylindrical Shell Under Hydrostatic Pressure," *Journal of Applied Mechanics*, vol. 24, no. 2, June 1957.
139. Baruch, M. and Singer, J., "Effect of Eccentricity of Stiffeners on the General Instability of Stiffened Cylindrical Shells Under Hydrostatic Pressure," *Journal of Mechanical Engineering Science*, vol. 5, no. 1, March 1963, pp 23-27.
140. Singer, J., Baruch, M., and Harari, O., "Further Remarks on the Effect of Eccentricity of Stiffeners on the General Instability of Stiffened Cylindrical Shells," *Journal of Mechanical Engineering Science*, vol. 8, no. 4, 1966, pp 363-373.
141. Kendrick, S., "The Buckling Under External Pressure of Circular Cylindrical Shells with Evenly Spaced Equal Strength Ring Frames – Part III," Naval Construction Research Establishment, Report R-244, September 1953.
142. Galletly, G. D., Slankard, R. C., and Wenk, E., Jr., "General Instability of Ring-Stiffened Cylindrical Shells Subject to External Hydrostatic Pressure – A Comparison of Theory and Experiment," *Journal of Applied Mechanics*, vol. 25, no. 2, June 1958, pp 259-266.
143. Yamamoto, Y., et al., "General Instability of Ring-Stiffened Cylindrical Shells under External Pressure," *Marine Structures*, vol. 2, 1989, pp 133-149.
144. Miller, C. D., and Kinra, R. K., "External Pressure Tests of Ring-Stiffened Fabricated Steel Cylinders," 13<sup>th</sup> Annual Offshore Technology Conference, Houston, May 1981, Paper no. OTC-4107, Proceedings OTC '81, vol. 3, 1981, pp 371-386.
145. Miller, C. D., Frieze, P. A., Zimmer, R. A., and Jan, H. Y., "Collapse Tests of Fabricated Stiffened Steel Cylinders under Combined Loads," presented at the ASME 4<sup>th</sup> National Congress of Pressure Vessels and Piping technology, Portland, June 1983, Paper 83-PVP-7.
146. Simitses, G. J., "Instability of Orthotropic Cylindrical Shells Under Combined Torsion and Hydrostatic Pressure," *AIAA Journal*, vol. 5 no.8, August 1967, pp 1463-1469.
147. Baruch, M., Singer, J., and Weller, T., "Effects of Eccentricity of Stiffeners on the General Instability of Cylindrical Shells Under Torsion," *Israel Journal of Technology*, vol. 4, no. 1, 1966, pp 144-154.
148. Milligan, R., and Gerard, G., "General Instability of Orthotropically Stiffened Cylinders Under Torsion," *AIAA Journal*, vol. 5, no. 11, November 1967, pp 2071-2073.
149. Block, D. L., "Buckling of Eccentrically Stiffened Orthotropic Cylinders Under Pure Bending," NASA TN-D3351, March, 1966.
150. Nemeth, M. P., "A Treatise on Equivalent-Plate Stiffnesses for Stiffened Laminated-Composite Plates and Plate-Like Lattices," NASA/TP-2011-216882, January 2011.
151. Schultz, M. R., Hilburger, M. W., Satyanarayana, A., and Oremont, L., "Buckling Analysis of the Space Launch System (SLS) Core Stage Ringless Cryotanks," NASA/TM-2014-218515, August 2014 (ITAR restricted distribution).
152. Hilburger, M. W., Schultz, M. R., and Oremont, L., "Buckling Analysis of the Space Launch System (SLS) Core Stage Ringless Cryotanks – Updated Buckling Load Predictions Based on As-Built SLS Cryotank Barrel Geometry," NASA/TM-2017-219373, February 2017 (ITAR restricted distribution).
153. SciTech reference on KDFs

154. Shanley, F. R., "Weight-Strength Analysis of Aircraft Structures," McGraw-Hill Book Co., Inc., 1952.
155. Block, D. L., "Influence of Ring Stiffeners on Instability of Orthotropic Cylinders in Axial Compression," NASA TN D-2482, 1964.
156. Stein, M., Sanders, J., L., and Crate, H., "Critical Stress of Ring-Stiffened Cylinders in Torsion," NACA Rept. 989, 1950.
157. Anon., "Sandwich Construction for Aircraft. Part II \_ Materials, Properties, and Design Criteria," ANC-23, Air Force-Navy-Civil Subcommittee on Aircraft Design Criteria, 1955.
158. Libove, C., and Hubka, R. E., "Elastic Constants for Corrugated Core Sandwich Plates," NACA TN 2289, 1951.
159. Plantema, F. G., "Sandwich Construction, The Bending and Buckling of Sandwich Beams, Plates, and Shells," John Wiley & Sons, Inc., 1966.
160. Zahn, J. J., and Kuenzi, E. W., "Classical Buckling of Cylinders of Sandwich Construction in Axial Compression – Orthotropic Cores," Rept. FPL-018, Forest Products Laboratories, 1963.
161. Anon., "Composite Construction for Flight Vehicles. Part I – Fabrication, Inspection, Durability, and Repair," MIL-HDBK-23, Part I, Armed Forces Supply Support Center, Oct. 1959.
162. Peterson, J. P., "Weight-Strength Studies on Structures Representative of Fuselage Construction," NACA TN 4114, 1957.
163. Norris, C., "Sorth-Column Compressive Strength of Sandwich Constructions as Affected by Size of Honeycomb Core Materials," FPL-026, Forest Products Laboratories, Jan. 1964.
164. Konishi, D. Y., et al., "Honeycomb Sandwich Structures Manual," Rept. NA58-899, North American Aviation, Inc., Los Angeles Division, July 1968.
165. Yusuff, S., "Face Wrinkling and Core Strength in Sandwich Construction," J. Roy. Aeron. Soc., vol. 64, no. 591, March 1960, pp 164-167.
166. Harris, B., and Crisman, W., "Face-Wrinkling Mode of Buckling of Sandwich Panels," EM3, ASCE Journal of Engineering, Mechanics Division, June 1965.
167. Kieiman, M. O., and Konishi, D. Y., "Stability of Honeycomb Sandwich Cylinders, Paper No.61-AV-36, ASME, 1961.
168. Holston, A., Jr., "Stability of Inhomogeneous Anisotropic Cylindrical Shells Containing Elastic Cores," *AIAA Journal*, vol. 5, no. 6, June 1967, pp. 1135-1138.
169. Brush, B. O., and Pittner, E. V., "Influence of Cushion Stiffness on the Stability of Cushion-Loaded Cylindrical Shells," *AIAA Journal*, vol. 3, no. 2, February 1965, pp 308-316.
170. Seide, P., "The Stability Under Axial Compression and Lateral Pressure of a Circular-Cylindrical Shell with an Elastic Core," *Journal of Aeronautical Sciences*, vol. 29, no. 7, July 1962, pp. 851-862.
171. Weingarten, V. I., "Stability Under Torsion of Circular Cylinder Shells with an Elastic Core," *ARS Journal*, vol. 32, no. 4, April 1962, pp. 637-639. (Article is available through the AIAA)
172. Peterson, J. P., and Whitley, R. O., "Local Buckling of Longitudinally Stiffened Curved Plates," NASA TN D-750, April 1961.
173. Peterson, J. P., and Dow, M. B., "Compression Tests on Circular Cylinders Stiffened Longitudinally by Closely Spaced Z-Section Stiffeners," Memo 2-12-59L, March 1959, NASA.

174. Murphey, T.W., Sanford, G.E., and Grigoriev, M.M., "Nonlinear Elastic Constitutive Modeling of Large Strains in Carbon Fiber Composite Flexures," *Proceedings of the 16<sup>th</sup> International Conference on Composite Structures (ICCS16)*, edited by A.J.M. Ferreira, FEUP, Porto, Portugal, 2011.
175. Schultz, M.R., Sleight, D.L., Gardner, N.W., Rudd, M.T., Hilburger, M.W., Palm, T.E., and Oldfield, N.J., "Test and Analysis of a Buckling-Critical Large-Scale Sandwich Composite Cylinder," *Proceedings of the 58<sup>th</sup> AIAA/ASME/ASCE/AHS/ASC Structures, Structural Dynamics & Materials Conference*, AIAA paper no. 2018-1693, Kissimmee, FL, January 2018.
176. Riks, E., Rankin, C. C., and Brogan, F. A., "On the solution of mode jumping phenomena in thin-walled shell structures," *Computer Methods in Applied Mechanics and Engineering*, vol. 136, pp. 59-92.